FLOW PATHS TO FLOODPLAINS: SCALING BIOGEOCHEMICAL CYCLES IN RIVERS

by

ASHLEY MCKENDREE HELTON

(Under the Direction of Geoffrey C. Poole)

ABSTRACT

Riverine processes play important roles in global biogeochemical cycles. However, current modeling frameworks for scaling biogeochemical processes in rivers lack fundamental hydrologic and ecological controls on biogeochemical cycles. We used several approaches to improve our understanding of scaling riverine biogeochemical processes. First, we evaluated common modeling assumptions about river and catchment hydrogeomorphology and biogeochemistry, by scaling headwater stream denitrification measurements to eight small river networks. Using the model results, we identified additional factors important for understanding biogeochemical cycling, and illustrated strategies for improving river biogeochemistry simulation. River network model results revealed the importance of incorporating hydrologic linkages between the river channel, floodplain surface, and hyporheic zone as a basis for scaling biogeochemical cycles. Thus, we parameterized a detailed three-dimensional hydrogeomorphic model for the 16 km^2 Nyack Floodplain on the Middle Fork Flathead River, Montana, and used hydrologic model results as a basis for 1) evaluating the influence of floodplain surface and hyporheic storage on hydrologic residence time (i.e., mean matrix traversal time; MTT), 2) analyzing observed patterns of hyporheic carbon quantity and quality, and 3) scaling an

interdependent set of flow path dissolved oxygen and nitrate models to the whole Nyack Floodplain study area.

Our hydrologic residence time results revealed the importance of floodplain surface and hyporheic storage for MTT, specifically that whole-floodplain MTT was strongly correlated with hyporheic exchange. Dissolved organic carbon (DOC) concentration decreased with MTT but DOC lability increased, suggesting that although the Nyack hyporheic zone is a net sink for DOC, recalcitrant DOC is replaced with more bioavailable DOC along hyporheic flow paths, increasing the lability of DOC transported downstream. Our biogeochemical model explained 67% and 27% of the variance in dissolved oxygen and nitrate measurements, respectively, that spanned the floodplain longitudinally, laterally, and vertically, and river discharge conditions and seasons. Paired with a realistic model of floodplain hydrogeomorphology, relatively simple biogeochemical models explained complex patterns of observed biogeochemical dynamics observed throughout the hyporheic zone. Thus, understanding the physical template that drives hydrologic flux and storage of biogeochemical constituents is fundamental for understanding biogeochemical cycles across large spatial and temporal scales.

INDEX WORDS: river, simulation model, hydrology, biogeochemistry, hyporheic zone, floodplain, nitrogen, dissolved organic carbon, carbon bioavailability

FLOW PATHS TO FLOODPLAINS: SCALING BIOGEOCHEMICAL CYCLES IN RIVERS

by

ASHLEY MCKENDREE HELTON

BS, University of Cincinnati, 2004

MS, University of Georgia, 2006

A Dissertation Submitted to the Graduate Faculty of The University of Georgia in Partial Fulfillment of the Requirements for the Degree

DOCTOR OF PHILOSOPHY

ATHENS, GEORGIA

2011

FLOW PATHS TO FLOODPLAINS: SCALING BIOGEOCHEMICAL CYCLES IN RIVERS

by

ASHLEY MCKENDREE HELTON

Major Professor:	Geoffrey C. Poole
Committee:	Emily S. Bernhardt
	Mark A. Bradford
	Miguel L. Cabrera
	Amy D. Rosemond

Electronic Version Approved:

Maureen Grasso
Dean of the Graduate School
The University of Georgia
May 2011

ACKNOWLEDGEMENTS

My committee members, Geoff Poole, Emily Bernhardt, Mark Bradford, Miguel Cabrera, and Amy Rosemond provided invaluable guidance, advice, and support. I especially thank my advisor, Geoff Poole, for being an extraordinary mentor, teacher, and friend during my program at the University of Georgia.

I am grateful for the Odum School of Ecology graduate students, faculty, and staff, especially the Rosemond lab group, office 199B past and present, and Cindy Tant, John Davis, Jake Allgeier, Andrew Mehring, and Chip Small. Thanks to Emily Bernhardt and the Bernhardt lab at Duke University, the Poole lab at Montana State University, and the Flathead Lake Biological Station faculty and staff, for office space, lab space, guidance, and support. Thanks also to Alison Appling, Meredith Wright, and Oriana Grubisic for field and lab collaborations.

I thank my family for being unwaveringly supportive for the past five years: my mother, Melissa McKendree; my sisters, Jessica Reitz and Lauren Peak; and my grandmother, Jackie Oliver. I am especially grateful for my husband, Nick Helton, who has always been the most encouraging and supportive person throughout graduate school and my life.

This work was funded by the Odum School of Ecology Small Grants Program, an Environmental Protection Agency Science to Achieve Results Fellowship, the US Department of Agriculture (2005-35102-16288), the National Science Foundation (DEB-0111410), and the Gordon and Betty Moore Foundation.

TABLE OF CONTENTS

Page

LIST OF TABLES

Page

LIST OF FIGURES

Page

CHAPTER 1

INTRODUCTION

Recent research highlights the importance of river ecosystems for global scale biogeochemical cycling (Cole et al. 2007). However, quantifying biogeochemical processes in whole river networks is difficult. Traditionally, the goal of watershed-scale riverine biogeochemical models has been to predict watershed nutrient export to receiving water bodies (Smith et al. 1997). However, in-stream processes, such as denitrification and respiration (i.e., ecosystem processes that produce greenhouse gases and/or permanently remove nutrients; Beaulieu et al. *In Press*; Mulholland et al. 2008), are important pathways for understanding river ecosystem biogeochemical cycling and its effects on larger scale biogeochemical cycles.

Stream reach biogeochemical process measurements have been scaled with traditional nutrient export modeling frameworks to predict patterns of ecosystem processes throughout river networks (e.g., denitrification, Mulholland et al. 2008; Alexander et al. 2000; Seitzinger et al. 2002; Wollheim et al. 2008). Estimates of denitrification produced from these models are typically based on mass balance or statistical analyses wherein nitrogen removal is represented as a one-way flux from the river channel (see Wollheim et al. 2006 for a review). Although these models have high predictive accuracy for annual watershed nitrogen export (Alexander et al. 2002), they represent neither complete biogeochemical cycles nor hydrologic flux between river ecosystem components (including the channel, floodplain surface, and hyporheic zone) that can drive important patterns of ecosystem processes (McClain et al. 2003).

In Chapter 2 (Helton et al. *In Press*), common modeling approaches and assumptions about river and catchment hydrogeomorphology and biogeochemistry are evaluated, by scaling *in situ* denitrification measurements from headwater streams (Mulholland et al. 2008) to river networks in eight different catchments. Using the model results, I identify additional dynamics and catchment characteristics that are important for understanding biogeochemical cycling, illustrate strategies for improving simulation of river biogeochemistry, and prioritize steps for future model development. I also present an initial approach for incorporating multiple elemental cycles and ecological stoichiometry into river-network models that integrates first principles of thermodynamics (i.e., free energy yield from metabolic pathways) with governing equations for surface and groundwater fluxes.

A primary finding from the model evaluation was the importance of interactions between the channel, hyporheic zone, and floodplain surface for scaling biogeochemical cycles. Thus, I also proposed integrating biogeochemical models and existing floodplain hydrology models to improve understanding of biogeochemical dynamics of multiple interacting flow paths within fluvial landscapes. In Chapters 3 through 5, I implement a floodplain hydrology model, and use the hydrology model to interpret observed biogeochemical patterns and to scale flow path biogeochemistry to a whole floodplain.

In Chapter 3, I parameterized and implemented a detailed three-dimensional hydrogeomorphic model for the 16 km^2 Nyack Floodplain on the Middle Fork Flathead River in northwest Montana, USA. The Nyack Floodplain river channel, hyporheic zone, and floodplain surface are well connected, and the Nyack Floodplain has an extensive hyporheic zone that ranges from ~5 to >25 meters in depth and spans the width of the floodplain (up to 1.5 km). I used a dynamic three-dimensional model to simulate surface and subsurface water flux and

storage (Poole et al. 2004), combined with a recently developed approach to delineate low-relief landscapes with high resolution topography data for hydrologic analysis (Jones et al. 2008). The model simulated four years of floodplain hydrology and nine particle releases across a range of river discharges. Model results were used to analyze temporal patterns of whole floodplain hyporheic exchange, and to determine mean matrix traversal time (MTT), a surrogate for hydrologic residence time, for the river channel, floodplain surface, hyporheic zone, and whole floodplain.

In Chapters 4 and 5, I used the hydrology model results as a basis for analyzing floodplain-scale biogeochemical patterns within the Nyack Floodplain. In Chapter 4, I measured dissolved organic carbon (DOC) concentration, bioavailable DOC (within laboratory assays), and optical properties of DOC in hyporheic well water sampled throughout the Nyack Floodplain during 10 sampling events in 2008 and 2009. I compare patterns of DOC concentration and quality to MTT (derived from the particle tracking model in Chapter 3) to determine the influence of hyporheic residence time on lability of DOC transported to downstream ecosystems. In Chapter 5, I developed a simulation model for oxygen and nitrate within the Nyack Floodplain and integrated the biogeochemical model with the detailed floodplain hydrogeomorphic model (Chapter 3). My primary goal was to determine whether simple biogeochemical models parameterized with flow path-scale data could explain variance in data observed across the whole floodplain (longitudinally, laterally, and vertically), river discharges, and seasons given a detailed representation of floodplain hydrology.

References

Alexander, R. B., P. J. Johnes, E. W. Boyer, and R. A. Smith. 2002. A comparison of models for estimating the riverine export of nitrogen from large watersheds. Biogeochemistry **57**:295-339.

Beaulieu, J.J. J.L. Tank, S.K. Hamilton, W.M. Wollheim, R.O. Hall Jr., P.J. Mulholland, B.J. Peterson, L.R. Ashkenas, L.W. Cooper, C.N. Dahm, W.K. Dodds, N.B. Grimm, S.L. Johnson, W.H. McDowell, G.C. Poole, H.M. Valett, C.P. Arango, M.J. Bernot, A.J. Burgin, C Crenshaw, A.M. Helton, L Johnson, J.M. O'Brien, J.D. Potter, R.W. Sheibley, D.J. Sobota, and S.M. Thomas. In Press. Nitrous oxide emission from denitrification in stream and river networks. Proceedings of the National Academy of Sciences of the United States of America.

Alexander, R. B., R. A. Smith, and G. E. Schwarz. 2000. Effect of stream channel size on the delivery of nitrogen to the Gulf of Mexico. Nature **403**:758-761.

Cole, J. J., Y. T. Prairie, N. F. Caraco, W. H. McDowell, L. J. Tranvik, R. G. Striegl, C. M. Duarte, P. Kortelainen, J. A. Downing, J. J. Middelburg, and J. Melack. 2007. Plumbing the global carbon cycle: Integrating inland waters into the terrestrial carbon budget. Ecosystems **10**:171-184.

Helton, A. M., G. C. Poole, J. L. Meyer, W. M. Wollheim, B. J. Peterson, P. J. Mulholland, E. S. Bernhardt, J. A. Stanford, C. Arango, L. R. Ashkenas, L. W. Cooper, W. K. Dodds, S. V. Gregory, R. O. Hall Jr, S. K. Hamilton, S. L. Johnson, W. H. McDowell, J. D. Potter, J. L. Tank, S. M. Thomas, H. M. Valett, J. R. Webster, and L. Zeglin. In Press. Thinking outside the channel: modeling nitrogen cycling in networked river ecosystems. Frontiers in Ecology and the Environment.

Jones, K. L., G. C. Poole, S. J. O'Daniel, L. A. K. Mertes, and J. A. Stanford. 2008. Surface hydrology of low-relief landscapes: Assessing surface water flow impedance using LIDAR-derived digital elevation models. Remote Sensing of Environment **112**:4148-4158.

McClain, M. E., E. W. Boyer, C. L. Dent, S. E. Gergel, N. B. Grimm, P. M. Groffman, S. C. Hart, J. W. Harvey, C. A. Johnston, E. Mayorga, W. H. McDowell, and G. Pinay. 2003. Biogeochemical hot spots and hot moments at the interface of terrestrial and aquatic ecosystems. Ecosystems **6**:301-312.

Mulholland, P. J., A. M. Helton, G. C. Poole, R. O. Hall, S. K. Hamilton, B. J. Peterson, J. L. Tank, L. R. Ashkenas, L. W. Cooper, C. N. Dahm, W. K. Dodds, S. E. G. Findlay, S. V. Gregory, N. B. Grimm, S. L. Johnson, W. H. McDowell, J. L. Meyer, H. M. Valett, J. R. Webster, C. P. Arango, J. J. Beaulieu, M. J. Bernot, A. J. Burgin, C. L. Crenshaw, L. T. Johnson, B. R. Niederlehner, J. M. O'Brien, J. D. Potter, R. W. Sheibley, D. J. Sobota, and S. M. Thomas. 2008. Stream denitrification across biomes and its response to anthropogenic nitrate loading. Nature **452**:202-U246.

Poole, G. C., J. A. Stanford, S. W. Running, C. A. Frissell, W. W. Woessner, and B. K. Ellis. 2004. A patch hierarchy approach to modeling surface and subsurface hydrology in complex flood-plain environments. Earth Surface Processes and Landforms **29**:1259-1274.

Seitzinger, S. P., R. V. Styles, E. W. Boyer, R. B. Alexander, and G. Billen. 2002. Nitrogen retention in rivers: model development and application to watersheds in the northeastern U.S.A. Biogeochemistry **57**:199-237.

Smith, R. A., G. E. Schwarz, and R. B. Alexander. 1997. Regional interpretation of water-quality monitoring data. Water Resources Research **33**:2781-2798.

Wollheim, W. M., B. J. Peterson, S. M. Thomas, C. H. Hopkinson, and C. J. Vorosmarty. 2008. Dynamics of N removal over annual time periods in a suburban river network. Journal of Geophysical Research-Biogeosciences **113**.

Wollheim, W. M., C. J. Vorosmarty, B. J. Peterson, S. P. Seitzinger, and C. S. Hopkinson. 2006. Relationship between river size and nutrient removal. Geophysical Research Letters **33**:doi:10.1029/2006GL025845.

CHAPTER 2

THINKING OUTSIDE THE CHANNEL: MODELING NITROGEN CYCLING IN NETWORKED RIVER ECOSYSTEMS[1]

---

[1]Ashley M Helton, Geoffrey C Poole, Judy L Meyer, Wilfred M Wollheim, Bruce J Peterson, Patrick J Mulholland, Emily S Bernhardt, Jack A Stanford, Clay Arango, Linda R Ashkenas, Lee W Cooper, Walter K Dodds, Stanley V Gregory, Robert O Hall Jr, Stephen K Hamilton, Sherri L Johnson, William H McDowell, Jody D Potter, Jennifer L Tank, Suzanne M Thomas, H Maurice Valett, Jackson R Webster, and Lydia Zeglin. In Press. *Frontiers in Ecology and the Environment*.

Abstract

Agricultural and urban development alters nitrogen and other biogeochemical cycles in rivers worldwide. Because such biogeochemical processes cannot be measured empirically across whole river networks, simulation models are critical tools for understanding river-network biogeochemistry. However, limitations inherent in current models restrict our ability to simulate biogeochemical dynamics among diverse river networks. We illustrate these limitations using a river-network model to scale up *in situ* measures of nitrogen cycling in eight catchments spanning various geophysical and land-use conditions. Our model results provide evidence that catchment characteristics typically excluded from models may control river-network biogeochemistry. Based on our findings, we identify important components of a revised strategy for simulating biogeochemical dynamics in river networks, including approaches to modeling terrestrial–aquatic linkages, hydrologic exchanges between the channel, floodplain/riparian complex, and subsurface waters, and interactions between coupled biogeochemical cycles.

Introduction

Rivers receive, transport, and process nutrients, contaminants, and other natural and human-derived materials from the landscape and deliver these constituents to downstream waters. Because river networks link terrestrial landscapes to lakes and oceans, perturbations to river ecosystems can influence biogeochemical cycling at local, regional, and global scales. Select human activities, such as fertilizing agricultural lands and burning fossil fuels, have delivered excess nitrogen to rivers, thereby increasing nitrogen export to coastal areas and exacerbating hypoxic zones in nearshore seas worldwide (Diaz and Rosenberg 2008). However, as nitrogen is transported downstream, some may be lost to the atmosphere via denitrification,

the microbially mediated reduction of nitrate (NO_3^-) to nitrogen gas. Mass-balance accounting across broad regions suggests that denitrification losses substantially reduce riverine nitrogen loads to the ocean (Seitzinger et al. 2006).

Recent research has focused on modeling nitrogen dynamics in river networks, partly because biogeochemical processes cannot be measured contiguously across river networks. Initial applications of riverine nitrogen models focused on predicting nitrogen export from large watersheds (reviewed by Alexander et al. 2002). Additional applications have included efforts to model biogeochemical processes that reduce downstream nitrogen transport, such as denitrification (Alexander et al. 2000; Seitzinger et al. 2002; Darracq and Destouni 2005; Mulholland et al. 2008; Alexander et al. 2009). Unfortunately, difficulty in accounting for spatial and temporal variations in the biogeochemical controls of denitrification (Boyer et al. 2006) has created major uncertainties in simulation results, which hamper forecasting of river-network biogeochemistry under future scenarios of climate disruptions, urbanization, and human population growth.

Here, we evaluate common modeling approaches and assumptions about river and catchment hydrogeomorphology and biogeochemistry, by scaling *in situ* denitrification measurements from headwater streams (Mulholland et al. 2008) to river networks in eight different catchments (Table 2.1). Using the model results, we identify additional dynamics and catchment characteristics that are important for understanding biogeochemical cycling, illustrate strategies for improving simulation of river biogeochemistry, and prioritize steps for future model development.

A river network modeling experiment

We conducted simulation experiments using a model of river-network NO_3^- dynamics described by Mulholland et al. (2008) to systematically evaluate assumptions about river and catchment hydrogeomorphology and biogeochemistry (Appendix A; Figure 2.1). The model incorporates equations and assumptions commonly used in river network models to represent downstream changes in channel morphology, hydrology, and biogeochemistry (Appendix A), as well as a recently documented reduction in streambed denitrification efficiency with increasing NO_3^- concentration (Mulholland et al. 2008).

We treated the model and its assumptions as a hypothesis describing downstream transport and denitrification of NO_3^- in river networks and explicitly tested this hypothesis by evaluating model performance in eight small river networks (Table 2.1). We conducted sampling of NO_3^- concentrations (the model response variable), channel width, and discharge at locations across each network (Figure 2.2) during low-flow conditions for 2 years. Observed patterns of downstream changes in width and discharge, combined with network topology from 1:24 000 US Geological Survey (USGS) maps, served to parameterize network morphology and hydrology. We determined model parameters for denitrification from *in situ* measurements of whole stream-reach denitrification replicated across nine headwater (1st- to 3rd- order) streams in or near each catchment (Mulholland et al. 2008; Appendix B).

We used inverse modeling to estimate the spatial pattern of NO_3^- loading rates to streams by applying a model-independent parameter optimizer (ParameterESTimation, version 10.1, SS Papadopoulos and Associates Inc). We estimated NO_3^- loading rates necessary for the model to exactly reproduce observed patterns of NO_3^- concentrations across each network. This approach allowed us to calculate spatial variation in NO_3^- loading rates across each catchment (Figure

2.2), assuming that our hypothesized representation of nitrogen cycling (Appendix A) was correct. Thus we were able to falsify our hypothesis (i.e., reject the model) anywhere that estimated loading patterns were clearly unrealistic. To hedge against rejecting a reasonable representation of river-network biogeochemistry (e.g., rejecting the model because of the possibility of sampling error or localized dynamics atypical of conditions across the larger catchment), we rejected the model only when >10% of loading estimates for a catchment fell outside of a realistic range (0 to 6.96 kg km^{-2} d^{-1}, the highest loading estimate from a literature review of 140 catchments; Appendix C).

On the basis of these criteria, we accepted the model in only two of the eight catchments: the Little Tennessee River, North Carolina, and Mill Creek, Kansas (Figure 2.2). Thus, we conclude that aspects of these two river networks are largely consistent with model assumptions, including: (1) catchment topography drives water and NO_3^- accumulation; (2) channel width increases in proportion to discharge; (3) streambed denitrification is the primary mechanism of nitrogen removal; and (4) NO_3^- concentration is the primary determinant of streambed denitrification rate. In the remaining six catchments, we used model results, catchment characteristics, and findings from published research to identify deviations between model assumptions and catchment dynamics as potential sources of model failure. This information highlights important shortcomings in existing approaches to simulating river-network biogeochemistry and provides a basis for prioritizing needs for future model improvements.

Model assumptions versus catchment conditions

Our assessment suggests that model errors likely result from important deviations between catchment conditions and commonly applied model assumptions, including assumptions

that: (1) oversimplify catchment hydrology; (2) oversimplify river-network hydrogeomorphology; (3) incorporate unidirectional uptake of nitrogen rather than cycling in the context of other elements (i.e., stoichiometric constraints); and (4) focus on base-flow or annual mean conditions, ignoring the ecological relevance of seasonal cycles and temporal dynamics.

Catchment hydrology and nitrogen delivery to streams

Five of the modeled catchments provide examples of the influence of catchment hydrology on river-network biogeochemistry. In the Tualatin River, Oregon (13% unrealistic loading rates; Figure 2.2), two wastewater treatment facilities discharge 60 million gallons (over 227 million L) per day of treated wastewater into the river (Clean Water Services unpublished data), and agricultural water withdrawals occur throughout the network (Oregon Water Resources Department, www.wrd.state.or.us). When we reparameterized our model to incorporate the spatial arrangement of nitrogen and water delivery from these point-source inputs, unrealistic loading estimates were nearly eliminated from the model results (reduced from 13% to 3%).

The Río Piedras, Puerto Rico, Little Rabbit River, Michigan, and Flat Creek, Wyoming, catchments had high percentages of unrealistic loading rates (23%, 27%, and 24%, respectively; Figure 2.2). Most land in the Little Rabbit River catchment is agricultural (72% of catchment area; Table 2.1), with numerous high-density animal operations (USDA 2002) and extensive tile drainage systems (e.g., Figure 2.3a). The Río Piedras catchment has 42% urban land cover (Table 2.1) and contains many straight-pipe sewage lines from residential buildings to streams (e.g., Figure 2.3b). Water withdrawals from Flat Creek reduce flow substantially (e.g., to dryness; Figure 2.3c) in its headwaters, before water is added downstream by both a diversion

from Gros Ventre River and spring flows. In these three catchments, anthropogenic delivery systems (e.g., tile drains, sewers, irrigation systems), rather than catchment topography, dominate patterns of water and nitrogen delivery to streams, thus violating important model assumptions (Appendix A).

The case of the Rio Grande, New Mexico, is even more extreme. Patterns of base flow in the system are so completely dominated by dams, headgates (e.g., Figure 2.3d), and other flow regulation structures that no semblance of a convergent flow network remains along the river corridor. The hydrology of the river deviates so far from the underlying hydrologic basis of our model (i.e., topographically driven flow accumulation) that we were unable to apply our model to the system (Figure 2.2).

These five catchments illustrate the importance of incorporating the spatial patterns of water and nitrogen delivery to river networks into models. Indeed, previous modeling work has shown that accounting for the spatial arrangement of nitrogen inputs to rivers can improve model estimates of nitrogen export (Alexander et al. 2002), and spatial and temporal heterogeneity in water and nitrogen delivery increases uncertainty in modeled nitrogen export (Lindgren and Destouni 2004). Despite the need to incorporate spatiotemporal patterns of nitrogen delivery, many river-network models rely on a mass balance or a statistical approach to estimate nitrogen sources, resulting in steady-state mean annual estimates of nitrogen delivery to rivers. Such model applications are useful and appropriate for scaling up annual catchment nitrogen exports, based on data from distributed monitoring stations. However, more realistic representations of spatiotemporal variation in water and nitrogen delivery will be necessary for imperatives such as forecasting river biogeochemical responses to continued human population growth coupled with climate change.

River hydrogeomorphology

Both the Ipswich River, Massachusetts, and Flat Creek, Wyoming, catchments provide intriguing examples of hydrogeomorphic controls on river-network biogeochemistry. The Ipswich River has extensive water withdrawals for urban use in its headwaters (Zarriello and Ries 2000) and it flows through numerous wetland complexes, which comprise 20% of catchment land cover (e.g., Figure 2.4a). The Flat Creek network, in addition to hydrologic alteration (described above), has a large wetland (~2.3 km^2) along the main stem of Flat Creek, and high rates of exchange between the channel and an extensive hyporheic zone (the area directly beneath the channel and floodplain where surface and subsurface waters are freely exchanged) typical of western US alluvial streams (e.g., Figure 2.4b). In both catchments, our analysis yielded large percentages of negative loading estimates (Figure 2.2), indicating that our model underpredicts nitrogen removal in many reaches of each network.

Incorporating headwater withdrawals from the Ipswich River into the model did not reduce the percentage of unrealistic loading estimates. However, loading estimates were negatively correlated with the fraction of stream length intersecting wetlands (Appendix D), suggesting that wetlands are an important nitrogen sink not represented by the model. In Flat Creek, biotic removal of NO_3^- in the hyporheic zone (sensu Triska et al. 1989; Dahm et al. 1998; Hill et al. 1998; Dent et al. 2001) probably creates an NO_3^- sink that is not addressed by the model and therefore is a potential cause of the estimated negative loading rates.

The Ipswich River and Flat Creek networks illustrate the importance of considering patterns of hydrologic connections among river channels and adjacent wetlands, riparian corridors, floodplains, and hyporheic zones (Figure 2.5). As flow paths from different river ecosystem components converge throughout a river network, they create important spatial areas

and times of biogeochemical reactions (e.g., McClain et al. 2003; Hall et al. 2009) that vary in magnitude and frequency along stream courses. The potential importance of small lakes (Harrison et al. 2009), floodplains (within the Ipswich River catchment; Wollheim et al. 2008), and hyporheic zones (Thouvenot et al. 2007) on river-network nitrogen cycling has been acknowledged in some modeling studies. However, apart from reservoirs (e.g., Seitzinger et al. 2002; Bosch 2008), the influence of non-channel hydrogeomorphology has not been incorporated into river-network biogeochemical models, including our own (Appendix A).

Associated simplifying assumptions mean that such models do not represent natural mechanisms of nitrogen retention or the effects of common perturbations that disrupt them. For instance, streams with well-connected, intact riparian zones/floodplains may both denitrify and store nitrogen in vegetation and sediments for long periods, reducing and delaying downstream transport. Yet agricultural and urban development in stream corridors, stream channel engineering, and water abstraction tend to sever hydrologic connections between channel and non-channel components of streams (Cardenas and Wilson 2004; Kondolf et al. 2006), leaving the primary location of nitrogen uptake and storage as the channelized streambed, from which carbon and nutrients are easily remobilized and transported downstream (e.g., Noe and Hupp 2005). These critical changes in riverine biogeochemical processing cannot be adequately investigated by models that consider only channel water and the streambed as the hydrogeomorphic basis of stream ecosystems.

Nitrogen cycling and stoichiometry

Consistent with other models of river-network nitrogen dynamics (Boyer et al. 2006; Wollheim et al. 2006), our model (Appendix A) assumes that denitrification is the primary

nitrogen removal pathway and views the nitrogen cycle as a one-way flux of nitrogen from channel water (Figure 2.5). In our parameterization dataset (Mulholland et al. 2008), "direct" denitrification accounted for a wide percent of total NO_3^- taken up by biota (0.05–100%; median 16%). However, in most streams, NO_3^- assimilation into biomass was the largest removal flux, and assimilated nitrogen may either be stored temporarily and re-released to the water column as inorganic or organic nitrogen, or removed permanently via coupled nitrification–denitrification (e.g., Whalen et al. 2008) or other microbial pathways (e.g., reviewed by Burgin and Hamilton 2007; Figure 2.5). Unfortunately, the field methods (Mulholland et al. 2008) used to parameterize our model (Appendix A) quantify neither the subsequent cycling nor the ultimate fate of the nitrogen removed from the water column by assimilation. Furthermore, our parameterization dataset is based on denitrification measurements from headwater (1st- to 3rd-order) streams. Measuring the role of large rivers in biogeochemical cycling (e.g., Tank et al. 2008) will provide improved empirical estimates of denitrification throughout river networks, allowing us to parameterize and verify models. Coupled field and modeling efforts that attempt to iteratively investigate and simulate nitrogen storage, cycling, and mass balance in streams and rivers would further accelerate understanding of spatiotemporal patterns of nitrogen cycling within, and export from, river networks.

Our model also incorporates a decline in denitrification efficiency (υ_{fden}) with increasing NO_3^- concentration (Mulholland et al. 2008; Böhlke et al. 2009; Appendix A). The relationship is especially apparent when data from the eight catchments are combined (Mulholland et al. 2008). Yet the strength of the relationship varies markedly when considered for each of the eight catchments individually (Appendix B), suggesting that NO_3^- concentration was a primary driver of υ_{fden} in some study catchments (e.g., Little Tennessee River, North Carolina; $r^2 = 0.72$), but

not in others (e.g., Río Piedras, Puerto Rico; $r^2 = 0.01$). Stoichiometric relationships between nitrogen and other elements (e.g., carbon, Bernhardt and Likens 2002; phosphorus, Cross et al. 2005; sulfur, Burgin and Hamilton 2008) or whole-stream respiration rates (Mulholland et al. 2008) may also drive nitrogen cycling rates. However, such dynamics cannot be addressed by river-network models that track nitrogen dynamics in isolation and use statistical representations of nitrogen uptake. More mechanistic models that consider microbial biomass and respiration, along with coupling of the nitrogen cycle to other elemental cycles (i.e., an ecological stoichiometry approach), would improve the heuristic value and predictive power of simulations (see also Boyer et al. 2006), yielding more robust approaches for scaling biogeochemical cycles in river networks.

Temporal dynamics

Most river-network models, including our own (Appendix A), simulate steady-state (e.g., base-flow or mean annual) hydrologic conditions (but see Wollheim et al. 2008; Böhlke et al. 2009). Steady-state hydrologic assumptions prevent simulation of dynamics that may drive most biogeochemical processing or transport. For instance, in river channels, the fraction of catchment nitrogen exported downstream is highest during peak flows, when streambed biotic nitrogen removal efficiency is lowest (Royer et al. 2004; Alexander et al. 2009). In contrast, transient hydrologic connections with non-channel ecosystem components may buffer excess nitrogen export during high flows (Richardson et al. 2004; Hall et al. 2009). For example, transient hydrologic simulation of the Ipswich River network explored how variations in daily runoff influenced predicted denitrification patterns (Wollheim et al. 2008). The model appeared to underpredict nitrogen removal during periods of peak flow in the river network, suggesting that

nitrogen may be removed by off-channel components of the stream ecosystem (e.g., when floodwaters spill onto floodplains or into adjacent wetlands). Indeed, storm pulses expand hydrologic connections among river ecosystem components (Stanley et al. 1997), wetting ephemeral channels and floodplains, and thereby initiating contact between different suites of solutes and activating biogeochemical processes in areas adjacent to river channels (Valett et al. 2005). Developing models that can both incorporate and scale dynamic hydrology across river networks presents a formidable challenge yet is a critical necessity for improving models of river network biogeochemistry.

The way forward

Four fundamental and widely applied assumptions caused our model to fail in six out of eight catchments. Our model: (1) assumes that catchment topography drives water and nitrogen accumulation in river networks; (2) represents streams as channels, ignoring the floodplain, wetland, riparian, and hyporheic components of streams; (3) simulates nitrogen uptake in isolation rather than nitrogen cycling in the context of ecological stoichiometry; and (4) assumes a steady-state discharge regime. We believe, therefore, that overcoming these assumptions will extend the applicability and predictive accuracy of river-network biogeochemical models across a range of catchments. On the basis of these findings, we recommend several specific strategies to help extend and improve current modeling approaches.

Integration of river-network and catchment ecohydrologic models

Hydrologic and physical properties of catchments strongly control nitrogen delivery to rivers, but river-network models do not normally simulate hydrologic nitrogen delivery to rivers.

Ecohydrologic models (reviewed by Boyer et al. 2006; Kulkarni et al. 2008) simulate hydrologically explicit hillslope nitrogen dynamics across catchments, even predicting observed patterns and timing of water and nutrient delivery to streams (Band et al. 2001). Such catchment ecohydrologic models could be linked to river-network models, to provide spatially explicit and temporally dynamic estimates of water and nutrient delivery to streams – an important first step for understanding biogeochemical dynamics at the terrestrial–aquatic interface.

Catchment ecohydrologic models, however, still typically rely on topography as the primary determinant of catchment water and solute routing. Yet existing modeling techniques that accurately represent the hydrologic dynamics of human-dominated catchments generally require detailed and difficult-to-obtain information, such as patterns of tile drainage in agricultural lands or sewer system maps in urbanized settings (e.g., Hsu et al. 2000; Northcott et al. 2002). Thus, improved simulation of river-network biogeochemistry may also arise from the development of new, less data-intensive techniques that could quantify water and nutrient routing dynamics in urban and agricultural catchments without requiring detailed maps and descriptions of sewer or drain systems.

Modeling stoichiometric controls on biogeochemical cycles

River-network nitrogen models tend to simulate one-way removal of nitrogen. Such an approach has been quite successful when used to quantify annual nitrogen budgets of large catchments (Alexander et al. 2002). However, the nitrogen cycle is driven by multiple nitrogen pools and fluxes (Figure 2.5) and its relationships with other elemental cycles (e.g., carbon and oxygen). A more mechanistic representation of nitrogen dynamics might therefore help to

explain complex patterns of biogeochemical dynamics within river networks, and improve forecasts of biogeochemical responses to land-use or climate-change perturbations.

Biogeochemical cycling depends on the changing availability of various electron donors and acceptors, given the thermodynamically constrained metabolism of microorganisms (Hedin et al. 1998; Fisher et al. 2004). Thus, stoichiometric constraints on microbial metabolism link multiple elemental cycles in complex yet predictable ways. Indeed, microbial ecology models can predict carbon and nitrogen uptake, assimilation, and loss, based on the assumption that the aggregate metabolic activity of the microbial assemblage present will respond to oxygen, carbon, and nitrogen availability in such a way as to maximize overall growth (e.g., Vallino et al. 1996; Figure 2.6a). Such an approach, based on the first principles of thermodynamics (i.e., free energy yield from metabolic pathways), provides an avenue for addressing shifting drivers of the nitrogen cycle across systems. This comprehensive biogeochemical approach also highlights important contemporary research challenges, including: quantifying the fraction of nitrogen forms that make up the total nitrogen pool, understanding the interaction of nitrogen with other elements, and understanding the role and shifting frequency of alternate nitrogen removal pathways (e.g., coupled nitrification–denitrification).

Using river hydrogeomorphology to scale biogeochemistry

Although river-network models typically incorporate general trends of channel geometry and in-channel hydrology (e.g., Appendix A), they often disregard geomorphic variation in, and hydrologic connections between, the channel, riparian zone/floodplain, and hyporheic zone (Figure 2.5), even though such connections are key to understanding river biogeochemical dynamics (McClain et al. 2003; Groffman et al. 2009). Thus, to simulate river-network

biogeochemistry, a reliable approach for scaling biogeochemistry to flow paths is needed. For example, we have begun to integrate the aforementioned stoichiometric biogeochemical model (Figure 2.6a) into a spatially explicit and temporally dynamic model of hydrologic flow paths (Poole et al. 2006; Figure 2.6b). Initial results suggest the combined models yield realistic patterns of nitrogen (Figure 2.6c), oxygen, and organic carbon (Figure 2.6d), as well as microbial biomass and respiration (Figure 2.6e), along hyporheic flow paths. By using the hydrologic model to simulate floodplain surface and subsurface flow paths (Figure 2.7), we will be able to develop realistic, multi-element models of whole floodplain biogeochemistry.

Still, direct application of a spatially explicit, flow-path-centric approach (Figure 2.6) to an entire river network is not feasible because of the intensive data needs for parameterization and verification, along with the computational requirements needed to execute such a model. We believe, however, that river-network models incorporating both hydrogeomorphic and stoichiometric controls on biogeochemistry could be developed within the next decade. One promising approach would pair stream biogeochemical models with contemporary efforts by hydrologists to use theoretical approaches (Cardenas 2008) and simulation modeling (Deng and Jung 2009) as a means of scaling up the net effect of localized, off-channel hydrologic processes, such as hyporheic water exchange. Thus, the next generation of models might emerge from coupling network-scale hydrologic residence-time distributions with a robust understanding of flow-path biogeochemistry. Maturation of emerging geospatial technologies, such as LIDAR (Light Detection and Ranging; Jones et al. 2007, 2008) and SRTM (Shuttle Radar Topography Mission; Farr et al. 2007), will ultimately improve the practicality of quantifying hydrogeomorphic variation (sensu Wörman et al. 2006) across river networks to parameterize associated models of river network hydrologic residence time distributions.

Conclusions

We recommend an admittedly ambitious roadmap for developing the next generation of river-network models. Rather than attempting to implement all of our recommendations simultaneously, which may lead to overly cumbersome models that are difficult to parameterize and run, incremental improvements coupled with experimentation is more likely to succeed. We have outlined three specific paths to improve river-network biogeochemistry models, which can be accomplished incrementally and independently of one another. First, we propose using ecohydrologic models to improve estimated spatiotemporal patterns of water and nutrient delivery to river networks. Human alterations will complicate these patterns, and methods to scale their effects – for example, effects of storm-sewer and tile drainage systems on nutrient and water routing to whole river networks – will be essential, particularly as human impacts become increasingly prevalent. Second, we propose incorporating multiple elemental cycles and ecological stoichiometry into river-network models. Our initial approach (Figure 2.6) integrates first principles of thermodynamics (i.e., free energy yield from metabolic pathways) with governing equations for surface and groundwater fluxes, and should therefore be widely applicable. Maturation of such an approach, however, will require increased collaboration between empirical, simulation, remote sensing, geographical, and computer sciences to create, model, and understand datasets describing biogeochemical fluxes across an array of environmental conditions and scales. Finally, we propose integrating biogeochemical models and floodplain-scale hydrology models (e.g., Figure 2.7), which will provide important insights into the biogeochemical dynamics of multiple interacting flow paths within fluvial landscapes. The challenge will be to develop methods to scale these integrated biogeochemistry–hydrology models to whole river networks.

Developing models that can accurately represent hydrogeomorphic and biogeochemical dynamics across river networks will require the melding of concepts and approaches from both terrestrial and aquatic biogeochemical modeling, as well as hydrologic modeling and remote-sensing sciences. Application of these models will yield insights into the river-network biogeochemistry necessary for understanding carbon and nutrient cycling across a variety of fluvial landscapes and among diverse biomes. As anthropogenic activities, such as land-use conversion and fossil-fuel production, push ecosystems toward unprecedented states, a holistic and mechanistic approach to biogeochemical modeling of rivers will provide a valuable tool for forecasting the responses of biogeochemical cycles across river networks worldwide.

Acknowledgments

This research was supported by NSF (DEB-0111410). Additional support was provided by NSF for BJP and SMT (DEB-0614301), for WMW (OCE-9726921 and DEB-0614282), for WHM and JDP (DEB-0620919), for SKH (DEB-0423627), and by the Gordon and Betty Moore Foundation for AMH, GCP, ESB, and JAS, and by an EPA Star Fellowship for AMH. EPA has not officially endorsed this publication and the views expressed herein may not reflect the views of the EPA. We thank C Bennett for programming assistance and the Rosemond Lab Group at the University of Georgia for helpful comments on earlier versions of this manuscript.

References

Alexander RB, Böhlke JK, Boyer EW, *et al.* 2009. Dynamic modeling of nitrogen losses in river networks unravels the coupled effects of hydrological and biogeochemical processes. *Biogeochemistry* **93**: 91–116.

Alexander RB, Johnes PJ, Boyer EW, *et al.* 2002. A comparison of models for estimating the riverine export of nitrogen from large watersheds. *Biogeochemistry* **57**: 295–339.

Alexander RB, Smith RA, and Schwarz GE. 2000. Effect of stream channel size on the delivery of nitrogen to the Gulf of Mexico. *Nature* **403**: 758–61.

Band LE, Tague CL, Groffman P, *et al.* 2001. Forest ecosystem processes at the watershed scale: hydrological and ecological controls of nitrogen export. *Hydrol Process* **15**: 2013–28.

Bernhardt ES and Likens GE. 2002. Dissolved organic carbon enrichment alters nitrogen dynamics in a forest stream. *Ecology* **83**: 1689–1700.

Böhlke JK, Antweiler RC, Harvey JW, *et al.* 2009. Multi-scale measurements and modeling of denitrification in streams with varying flow and nitrate concentration in the upper Mississippi River basin, USA. *Biogeochemistry* **93**: 117–41.

Bosch NS. 2008. The influence of impoundments on riverine nutrient transport: an evaluation using the Soil and Water Assessment Tool. *J Hydrol* **355**: 131–37.

Boyer EW, Alexander RB, Parton WJ, *et al.* 2006. Modeling denitrification in terrestrial and aquatic ecosystems at regional scales. *Ecol Appl* **16**: 2123–42.

Burgin AJ and Hamilton SK. 2007. Have we overemphasized the role of denitrification in aquatic ecosystems? A review of nitrate removal pathways. *Front Ecol Environ* **5**: 89–96.

Burgin AJ and Hamilton SK. 2008. NO_3^--driven SO_4^{2-} production in freshwater ecosystems: implications for N and S cycling. *Ecosystems* **11**: 908–22.

Cardenas MB. 2008. Surface water–groundwater interface geomorphology leads to scaling of residence times. *Geophys Res Lett* **35**: doi:10.1029/2008GL033753.

Cardenas MB and Wilson JL. 2004. Impact of heterogeneity, bed forms, and stream curvature on subchannel hyporheic exchange. *Water Resour Res* **40**: doi:10.1029/2004WR003008.

Cross WF, Benstead JP, Frost PC, *et al.* 2005. Ecological stoichiometry in freshwater benthic systems: recent progress and perspectives. *Freshwater Biol* **50**: 1895–912.

Dahm CN, Grimm NB, Marmonier P, *et al.* 1998. Nutrient dynamics at the interface between surface waters and groundwaters. *Freshwater Biol* **40**: 427–51.

Darracq A and Destouni G. 2005. In-stream nitrogen attenuation: model-aggregation effects and implications for coastal nitrogen impacts. *Environ Sci Technol* **39**: 3716–22.

Deng ZQ and Jung HS. 2009. Variable residence time-based model for solute transport in streams. *Water Resour Res* **45**: doi:10.1029/2008WR007000.

Dent CL, Grimm NB, and Fisher SG. 2001. Multiscale effects of surface–subsurface exchange on stream water nutrient concentrations. *J N Am Benthol Soc* **20**: 162–81.

Diaz RJ and Rosenberg R. 2008. Spreading dead zones and consequences for marine ecosystems. *Science* **321**: 926–29.

Farr TG, Rosen PA, Caro E, *et al.* 2007. The shuttle radar topography mission. *Rev Geophys* **45**: doi:10.1029/2005RG000183.

Fisher SG, Sponseller RA, and Heffernan JB. 2004. Horizons in stream biogeochemistry: flowpaths to progress. *Ecology* **85**: 2369–79.

Groffman PM, Butterbach-Bahl K, Fulweiler RW, *et al.* 2009. Challenges to incorporating spatially and temporally explicit phenomena (hotspots and hot moments) in denitrification models. *Biogeochemistry* **93**: 49–77.

Hall RO, Baker MA, Arp CD, and Koch BJ. 2009. Hydrologic control of nitrogen removal, storage, and export in a mountain stream. *Limnol Oceanogr* **54**: 2128–42.

Harrison JA, Maranger RJ, Alexander RB, *et al.* 2009. The regional and global significance of nitrogen removal in lakes and reservoirs. *Biogeochemistry* **93**: 143–57.

Hedin LO, von Fischer JC, Ostrom NE, *et al.* 1998. Thermodynamic constraints on nitrogen transformations and other biogeochemical processes at soil–stream interfaces. *Ecology* **79**: 684–703.

Hill AR, Labadia CF, and Sanmugadas K. 1998. Hyporheic zone hydrology and nitrogen dynamics in relation to the streambed topography of a N-rich stream. *Biogeochemistry* **42**: 285–310.

Hsu MH, Chen SH, and Chang TJ. 2000. Inundation simulation for urban drainage basin with storm sewer system. *J Hydrol* **234**: 21–37.

Jones AF, Brewer PA, Johnstone E, *et al.* 2007. High-resolution interpretative geomorphological mapping of river valley environments using airborne LiDAR data. *Earth Surf Proc Land* **32**: 1574–92.

Jones KL, Poole GC, O'Daniel SJ, *et al.* 2008. Surface hydrology of low-relief landscapes: assessing surface water flow impedance using LIDAR derived digital elevation models. *Remote Sens Environ* **112**: 4148–58.

Kondolf GM, Boulton AJ, O'Daniel S, *et al.* 2006. Process-based ecological river restoration: visualizing three-dimensional connectivity and dynamic vectors to recover lost linkages. *Ecol Soc* **11**: 5.

Kulkarni MV, Groffman PM, and Yavitt JB. 2008. Solving the global nitrogen problem: it's a gas! *Front Ecol Environ* **6**: 199–206.

Leopold LB and Maddock T. 1953. The hydraulic geometry of streams and some physiographic implications. US Geological Survey Professional Paper 252. United States Government Printing Office, Washington DC.

Lindgren GA and Destouni G. 2004. Nitrogen loss rates in streams: scale-dependence and up-scaling methodology. *Geophys Res Lett* **31**: doi:10.1029/2004GL019996.

McClain ME, Boyer EW, Dent CL, *et al.* 2003. Biogeochemical hot spots and hot moments at the interface of terrestrial and aquatic ecosystems. *Ecosystems* **6**: 301–12.

Mulholland PJ, Helton AM, Poole GC, *et al.* 2008. Stream denitrification across biomes and its response to anthropogenic nitrate loading. *Nature* **452**: 202–46.

Noe GB and Hupp CR. 2005. Carbon, nitrogen, and phosphorus accumulation in floodplains of Atlantic Coastal Plain rivers, USA. *Ecol Appl* **15**: 1178–90.

Northcott WJ, Cooke RA, Walker SE, *et al.* 2002. Modeling flow on a tile-drained watershed using a GIS-integrated DRAINMOD. *T ASAE* **45**: 1405–13.

Poole GC, Stanford JA, Running SW, *et al.* 2006. Multiscale geomorphic drivers of groundwater flow paths: subsurface hydrologic dynamics and hyporheic habitat diversity. *J N Am Benthol Soc* **25**: 288–303.

Poole GC, O'Daniel SJ, Jones KL, *et al.* 2008. Hydrologic spiralling: the role of multiple interactive flow paths in stream ecosystems. *River Res Appl* **24**: 1018–31.

Richardson WB, Strauss EA, Bartsch LA, *et al.* 2004. Denitrification in the Upper Mississippi River: rates, controls, and contribution to nitrate flux. *Can J Fish Aquat Sci* **61**: 1102–12.

Royer TV, Tank JL, and David MB. 2004. Transport and fate of nitrate in headwater agricultural streams in Illinois. *J Environ Qual* **33**: 1296–304.

Seitzinger SP, Harrison JA, Böhlke JK, *et al.* 2006. Denitrification across landscapes and waterscapes: a synthesis. *Ecol Appl* **16**: 2064–90.

Seitzinger SP, Styles RV, Boyer EW, *et al.* 2002. Nitrogen retention in rivers: model development and application to watersheds in the northeastern USA. *Biogeochemistry* **57**: 199–237.

Stanley EH, Fisher SG, and Grimm NB. 1997. Ecosystem expansion and contraction in streams. *BioScience* **47**: 427–35.

Tank JL, Rosi-Marshall EJ, Baker MA, and Hall RO. 2008. Are rivers just big streams? A pulse method to quantify nitrogen demand in a large river. *Ecology* **89**: 2935–45.

Thouvenot M, Billen G, and Garnier J. 2007. Modelling nutrient exchange at the sediment–water interface of river systems. *J Hydrol* **341**: 55–78.

Triska FJ, Kennedy VC, Avanzino RJ, *et al.* 1989. Retention and transport of nutrients in a third-order stream in northwestern California: hyporheic processes. *Ecology* **70**: 1893–1905.

USDA (US Department of Agriculture). 2002. Census of agriculture. National Agricultural Statistics Service. Washington, DC: USDA. www.nass.usda.gov/Census_of_Agriculture/index.asp. Viewed 13 Dec 2008.

Valett HM, Baker MA, Morrice JA, *et al.* 2005. Biogeochemical and metabolic responses to the flood pulse in a semiarid floodplain. *Ecology* **86**: 220–34.

Vallino JJ, Hopkinson CS, and Hobbie JE. 1996. Modeling bacterial utilization of dissolved organic matter: optimization replaces monod growth kinetics. *Limnol Oceanogr* **41**: 1591–1609.

Whalen SC, Alperin MJ, Nie Y, *et al.* 2008. Denitrification in the mainstem Neuse River and tributaries, USA. *Fund Appl Limnol* **171**: 249–61.

Wollheim WM, Peterson BJ, Thomas SM, *et al.* 2008. Dynamics of N removal over annual time periods in a suburban river network. *J Geophys Res-Biogeo* **113**: G03038.

Wollheim WM, Vorosmarty CJ, Peterson BJ, *et al.* 2006. Relationship between river size and nutrient removal. *Geophys Res Lett* **33**: doi:10.1029/2006GL025845.

Wörman A, Packman AI, Marklund L, *et al*. 2006. Exact three-dimensional spectral solution to surface–groundwater interactions with arbitrary surface topography. *Geophys Res Lett* **33**: doi:10.1029/2006GL025747.

Zarriello PJ and Ries KG. 2000. A precipitation-runoff model for the analysis of the effects of water withdrawals on stream flow, Ipswich River Basin, Massachusetts. US Geological Survey Water-Resources Investigation Report 00-4029. US Geological Survey Information Services. Denver, CO.

Table 2.1 Descriptions of study catchments

Site location	*Biome*	*Basin area (km^2)*	*% Agriculture*	*% Urban*
Little Tennessee River, North Carolina (NC)	Warm temperate deciduous forest	361	10	7
Mill Creek, Kansas (KS)	Grassland	1008	16	3
Tualatin River, Oregon (OR)	Humid coniferous	1828	27	21
Flat Creek, Wyoming (WY)	Semiarid coniferous	400	0.4	2
Ipswich River, Massachusetts (MA)	Cool temperate deciduous forest	381	6	31
Little Rabbit River, Michigan (MI)	Cool temperate deciduous forest	126	72	9
Río Piedras, Puerto Rico (PR)	Moist evergreen tropical forest	40	27	42
Rio Grande, New Mexico (NM)	Arid grassland	40 780	0.7	1

Notes: Land-cover data are derived from the USGS 2001 National (US) Land Cover Dataset (http://seamless.usgs.gov).

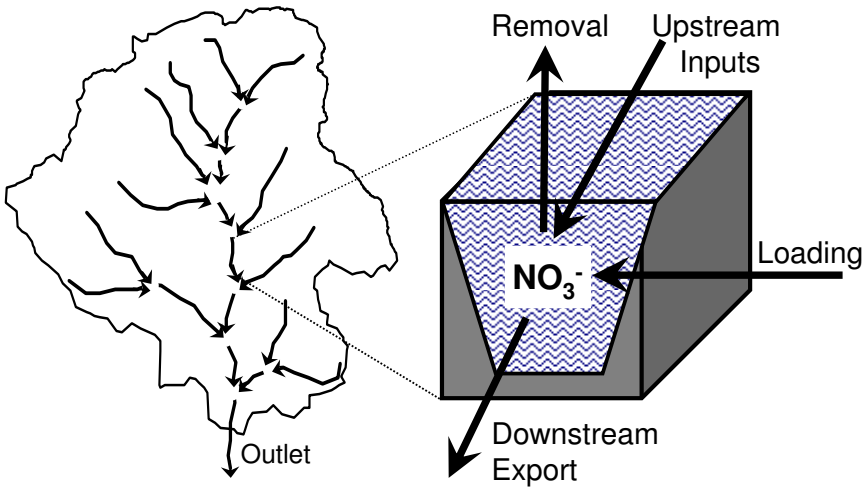

Figure 2.1. River-network model structure. Following the methods presented by Mulholland et al. (2008), river networks were divided into segments, defined as the length of stream between tributary junctions. Water and NO_3^- flux into (upstream inputs and loading from the terrestrial landscape) and out of (downstream export and removal via denitrification) each segment were modeled. Fluxes are described in Appendix A.

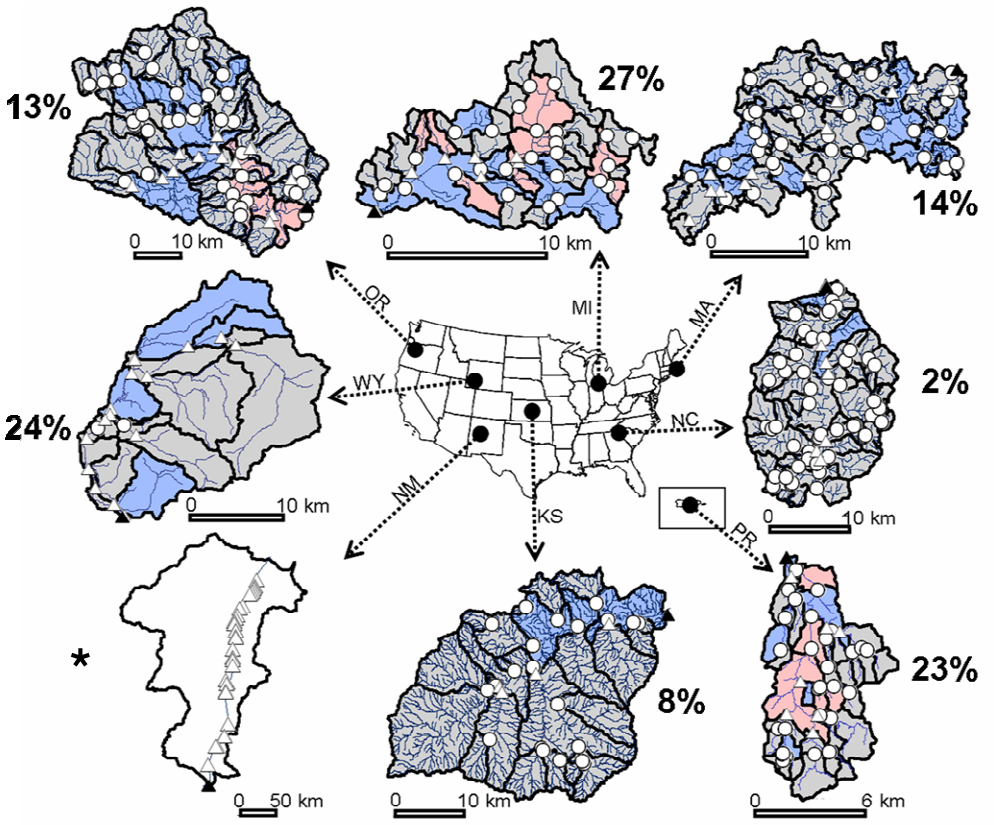

Figure 2.2. Maps of the eight modeled catchments, which include stream hydrography (blue lines), discharge sampling points (triangles; solid triangles indicate catchment outlet), NO_3^- sampling points (circles), and catchment contributing area (CCA) for each NO_3^- sampling point (black lines). Color of CCA represents average simulated loading estimates that are realistic (gray; between 0 and 6.96 kg km^{-2} d^{-1}), unrealistic (high = red; > 6.96 kg km^{-2} d^{-1} and low = blue; < 0 kg km^{-2} d^{-1}), or indeterminable given model assumptions (white; see text). The percent of CCAs with unrealistic modeled NO_3^- loading estimates is indicated for each catchment. *See text for discussion of NM river-flow issues.

Figure 2.3. Examples of anthropogenic alterations to hydrology and nitrogen delivery that deviate from assumptions within modeled catchments. (a) Agricultural tile drains, Rabbit River, MI, catchment. (b) Sanitary sewer overflow (left) and straight-pipe sewer discharge (right), Río Piedras, PR, catchment. (c) Alluvial stream reach irrigated to dryness, Flat Creek, WY, catchment; (d) Water abstraction, Isleta diversion, Rio Grande, NM.

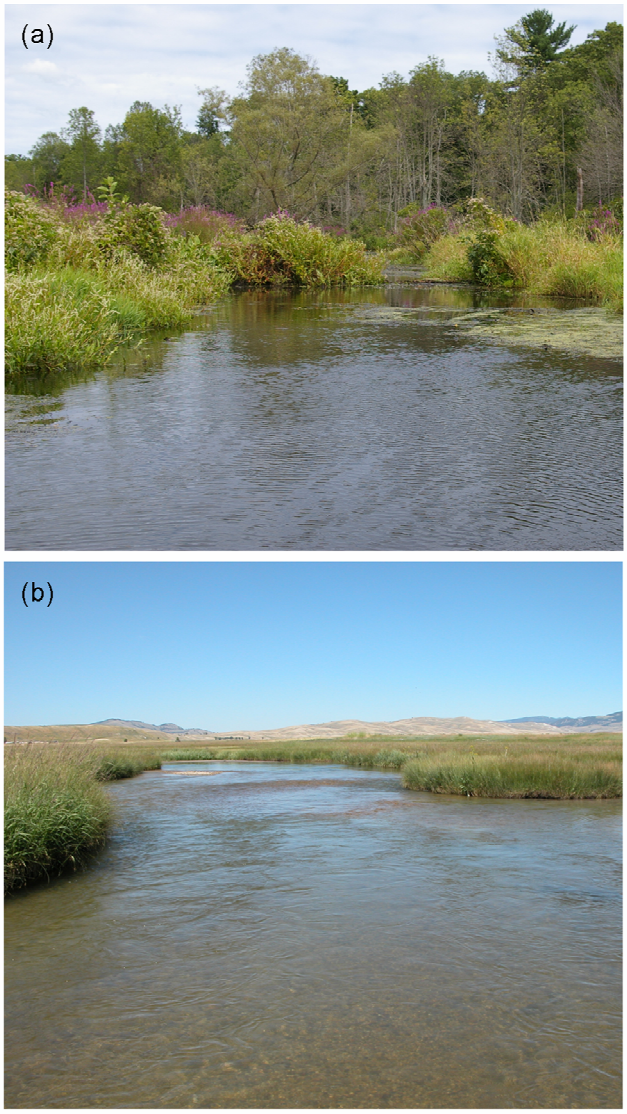

Figure 2.4. Examples of river hydrogeomorphology that deviate from assumptions within modeled catchments. (a) Riverine wetlands, Ipswich River, MA, catchment. (b) Spring-fed alluvial stream reach with high hyporheic exchange, Flat Creek, WY, catchment.

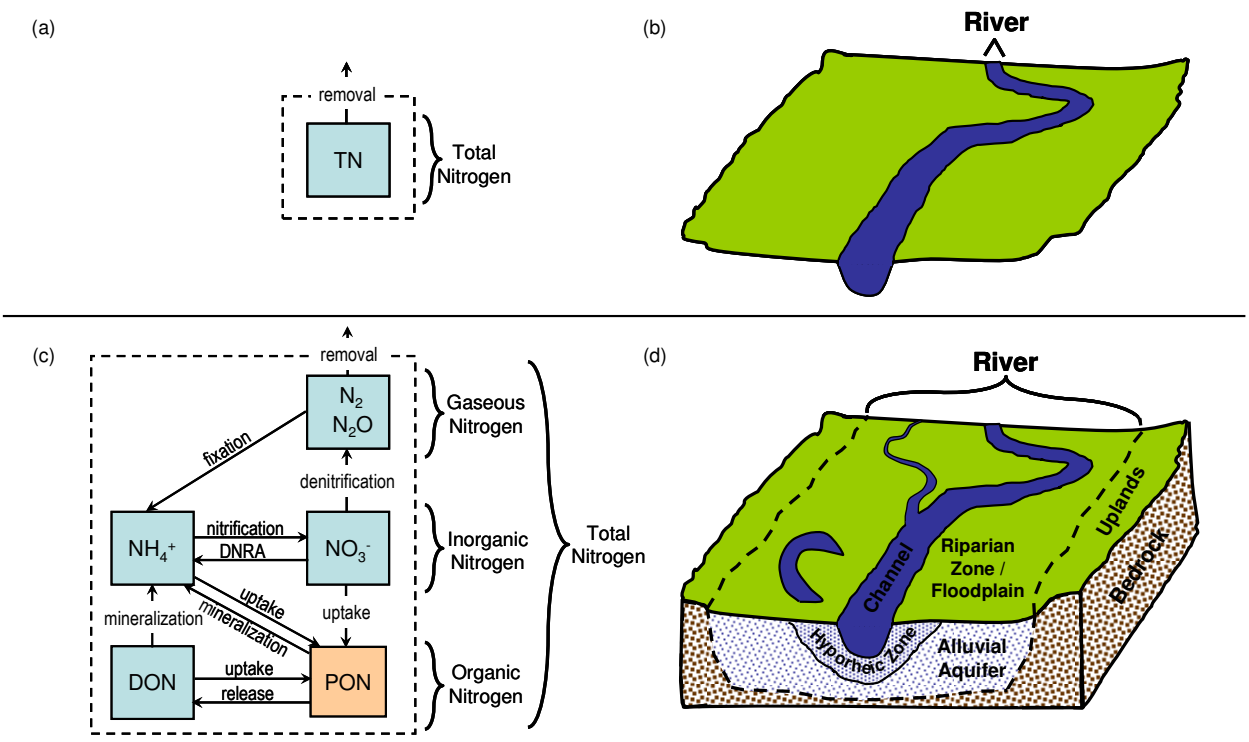

Figure 2.5 River-network models typically describe (a) one-way total nitrogen flux from (b) river channels. A more holistic conceptual model of nitrogen cycling in river ecosystems recognizes (c) multiple forms of nitrogen that undergo numerous transformations and (d) the role of non-channel river ecosystem components in nitrogen dynamics, including the hyporheic zone, alluvial aquifer, and floodplain/riparian complex. DON = dissolved organic nitrogen; PON = particulate organic nitrogen; NH_4^+ = ammonium; NO_3^- = nitrate; N_2 = dinitrogen gas; N_2O = nitrous oxide; DNRA = dissimilatory nitrate reduction to ammonium.

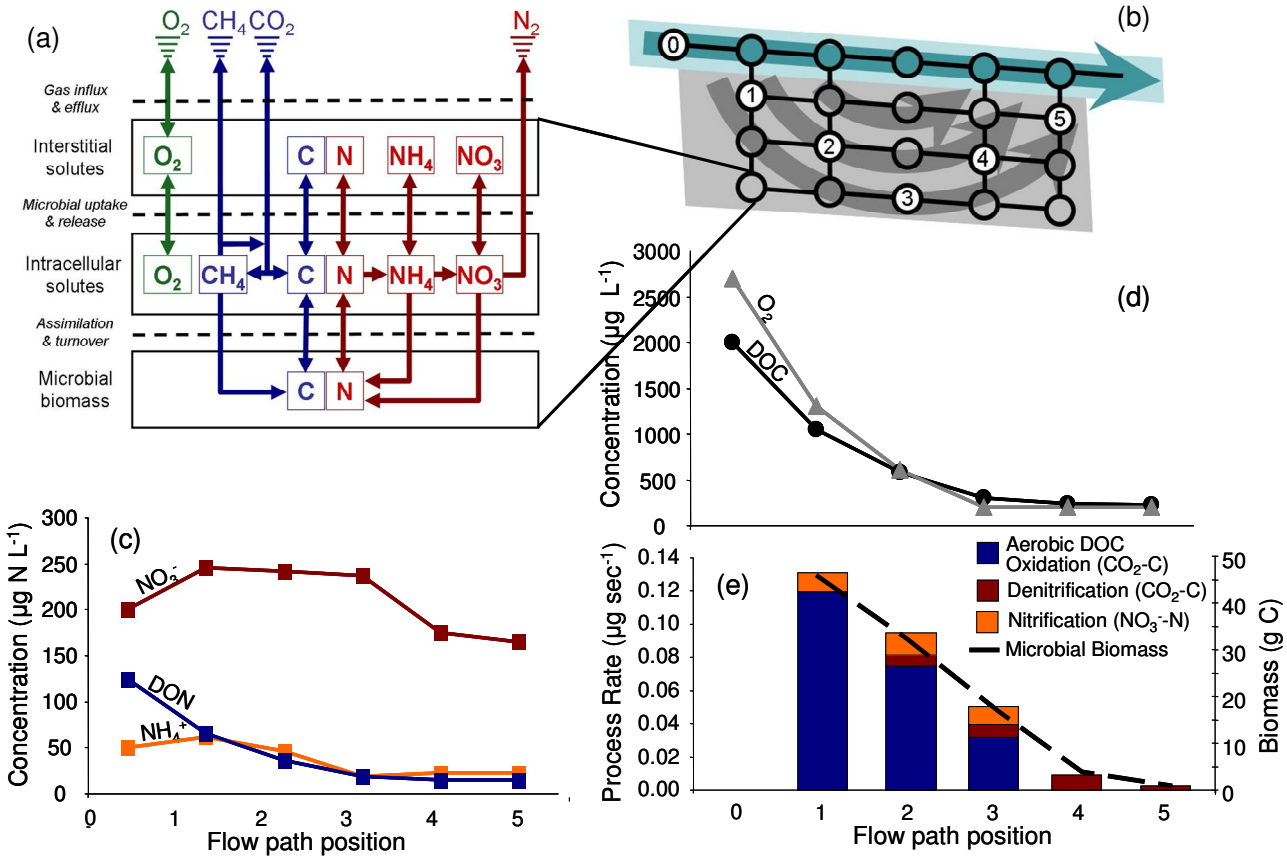

Figure 2.6. Simulation of multi-element biogeochemical cycles along a hyporheic flow path. (a) Schematic of a prototype biogeochemical model (AM Helton et al. unpublished) that simulates microbial uptake and utilization and/or production of dissolved organic matter, oxygen, nitrate, ammonium, and methane. The model operates by assuming that microbial assemblages will use the suite of metabolic pathways that will maximize microbial growth, as co-limited by the availability of carbon, nitrogen, and oxygen as electron donors/acceptors and the stoichiometric ratio of carbon and nitrogen required for building biomass. (b) Simulated hydrologic flow paths in a simple two-dimensional implementation of a mechanistic model of surface water flow and hyporheic exchange (hydrology model described by Poole et al. 2006). We combined the two

models to simulate hydrologic solute flux and (c) concentrations of different nitrogen forms (DON = dissolved organic nitrogen), (d) dissolved oxygen and dissolved organic carbon (DOC), and (e) microbial activity and biomass along an idealized hyporheic flow path (numbered circles in [b]).

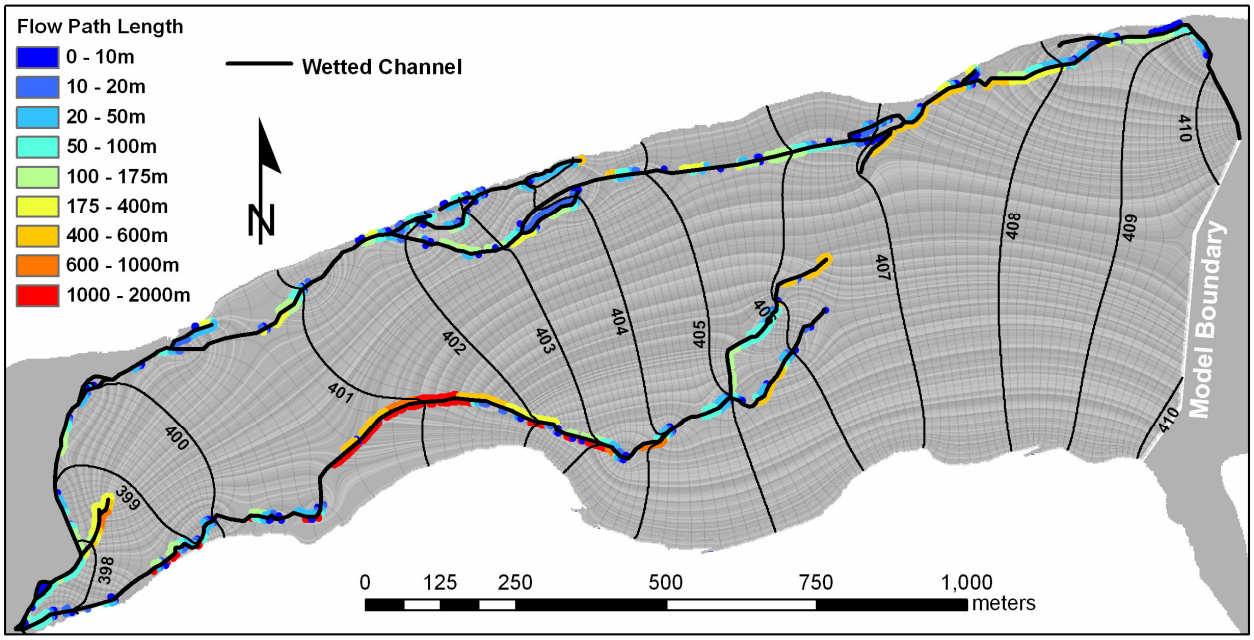

Figure 2.7. Simulated spatial juxtaposition of individual flow paths within a floodplain aquifer (modified from Poole et al. 2008; ©2008 John Wiley and Sons Ltd. Reproduced by permission). Heavy black lines show the center of active channels. Colors along the channels denote subsurface (hyporheic) flow-path length at each point of flow-path discharge back to the channel. Absence of color along the channel denotes points of hyporheic recharge from the channel. Black contours represent simulated water table elevations (m). Simulated aquifer flow paths are indicated by gray background striations.

CHAPTER 3

EFFECTS OF RIVER DISCHARGE AND HYDROLOGIC EXCHANGE BETWEEN THE RIVER CHANNEL, HYPORHEIC ZONE, AND FLOODPLAIN SURFACE ON WATER RESIDENCE TIME IN A ALLUVIAL RIVER[1]

---

[1]Ashley M Helton, Geoffrey C Poole, Robert Payn, Jack A Stanford. To be submitted to Water Resources Research.

Abstract

Understanding spatiotemporal patterns of hydrologic linkages between the river channel, hyporheic zone/alluvial aquifer, and floodplain/riparian surface is fundamental for understanding river ecosystem processes. We applied a spatially explicit, three-dimensional hydrologic model to simulate surface and hyporheic hydrology within the 16 km^2 Nyack Floodplain on the Middle Fork Flathead River in northwest Montana, USA. The model tracks surface and subsurface water flux and storage across the floodplain and is parameterized using a recently developed approach for hydrologic analysis of low-relief landscapes. We ran the model for four years and simulated nine conservative tracer particle releases across a range of river discharges. Whole-floodplain rates of hyporheic recharge showed a general positive relationship with river discharge, but peaks in hyporheic recharge and net exchange were associated with minor floods and/or the rising limbs of larger flood events. Model output showed that rates of whole-floodplain hyporheic exchange were driven by vertical hydraulic gradients at low to intermediate river discharges, but by inundated floodplain surface area during higher river discharges as water spread laterally onto the floodplain. Particle tracking simulations revealed when river discharge was below bankfull, mean residence time of surface water on the floodplain was inversely correlated to river discharge. However, during overbank flows, mean residence time increased with discharge due to storage of surface water on the floodplain. Conversely, when both surface and hyporheic water were considered, mean whole-floodplain hydrologic residence time was more than an order of magnitude greater than the residence time of surface water alone, and decreased exponentially with river discharge, due to a smaller percentage of channel water entering the hyporheic zone at high discharges. Our analyses illustrate the importance of

considering channel, floodplain, and hyporheic hydrologic residence times in determining the overall residence time of water within a river segment.

Introduction

River ecosystems are composed of hydrologically interdependent components, including the channel, hyporheic zone/alluvial aquifer, and floodplain/riparian surface (Stanford and Ward 1993; Helton et al. In Press). Complex and dynamic hydrologic interactions between river ecosystem components can create important areas and times of ecosystem processes (e.g., McClain et al. 2003) that vary in magnitude and frequency as flow paths diverge and converge within a river ecosystem. When and where these ecosystem components are tightly linked hydrologically, river ecosystem dynamics cannot be understood by studying the channel in isolation. An approach that includes understanding important hydrologic exchanges between components is needed.

Hyporheic exchange (the bidirectional flux of water between the channel and hyporheic zone) is an ecologically important link between a river's surface and subsurface (Findlay 1995; Boulton et al. 1998). Hyporheic exchange transports dissolved and particulate matter (Dahm et al. 1998; Baker et al. 2000) between the channel and hyporheic zone where physical and biological processes can retain and transform these constituents. Hyporheic zone microbial processes can account for the majority of whole ecosystem processes (e.g., Fellows et al. 2001). Hyporheic water discharged back to the channel influences surface water chemistry (Dent et al. 2001) and surface water temperature dynamics (Arrigoni et al. 2008), which, in turn, influence the distribution and abundance of aquatic biota and rates of ecosystem processes.

Perirheic exchange between the channel and floodplain surface is also ecologically important (Mertes 1997). For example, flood spates expand hydrologic connections (Stanley et al. 1997), wetting ephemeral channels and floodplains, which activates biogeochemical processes in surface areas adjacent to river channels (Valett et al. 2005). Floodplain storage and processing of nutrients during and after flooding events has the potential to explain river network scale variation in nitrogen removal (Wollheim et al. 2008).

Understanding river processes and geomorphic characteristics that mediate hydrologic exchange between river ecosystem components is challenging, particularly for large spatial scales (e.g., floodplains) where processes are difficult to measure using conventional stream tracer techniques (Gooseff et al. 2003). The utility of existing groundwater flow simulation models (e.g., MODFLOW, McDonald and Harbaugh 2003) for assessing cumulative effects of hydrologic exchanges between river ecosystem components is limited. Because such models are primarily designed to simulate groundwater, they often lack sophisticated capabilities to simulate detailed spatiotemporal inundation dynamics that drive hydrologic exchange between the channel, hyporheic zone, and floodplain surface.

Here we simulate hydrologic storage and exchange between the channel, floodplain surface, hyporheic zone, and alluvial aquifer of the 16 km^2 Nyack Floodplain on the Middle Fork Flathead River in northwest Montana, USA (Figure 3.1). We used a dynamic three-dimensional model to simulate surface and subsurface water flux and storage (Poole et al. 2004), parameterized by analyzing a high resolution digital elevation model to delineate geomorphic controls on inundation dynamics for this low-relief landscape (Jones et al. 2008). We ran the model for four years, encompassing one high, two intermediate, and one low flood spate. We also simulated nine particle releases within the modeled floodplain to determine simulated

"matrix traversal time" distribution (a surrogate measure of floodplain hydrologic residence time distribution; see *Methods*). The model results allowed us to examine the cumulative floodplain-scale patterns of hyporheic exchange and floodplain matrix traversal time across a range of river discharges.

Methods

Site description

The Nyack Floodplain is a 16 km^2 gravel- and cobble-bedded anabranched alluvial montane floodplain on the Middle Fork of the Flathead River located in northwest Montana (Figure 3.1). Hay production and low levels of riparian logging have occurred on the floodplain over the last 100 years and a railroad and highway traverse the eastern portion of the floodplain, but the river is unregulated and most of the upstream catchment is in federally protected wilderness, including the hillslopes adjacent to the floodplain. The hydrology and geomorphology of the Nyack hyporheic zone are well characterized (Poole et al. 2002; Diehl 2004; Poole et al. 2004; Poole et al. 2006). The floodplain is constrained laterally by bedrock valley walls and bounded upstream and downstream by canyon segments with bedrock streambeds. This fifth-order river has a snow-spate driven hydrograph with a mean discharge of 80 m^3/s and mean peak discharge of 600 m^3/s. Complex channel morphology and coarse, well-sorted sediments on the floodplain facilitate high rates of surface-subsurface water flux, creating an extensive hyporheic zone that ranges from ~5 to >25 meters in depth and spans the width of the floodplain (up to 1.5 km) (Stanford et al. 1994). Acoustic Doppler profiler data indicate that the main channel of the river loses ~30% of its base-flow discharge to the underlying alluvial aquifer as it flows across the first 1/3 of the floodplain (Mark Lorang, unpublished data). Water

recharged to the alluvial aquifer flows down-valley within the hyporheic zone and later re-emerges to the floodplain surface in the main channel or in spring channels scattered across the floodplain, which rejoin the main river channel before entering the downstream canyon (Poole et al. 2006). Patterns of surface and subsurface exchange are complex, and vary seasonally as surface water inundates the floodplain (Poole et al. 2006).

Hydrology Model

We applied a hydrologic model developed by Poole et al. (2004), and implemented the model with an improved parameterization (See *parameterization* sections, below). The model incorporates the surface and subsurface flow equations used in the Wetland Dynamic Water Budget Model (Walton et al. 1996). The three-dimensional model is a finite volume, or "link and node" model, in which the floodplain is divided into discrete cells, represented by nodes in a three-dimensional lattice network, and one-dimensional flows are calculated along links between adjacent nodes in all three spatial dimensions. Thus, the model represents: 1) horizontal surface water flow and floodplain inundation; 2) horizontal and vertical subsurface flow; and 3) vertical exchange between surface and subsurface waters. More detailed descriptions of the model are provided by Walton et al. (1996) and Poole et al. (2004).

Floodplain surface parameterization

The model requires that the floodplain surface be divided into spatially discrete patches, which each represent a model node (Figure 3.2a). A high-resolution (±10cm vertical accuracy, $1m^2$ grid cell size) Digital Elevation Model (DEM) derived from light detection and ranging (LIDAR) data was processed and patches were delineated according to Jones et al. (2008). This

patch delineation method was developed particularly for low-relief landscapes (e.g., floodplains) and analyzes patterns of hydrologic connectivity across the floodplain to delineate patch boundaries. Specifically, the algorithm creates a Digital Relative Elevation Model (DREM) – the floodplain DEM detrended by plotting the elevation of the floodplain relative to the channel water surface at a single arbitrary discharge (*sensu* Poole et al. 2002). The algorithm then identifies hydrologic sinks (low points) in the DREM and determines the boundaries of the floodplain area draining to each sink. Sink areas are aggregated into coarser-scale patches by preferentially dissolving boundaries with high hydrologic connectivity (e.g., a small difference between sink elevation and boundary elevation). Thus, sinks areas are aggregated into patches with high intra-patch surface water connectivity and low inter-patch surface water connectivity. The final distribution of patches represents an optimized set of patches that represent discrete but uniform hydrologic units, and final patch boundaries represent the most significant hydrologic divides controlling surface water flow and inundation across the floodplain. Surface water nodes within the model were located at the lowest sink within each patch and surface water links were created between nodes contained in adjacent patches (Figure 3.2).

For each patch, the relationship between water volume and both water depth and inundation area (required by the model) were determined from GIS analysis of the patch's DREM. The GIS analysis calculated the incremental increase in water depth and inundation with increasing water volume in each patch. These precise empirical relationships replaced prior assumptions of prismic channel shape and associated estimates of channel side slope and overbank elevation used to determine water volume, water depth, and inundation area in prior Nyack Floodplain modeling efforts (Poole et al. 2004, 2006).

For each surface water link (representing the flux of water across the boundary between two adjacent patches) in the model, we also used the DREM to develop similarly precise relationships between channel depth and both channel width and channel cross-sectional area (required by the model). From the elevation distribution traced along each divide, the GIS calculated the depth of water required to initiate flow across each divide, and then determined the wetted width and cross sectional area of flow for incrementally greater water depths. Again, these precise empirical relationships (one for each surface water link in the model) between channel depth, width, and cross-sectional area replaced model assumptions of prismic channel shape and associated estimated of channel bottom width and channel side slope used by Poole et al. (2004, 2006) to estimate relationships between channel depth, width, and cross-sectional area in prior efforts to model the Nyack Floodplain.

Horizontal link lengths were calculated as the flow path distance between connected nodes, traced along the path of lowest elevation between the nodes. These flow lengths replaced assumptions of straight-line distance between nodes used by Poole et al. (2004, 2006). Manning's n for horizontal surface water flux was estimated at 0.041, measured for the Middle Fork Flathead River at Essex, MT, on a similar floodplain segment approximately 25 km upstream (http://wwwrcamnl.wr.usgs.gov/sws/fieldmethods/Indirects/nvalues/). We also implemented surface water flow equation for nodes connected by culverts, using the equations reported by Walton et al. (1995). We measured culvert geometry and elevation in the field and used Manning's n of 0.02 to determine flux through culvert links.

The model network included 13 surface water inflow boundaries: the main stem inflow and 12 tributaries. We determined flux in surface water boundaries based on rating curves with the USGS West Glacier, MT gauging station (Poole et al. 2004). Previous mass balance analysis

shows evapotranspiration and precipitation provide a net contribution of <0.5% of the floodplain water budget (Poole 2000), so those fluxes are not included in the model. To reduce the influence of upstream and downstream boundary conditions on model simulations, an additional 2 km of river was added to the simulation domain upstream and downstream of the floodplain.

Floodplain subsurface parameterization

For each floodplain surface node, we delineated an underlying subsurface patch (Figure 3.2b). Subsurface nodes were centered directly below floodplain surface nodes. Surface boundaries were straightened to form subsurface boundaries, and subsurface link lengths were calculated as Euclidean (straight-line) distances between nodes (Figure 3.2c) because subsurface flow is not dependent on surface topography.

Alluvial sediments on the Nyack Floodplain consisted of two strata – "soil" and "aquifer" – the thicknesses of which were determined from 23 well logs spanning the lateral and longitudinal extent of the floodplain (20 wells from Diehl 2004; 3 additional wells from MGWIC 2009; Figure 3.3). The soil stratum varied spatially in depth from centimeters to approximately 3 meters thick, and the aquifer stratum ranged from approximately 6 to 25 meters thick.

The soil stratum is comprised primarily of sands, often with well developed organic horizons (especially beneath established floodplain forest canopies), and was generally unsaturated during base flow. Soil stratum thickness was related empirically to relative elevation, the elevation of a patch above the river surface elevation (Figure 3.3a). Thus, patch relative elevation (calculated from the DREM) was used to estimate soil stratum thickness for each subsurface patch. Channel patches lacked the soil stratum (Figure 3.4).

Beneath the soil stratum, the aquifer stratum (Figure 3.4) was comprised of sands, pebbles, gravels, and cobbles with little organic matter, was generally saturated at base flow, and overlay a relatively impermeable silt and clay deposit, which extends to bedrock (Diehl 2004). The aquifer stratum was wedge-shaped, decreasing from ~25m in thickness to ~6m in thickness in a downstream direction (Diehl 2004). Because floodplain elevation also decreased downstream, there was a strong empirical relationship between patch elevation and aquifer thickness (Figure 3.3b), which was used estimate the aquifer stratum thickness for each model patch. In the model, the aquifer stratum was subdivided into a "shallow" and "deep" layer to allow the model to represent both shallow and deep hyporheic flow paths. Unless constrained by bedrock (see below), the shallow aquifer layer thickness was set to 2 m. The deep aquifer layer comprised the remaining aquifer thickness.

Harrison (2004) estimated the depth to bedrock for the Nyack Floodplain by gravity modeling of 155 sites located within the Nyack Floodplain using a USGS program, GI3, which calculates three-dimensional gravity inversion by Cordell-Henderson method (Cordell and Henderson 1968). Where estimates of combined soil and aquifer thickness were greater than mapped depth to bedrock, we reduced the thickness of each layer, from the bottom up, until the thickness of the combined remaining layers equaled to depth to bedrock. In cases where bedrock constrained an aquifer layer to <1m in thickness, the layer was eliminated from the model. Thus, in some patches, shallow bedrock eliminated the deep aquifer layer. In a small number of patches near the upstream and downstream ends of the floodplain, shallow bedrock eliminated both aquifer layers, leaving only the soil layer in the modeled patch.

Vertical model links were used to connect surface nodes to directly underlying soil or streambed nodes, and to connect soil and aquifer nodes within a subsurface patch. The

elevations of surface nodes were set equal to the lowest surface elevation within each patch. The elevations of subsurface nodes were set at the middle of the layer they represented. Thus, surface-subsurface link lengths were set equal to one-half the thickness of the topmost subsurface layer. Link lengths between subsurface layers were calculated as the sum of one-half the thickness of each layer.

We parameterized hydraulic conductivity with measured horizontal K values within the Nyack aquifer (Diehl 2004). Other parameters were derived from K values and relationships used by Poole et al. (2004) (Table 3.1).

Model simulation

The final model network consisted of 2938 links, 916 nodes, and 14 surface water boundaries. Model spin up consisted of two phases. First, we initialized subsurface hydraulic head using river stage adjacent to each patch. We ran the model to steady-state using base-flow inflow rates and calculated surface water fluxes within the modeled domain using the "diffuse wave" equation (Walton et al. 1996). Second, with the resulting steady-state hydrology as initial values, we ran the model with the "dynamic wave" equation using observed river discharge for the 10 months from January 1, 1996 to October 31, 1996. The resulting surface stage and subsurface head distributions became the initial conditions for the model run.

We ran the model using observed river discharge from November 1, 1996 to December 31, 2000. These years encompassed a high, low, and two average flood spates (Figure 3.5). Based on the USGS West Glacier gauge record (average daily discharge from 1940 to 2008), the 1997 maximum flood peak was ranked in the 94th percentile, the 1998 maximum flood peak in the 6th percentile, the 1999 maximum flood peak in the 56th percentile, and the 2000 maximum

flood peak in the 22nd percentile. We ran the model using a 0.5 second time step with instantaneous and time-averaged output reported for each link and node hourly for the 4-year model run. It took approximately three weeks to complete the simulation on a computer node at the Rocky Mountain Supercomputing Center. We used model output to calculate whole-floodplain hyporheic net exchange (summed surface-subsurface water flux rate across all patches for each simulation day), and to simulate conservative tracer particle releases within the model network.

Particle tracking

We developed a particle tracking postprocessor to route particles through the model domain (the lattice network representing the channel/floodplain/aquifer hydrosystem) based on model output. The particle tracker simulates the release of conservative tracer "particles" at a user-specified time and model node. The particle tracker calculates the location of each particle within the modeled lattice network, over time, assuming that particles move along links as conservative tracers (i.e., at the same velocity as water). When a particle reaches a model node, the particle is routed along a random outflow link from the node, where the likelihood of entering each outflow link is proportional to the volume of water flowing through the link.

The floodplain and hyporheic matrix traversal times calculated for any particular particle through the Nyack matrix represents a surrogate for (not a direct estimate of) floodplain hydrologic residence time. Matrix traversal times likely overestimate residence time at any given location because particles are forced to travel along links in the networked representation of the Nyack Floodplain, even when links are not perpendicular to isopleths of groundwater head. For example, particles must travel straight down a vertical link connecting surface and

subsurface waters before traversing horizontal links within the subsurface. Additionally, the resolution of our representation of the Nyack Floodplain (i.e., patch areas range from 3000 to 475000 m^2), is too coarse to represent fine-scale geomorphology that drives short flow paths which often dominate hyporheic exchange in frequency (Poole et al. 2008). Thus, traversal time calculated by the particle tracker provides a measure of relative, not absolute, residence time and my data analysis focuses on relative changes (not absolute values) of matrix traversal time.

We tracked particles through the model for releases conducted on nine simulation dates (Figure 3.5). For each simulation date, we released 50000 particles at the upstream-most surface water node and tracked the location and residence time of each particle hourly as it traveled from the floodplain inlet to the outlet. We tracked particles for 1.5 years or until they reached the floodplain outlet. The nine conservative tracker particle release simulations were conducted at the Rocky Mountain Supercomputing Center.

For each particle, we calculated the whole-floodplain matrix traversal time (MTT) as the total amount of time the particle spent in the model domain. For each particle release, we calculated the mean MTT of all 50000 particles. We also calculated mean MTT of four subsets of particles: 1) particles that traversed the main river channel but did not enter the floodplain surface or subsurface (river channel particles), 2) particles that left the main river channel and entered the floodplain surface, but did not enter the subsurface (floodplain surface particles), 3) particles that either traversed only the main channel or entered the off-channel floodplain surface, but did not enter the hyporheic zone (river channel + floodplain surface particles), and 4) particles that, at some point, entered the floodplain subsurface (hyporheic particles).

Model Evaluation

We used several lines of evidence to evaluate the results generated by the model. First, we compared modeled discharge at the outlet of the Nyack Floodplain with empirical discharge data (derived from a rating curve (Poole et al. 2004) that predicts Nyack Floodplain outflow from discharge measured at the USGS gauging station at West Glacier, MT). Second, we compared simulated subsurface head distributions to observed heads in sampling wells throughout the alluvial aquifer. We measured water level and calculated head in floodplain wells (Figure 3.1) on three dates that spanned a range of river discharges (15 wells on May 28, 2009 at 445 m^3/s, 21 wells on August 17, 2009 at 43 m^3/s, and 11 wells on October 15, 2009 at 10 m^3/s). Since head was measured for dates not simulated within our model scenarios, we compared measured values to averaged mean daily head values from simulated days when river discharge reported at the USGS gauging station at West Glacier, MT was +/- 5% of river discharge when observed head data were collected.

Third, we analyzed the relationship between matrix traversal time and observed temperature dynamics in floodplain wells. Previous research shows that heat (i.e., temperature measurements) can be used as a groundwater tracer (reviewed by Anderson et al. 2005) and that the range and phase of annual temperature cycles in extensive hyporheic zones is correlated with subsurface flow path length (Poole et al. 2008). Thus, a strong correlation between the annual temperature cycle and simulated traversal time would indicate that matrix traversal time is an accurate representation of the relative residence times within the Nyack Floodplain. We obtained hourly temperature logger data for one to two years (data collected from 7/23/2002 to 11/22/2004 and from 7/3/2008 to 10/15/2009) for each of 12 wells and three surface water sites, and manual monthly temperature measurements for 5 additional wells from 5/1/2008 to

10/15/2009, for a total of 20 annual temperature records. These temperature records were derived from loggers deployed in surface water, the "shallow aquifer" layer, and the "deep aquifer" layer (Figure 3.4) and spanned the floodplain longitudinally (Figure 3.1). We analyzed each temperature record according to Arrigoni et al. (2008), except we fit the cosine wave to observed annual rather than diel temperature cycle. Specifically, we fit the mean temperature (M) in ^{o}C, temperature range (R) in ^{o}C, and phase (P) in days of a cosine wave to the observed annual cycle of temperature in each well by minimizing RMSE for the following sinusoidal equation (Arrigoni et al. 2008):

$$T_d = (0.5R) \cos((h-P)c) + M \quad (1)$$

where T_d is the mean daily water temperature (^{o}C) for a given day of the year (d), and c is $2\pi/365$, a constant to convert radians to day of the year. Since P is cyclical over a 365 day period (i.e., it represents the day of the year upon which the well temperature peaks), we constrained P to range between 0 and 365 when fitting parameters.

From the particle tracking output, we calculated the node mean matrix traversal time (MTT) for each model node that contained a temperature monitoring well. Node MTT was calculated as the time required to reach the model node for all particles that reached the node across all nine particle releases. To evaluate the importance of considering deep vs. shallow subsurface flow paths within the model, we compared the annual water temperature range and phase to: 1) the node MTTs calculated for shallow and deep aquifer layers; and 2) the node MTTs for only the model layer which corresponded to the deployment depth of the data logger within the well.

Results

Simulated river discharge at the outlet of the Nyack Floodplain is strongly correlated to estimated river discharge from the Middle Fork rating curve well (Figure 3.6a), but the model tended to over-predict discharge at higher river discharges (i.e., points consistently fall above 1:1 line with increasing discharge, except for the three highest points; Figure 3.6a). Simulated head values were also strongly correlated to observed head on each date. Similar to river discharge, the model tended to over-predict head for the highest discharge (i.e., white diamonds in Figure 3.6b tend to fall above the 1:1 line).

Annual temperature range (R, fit from equation 1) decreased (Figure 3.7) and annual temperature phase (P, fit from equation 1) increased (Figure 3.8) with node MTT (i.e., the average time required for particles to reach a particular model node), derived from our simulated particle releases. As further verification of the shallow and deep aquifer vertical model structure, the relationships between node MTT and phase and range substantially improved when the deployment depths of data loggers were considered in the calculation of node MTT (Figures 3.7 and 3.8).

Whole-floodplain hyporheic recharge (the flux of water from surface to subsurface model nodes summed across the floodplain) was positively related to river discharge (Figure 3.9a, black line). Hyporheic recharge as a percent of river discharge had the opposite temporal trend: as a percent, hyporheic recharge was negatively related to river discharge (Figure 3.9a, grey line). Thus, at low river discharge, a lower flux, but a higher percent of water was exchange between the channel and hyporheic zone. Conversely, at high river discharge, a higher flux, but a lower percent was exchanged.

The highest rates of hyporheic recharge and resultant negative peaks of net hyporheic exchange (Figure 3.9b) correspond to the rising limbs, rather than peak flows, on the hydrograph. Indeed, hyporheic recharge generally increased with discharge, but with the highest rates of hyporheic recharge occurring at intermediate levels of discharge (Figure 3.10a). This pattern is driven by the interplay between inundated floodplain area and the vertical hydraulic gradient weighted by inundated floodplain area. The inundated floodplain area increased consistently with river discharge (Figure 10b), while the vertical hydraulic gradient peaked at intermediate discharges (Figure 10c).

Matrix traversal time, the total amount of time each particle spent in the model domain, varied among particles that traversed different river ecosystem components (the channel, hyporheic zone/aquifer, and floodplain/riparian surface), and was strongly correlated with river discharge. River channel MTT (i.e., mean MTT of particles that traverse the main river channel and do not enter the subsurface or the floodplain surface) ranged from 0.96 to 1.18 days and decreased with river discharge (Figure 3.11a). Floodplain surface MTT (i.e., mean MTT of particles that, at some point, travel from the main river channel out onto the floodplain surface but do not enter the subsurface) was higher than river channel MTT, ranging from 1.29 to 1.87 days (Figure 3.11a). Combined river channel and floodplain surface MTT (i.e., mean MTT of all particles that travel across the surface, including the river channel and the floodplain surface, but do not enter the subsurface) ranged from 1.06 to 1.33 and decreased with discharge below bankfull flow, but then increased with discharge above bankfull flow (Figure 3.11b), likely do to out-of-channel storage of surface water on the floodplain. Indeed, the percent of particles that leave the channel and enter the floodplain surface increased with river discharge (Figure 3.12a).

Hyporheic MTT (i.e., mean MTT of particles that, at some point, enter the subsurface) was high, ranging from 194 to 238 days, but is unrelated to river discharge (Figure 3.11c). Whole-floodplain MTT (i.e., mean MTT of all particles released) ranges from 10 to 56 days and decreased with increasing river discharge (Figure 3.11d). At low discharge, a larger fraction of the water entered the hyporheic zone (Figure 3.12b), driving up whole-floodplain MTT under low flow conditions. In fact, the percent of particles entering the hyporheic zone is a strong predictor of whole-floodplain MTT (Figure 3.13).

Discussion

Our model evaluation indicates the three-dimensional simulation model of hydrologic storage within and fluxes between the river channel, floodplain surface, and alluvial aquifer provides a realistic representation of Nyack Floodplain hydrology (Figure 3.6, 3.7, and 3.8). Over-prediction of river discharge and subsequent over-prediction of head at high USGS gauged river discharges may be because the rating curves used to estimate main stem and tributary influxes to the system as well as to compare to simulated main stem outflow are based on empirical relationships developed from USGS gauged discharges below 250 m^3/s (Poole et al. 2004). The USGS hydrograph for simulated years, 1996 thru 2000, had peak flood flows that ranged from 330 to 880 m^3/s, although 92% of daily river discharges fell below 250 m^3/s. Another explanation may be that our floodplain roughness coefficient was too low. We used a constant value across the floodplain (0.041), which fell within the range of floodplain pasture and lightly forested land types (Chow 1959). Roughness coefficients for the Nyack Floodplain have not been measured. Although the model overestimates infrequent large flood peaks,

correspondence between simulated and observed discharge and water levels illustrate the model represents Nyack Floodplain hydrology well.

Our temperature analysis provides further evidence that the model was an adequate representation of hydrologic dynamics within the Nyack Floodplain, and that the particle tracking model provided accurate distributions of relative floodplain residence times (Figures 3.7 and 3.8). Our observations with annual temperature cycles correspond qualitatively to patterns observed by Arrigoni et al. (2008) for diel temperature cycles: as hyporheic residence time increases, water temperature cycles are buffered (i.e., the range is reduced) and lagged (i.e., the phase, or day of year to peak temperature is increased) relative to surface water.

The temperature analysis also revealed the importance of our three-dimensional representation of subsurface structure (Figure 3.4) for accurately simulating hydrologic flux throughout the Nyack Floodplain subsurface. The relationships between temperature metrics and MTT improved when we compared temperature metrics to MTT in model nodes that corresponded to the depth at which the temperature loggers were installed, rather than comparing temperature metrics to MTT in either the shallow or deep aquifer model layers (Figures 3.7 and 3.8). Physical heterogeneity of the alluvial material that makes up the hyporheic zone can control hydrologic retention of solutes and residence time (Morrice et al. 1997; Cardenas et al. 2004). Likewise, our temperature analysis suggests hyporheic heterogeneity is an important control for hydrologic residence times and may help explain variance observed in field data (e.g., temperature data). Thus, in rivers with extensive hyporheic zones, a two-dimensional homogenous representation of the subsurface may be insufficient when interpreting longitudinal patterns of temperature and other physical and chemical parameters that drive ecological processes.

Hyporheic exchange drives ecological patterns and processes in streams and rivers, and much research has focused on determining the influence of hyporheic exchange on ecosystem processes (Findlay 1995; Boulton et al. 1998; Fellows et al. 2001). Many studies have calculated spatial and temporal trends in hyporheic exchange on the stream reach scale (Wondzell 2006, Gooseff et al. 2006), typically using a two-dimensional representation of water flux through the channel and hyporheic zone (Harvey and Wagner 2000). Much less is understood about the cumulative effects of hyporheic exchange across large spatial and temporal scales.

Our simulation model allowed us to calculate the hyporheic exchange across the whole floodplain daily for >4 years. General temporal patterns of hyporheic recharge (as a flux and percent of river discharge) follow temporal trends in the hydrograph (Figure 3.9a). However, peak net exchange events (and corresponding peak recharge events) were associated with minor floods or the initial rising limb of annual flood spates (Figure 3.9b). During the rising limb, high peak hyporheic recharge and net exchange occur as average vertical hydraulic gradient peaks (Figure 3.10c) and surface water fills the alluvial aquifer. As water levels exceed channel banks and water spreads laterally onto the floodplain, inundated floodplain surface area rather than hydraulic gradient, drives hyporheic exchange (Figure 3.10b). Since the water table in the alluvial aquifer is higher during the falling limb than during the rising limb, the peak net exchanges that occurred during the rising limbs do not occur during the falling limbs. Maximum values of vertical hydraulic gradient corresponding to intermediate flows were also observed by Jung et al. 2004 in a lowland river floodplain. Thus, the temporal pattern of whole-floodplain hyporheic exchange is driven by the interaction between changes in the magnitude of vertical hydrologic exchange and changes in inundated area, both driven by variation in river channel discharge.

Hydrologic residence time is a driving variable for many physical (e.g., temperature, weathering) and biological (e.g., microbially mediated transformations) processes in rivers. Our simulation model allowed us to calculate whole-floodplain residence time and residence time for particles traversing various river ecosystem components, including the channel, floodplain surface, and hyporheic zone/alluvial aquifer (i.e., mean matrix traversal time, MTT). Our analyses illustrate the importance of considering hydrologic exchanges and storage among components of whole-floodplain hydrologic residence times. For example, independently, MTT for both channel and floodplain surface particles decreased with increasing river discharge (Figure 3.11a). However, when channel and floodplain particles were combined, MTT only decreased below bankfull river discharge (Figure 3.11b). During higher river discharges, MTT increased as a higher proportion of particles traveled from the channel onto the floodplain surface (Figure 3.12a). These results highlight the importance of understanding the effects of inundation hydrology (sensu Mertes 2000) on hydrologic residence times in rivers.

Our findings show a shift from the dominance of floodplain surface fluxes at high flow to hyporheic fluxes at low flow (Figure 3.12). Relative to floodplain and channel MTT, hyporheic MTT was long (i.e., 1-2 days versus ~200 days). Because hyporheic MTT was so much longer than surface MTT, the fraction of particles entering the hyporheic zone determined whole-floodplain scale patterns of MTT (Figure 3.13). These results highlight the potential influence of the hyporheic zone on whole-floodplain scale patterns of hydrologic residence time. The strong correlation between whole-floodplain residence time and hyporheic exchange underscores the limitations of using transient storage models based on empirical tracer measurements for representing hyporheic influences on hydrologic residence time in large-floodplain systems –

especially those with extensive alluvial aquifers comprised of coarse (pebble/gravel/cobble) bed materials.

The influence of the floodplain/riparian surface and the hyporheic zone on hydrologic residence time has important implications for models that scale stream reach dynamics to river networks. For example, Helton et al. (In Press) point out that river network models that simulate nitrogen dynamics generally consider channel hydrology alone. However, here, we found that linkages between non-channel ecosystem components substantially influence the residence time of particles traversing the river system. The range of geomorphic conditions within rivers (e.g., bedrock dominated channels versus gravel bedded rivers) will likely influence the relative effects of non-channel river components on variables such as hydrologic residence time and resultant ecosystem process rates. Our work suggests that, at least for river systems with well-connected hyporheic zones and floodplains, models that omit descriptions of non-channel hydrologic exchange likely underestimate the role of river ecosystems in biogeochemical cycling. Because large gravel-bedded rivers are prevalent in many regions around the world, the influence of non-channel storage could have a substantial influence on biogeochemical cycling across large scales.

Conclusions

Our simulation of hydrologic dynamics within and flux between the channel, hyporheic zone/alluvial aquifer, and floodplain/riparian surface illustrates the importance of dynamic hydrologic linkages between ecosystem components for whole-floodplain scale patterns in hydrologic residence time. When ecosystem components are well connected, adequate representation of hydrologic linkages among channels, floodplains, and alluvial aquifers is likely fundamental for understanding hydrologic patterns that drive ecological dynamics. As

researchers continue to extrapolate fine scale hydrologic and biogeochemical measurements, a more holistic representation of river system hydrology will be fundamental in describing patterns across large spatial and temporal scales.

Acknowledgements

This research was supported by the National Research Initiative of the USDA Cooperative State Research, Education and Extension Service (2005-35102-16288), by the Gordon and Betty Moore Foundation, by the Rocky Mountain Supercomputing Center, and by an EPA Star Fellowship for AMH. EPA has not officially endorsed this publication and the views expressed herein may not reflect the views of the EPA. We thank Tom Bansak, Tyler Tappenbeck, Meredith Wright, and Oriana Grubisic for assistance in the field. We thank Michael Paulson and Clemente Izurieta for software engineering assistance.

References

Anderson, M. P. 2005. Heat as a Ground Water Tracer. Ground Water **43**:951-968.

Arrigoni, A. S., G. C. Poole, L. A. K. Mertes, S. J. O'Daniel, W. W. Woessner, and S. A. Thomas. 2008. Buffered, lagged, or cooled? Disentangling hyporheic influences on temperature cycles in stream channels. Water Resources Research **44**.

Baker, M. A., H. M. Valett, and C. N. Dahm. 2000. Organic carbon supply and metabolism in a shallow groundwater ecosystem. Ecology **81**:3133-3148.

Boulton, A. J., S. Findlay, P. Marmonier, E. H. Stanley, and H. M. Valett. 1998. The functional significance of the hyporheic zone in streams and rivers. Annual Review of Ecology and Systematics **29**:59-81.

Cardenas, M. B., J. L. Wilson, and V. A. Zlotnik. 2004. Impact of heterogeneity, bed forms, and stream curvature on subchannel hyporheic exchange. Water Resources Research **40**:W08307.

Chow, V.T. 1959. Open Channel Hydraulics. McGraw-Hill, New York, USA.

Cordell, L. and Henderson, R.G. 1968. Iterative three-dimensional solution of gravity anomaly data using a digital computer: Geophysics, **33**(4):596-601.

Dahm, C. N., N. B. Grimm, P. Marmonier, H. M. Valett, and P. Vervier. 1998. Nutrient dynamics at the interface between surface waters and groundwaters. Freshwater Biology **40**:427-451.

DeBorde, D.C., W.W. Woessner, Q.T. Kiley, and P. Ball. 1999. Rapid transport of viruses in a floodplain aquifer. Water Research **33**: 2229-38.

Dent, C. L., N. B. Grimm, and S. G. Fisher. 2001. Multiscale effects of surface-subsurface exchange on stream water nutrient concentrations. Journal of the North American Benthological Society **20**:162-181.

Diehl, J.C. 2004. Hydrogeological characteristics and groundwater / river exchange in a gravel-dominated floodplain, Middle Fork of the Flathead River, Northwestern Montana. Unpublished Master's Thesis. University of Montana, Missoula.

Fellows, C. S., H. M. Valett, and C. N. Dahm. 2001. Whole-stream metabolism in two montane streams: Contribution of the hyporheic zone. Limnology and Oceanography **46**:523-531.

Fetter. 1994. Applied hydrogeology. MacM\millan College Publishing Company, New York, New York.

Findlay, S. 1995. Importance of Surface-Subsurface Exchange in Stream Ecosystems - the Hyporheic Zone. Limnology and Oceanography **40**:159-164.

Gooseff, M.N., D.M. McKnight, R.L. Runkel, and B.H. Vaughn. 2003. Determining long time-scale hyporheic zone flow paths in Antarctic streams. Hydrological Processes **17**:1691-1710.

Gooseff, M. N., J. K. Anderson, S. M. Wondzell, J. LaNier, and R. Haggerty. 2006. A modelling study of hyporheic exchange pattern and the sequence, size, and spacing of stream bedforms in mountain stream networks, Oregon, USA. Hydrological Processes **20**:2443-2457.

Harrison, N.E. 2004. Gravity, radar, and seismic investigation to help determine geologic, hydrologic, and biologic relations in the Nyack Valley, Northwestern Montana. Unpublished Master's Thesis. University of Montana, Missoula.

Harvey, J.W., and Wagner, B.J. 2000. Quantifying hydrologic interactions between streams and their subsurface hyporheic zones. In: Jones, J.B. and Mulholland, P.J. (eds) Streams and ground waters. San Diego, CA: Academic Press, pp. 3–44.

Helton, A. M., G. C. Poole, J. L. Meyer, W. M. Wollheim, B. J. Peterson, P. J. Mulholland, E. S. Bernhardt, J. A. Stanford, C. Arango, L. R. Ashkenas, L. W. Cooper, W. K. Dodds, S. V. Gregory, R. O. Hall Jr, S. K. Hamilton, S. L. Johnson, W. H. McDowell, J. D. Potter, J. L. Tank, S. M. Thomas, H. M. Valett, J. R. Webster, and L. Zeglin. Thinking outside the channel: modeling nitrogen cycling in networked river ecosystems. Frontiers in Ecology and the Environment.

Jones, K. L., G. C. Poole, S. J. O'Daniel, L. A. K. Mertes, and J. A. Stanford. 2008. Surface hydrology of low-relief landscapes: Assessing surface water flow impedance using LIDAR-derived digital elevation models. Remote Sensing of Environment **112**:4148-4158.

Jung, M., T. P. Burt, and P. D. Bates. 2004. Toward a conceptual model of floodplain water table response. Water Resources Research **40**:W12409.

MGWIC. Montana's Ground-Water Information Center. Online database: http://mbmggwic.mtech.edu. Accessed 5 November 2009.

McClain, M. E., E. W. Boyer, C. L. Dent, S. E. Gergel, N. B. Grimm, P. M. Groffman, S. C. Hart, J. W. Harvey, C. A. Johnston, E. Mayorga, W. H. McDowell, and G. Pinay. 2003. Biogeochemical hot spots and hot moments at the interface of terrestrial and aquatic ecosystems. Ecosystems **6**:301-312.

McDonald, M. G. and A. W. Harbaugh. 2003. The History of MODFLOW. Ground Water **41**:280-283.

Mertes, L.A.K. 1997. Documentation of the significance of the perirheic zone on inundated floodplains. Water Resources Research **33**:1749-1762.

Mertes, L.A.K. 2000. Inundation hydrology. Pages 146-166 in E. E. Wohl (editor). Inland Flood Hazards. Cambridge University Press, Cambridge, UK.

Morrice, J. A., H. M. Valett, C. N. Dahm, and M. E. Campana. 1997. Alluvial characteristics, groundwater-surface water exchange, and hydrological retention in headwater streams. Hydrological Processes **11**:253-267.

Poole G.C. 2000. Analysis and Dynamic Simulation of Morphologic Controls on Surface- and Ground-water Flux in a Large Alluvial Flood Plain. PhD dissertation, University of Montana, Missoula.

Poole G.C., J.A. Stanford, C.A. Frissell, S.W. Running. 2002. Three-dimensional mapping of geomorphic controls on flood-plain hydrology and connectivity from aerial photos. Geomorphology 48(4): 329–347.

Poole, G. C., S. J. O'Daniel, K. L. Jones, W. W. Woessner, E. S. Bernhardt, A. M. Helton, J. A. Stanford, B. R. Boer, and T. J. Beechie. 2008. Hydrologic spiralling: the role of multiple

interactive flow paths in stream ecosystems. River Research and Applications **24**:1018-1031.

Poole, G. C., J. A. Stanford, S. W. Running, and C. A. Frissell. 2006. Multiscale geomorphic drivers of groundwater flow paths: subsurface hydrologic dynamics and hyporheic habitat diversity. Journal of the North American Benthological Society **25**:288-303.

Poole, G. C., J. A. Stanford, S. W. Running, C. A. Frissell, W. W. Woessner, and B. K. Ellis. 2004. A patch hierarchy approach to modeling surface and subsurface hydrology in complex flood-plain environments. Earth Surface Processes and Landforms **29**:1259-1274.

Schroeder, P.R., T.S. Dozier, P.A. Zappi, B.M. McEnroe, J.W. Sjostrom, and R.L. Peyton. 1994. The hydrologic evaluation of landfill performance (HELP) model: engineering documentation for version 3. US Environmental Protection Agency, Risk Reduction Engineering Laboratory #EPA/600/R-94/168b.

Schroeder, P.R., B.M. McEnroe, R.L. Peyton, T.S. Dozier, and J.W. Sjostrom. 1992. The hydrologic evaluation of landfill performance (HELP) model, volume IV: documentation for version 2. US Army Corps of Engineers Envrionmental Laboratory, Waterways Experiment Station #Internal working document EL-92-1.

Shaver, R.B. 1998. The Determination of Glacial Till Specific Storage in North Dakota. Ground Water **63**: 552-7.

Stanford, J. A., and J. V. Ward. 1993. An ecosystem perspective of alluvial rivers: connectivity and the hyporheic corridor. Journal of the North American Benthological Society **12**:48-60.

Stanford, J.A., J.V. Ward, and B.K. Ellis. 1994. Ecology of the alluvial aquifers of the Flathead River, Montana. Pages 367-390 in J. Gibert, D. L. Danielopol, and J. A. Stanford (editors). Groundwater Ecology. Academic Press, San Diego, California.

Stanley, E. H., S. G. Fisher, and N. B. Grimm. 1997. Ecosystem expansion and contraction in streams. Bioscience **47**:427-425.

Valett, H. M., M. A. Baker, J. A. Morrice, C. S. Crawford, M. C. Molles, C. N. Dahm, D. L. Moyer, J. R. Thibault, and L. M. Ellis. 2005. Biogeochemical and metabolic responses to the flood pulse in a semiarid floodplain. Ecology **86**:220-234.

Walton, R., T.H. Martin, Jr., R.S. Chapman, and J.E. Davis. 1995. Investigation of wetlands hydraulic and hydrological processes, model development, and application. US Army Corps of Engineers, Waterways Experiment Station, Technical Report No. WRP-CP-6, Vicksburg, MS.

Walton, R., R. S. Chapman, and J. E. Davis. 1996. Development and application of the wetlands dynamic water budget model. Wetlands **16**:347-357.

Wollheim, W. M., B. J. Peterson, S. M. Thomas, C. H. Hopkinson, and C. J. Vorosmarty. 2008. Dynamics of N removal over annual time periods in a suburban river network. Journal of Geophysical Research-Biogeosciences **113**.

Wondzell, S. M. 2006. Effect of morphology and discharge on hyporheic exchange flows in two small streams in the Cascade Mountains of Oregon, USA. Hydrological Processes **20**:267-287.

Table 3.1. Hydrology model parameters.

Subsurface node type	Horiz. Saturated K[a] ($m\ s^{-1}$)	Vert. Saturated K[b] ($m\ s^{-1}$)	Residual soil water content[c] ($m^3\ m^{-3}$)	Field Capacity[c] ($m^3\ m^{-3}$)	Porosity[d] ($m^3\ m^{-3}$)	Specific Storage[e] (m^{-1})
Soil	0.001	0.0001	0.015	0.047	0.2	0.0006
Shallow Aquifer	0.010	0.001	0.006	0.016	0.2	0.0006
Deep Aquifer	0.0035	0.00035	0.009	0.026	0.2	0.0006

[a] Estimated from Nyack aquifer hydraulic conductivities measured by Diehl (2004).
[b] Set equal to 1/10 of horizontal hydraulic conductivity (Fetter 1994).
[c] Derived from relationship between model parameter and hydraulic conductivity (Poole et al. 2004) with data from Schroeder et al. (1992, 1994)
[d] Estimate from Poole et al. 2004 Nyack hydrology model, based on data from Deborde et al. (1999).
[e] Estimate from Poole et al. 2004 Nyack hydrology model, value from Shaver (1998) for specific storage in an unconfined glacial till aquifer.

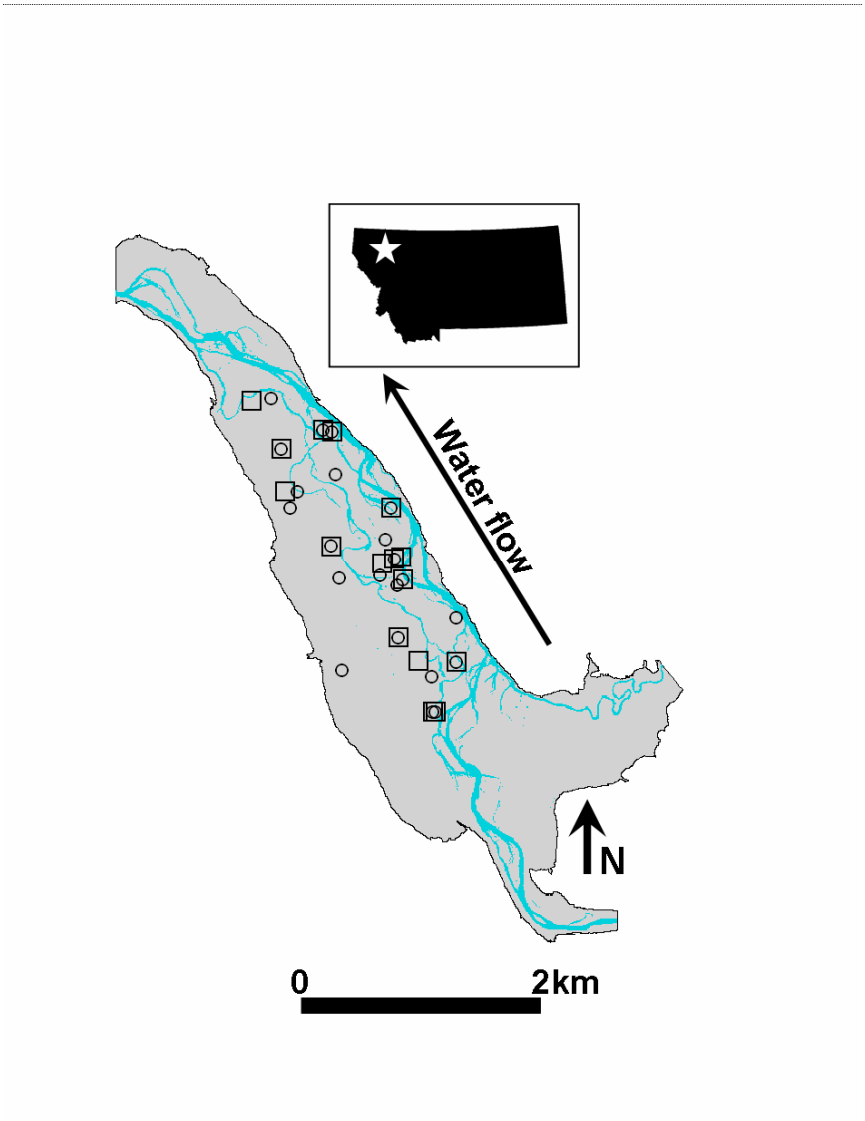

Figure 3.1. Plan view of Nyack Floodplain extent (grey), on the Middle Fork Flathead River located in Northwest Montana (shown in inset). Circles indicate well locations with measured water level (see Figure 3.6b), and squares indicate well locations with temperature records (see Figures 3.7 and 3.8) used to evaluate the model.

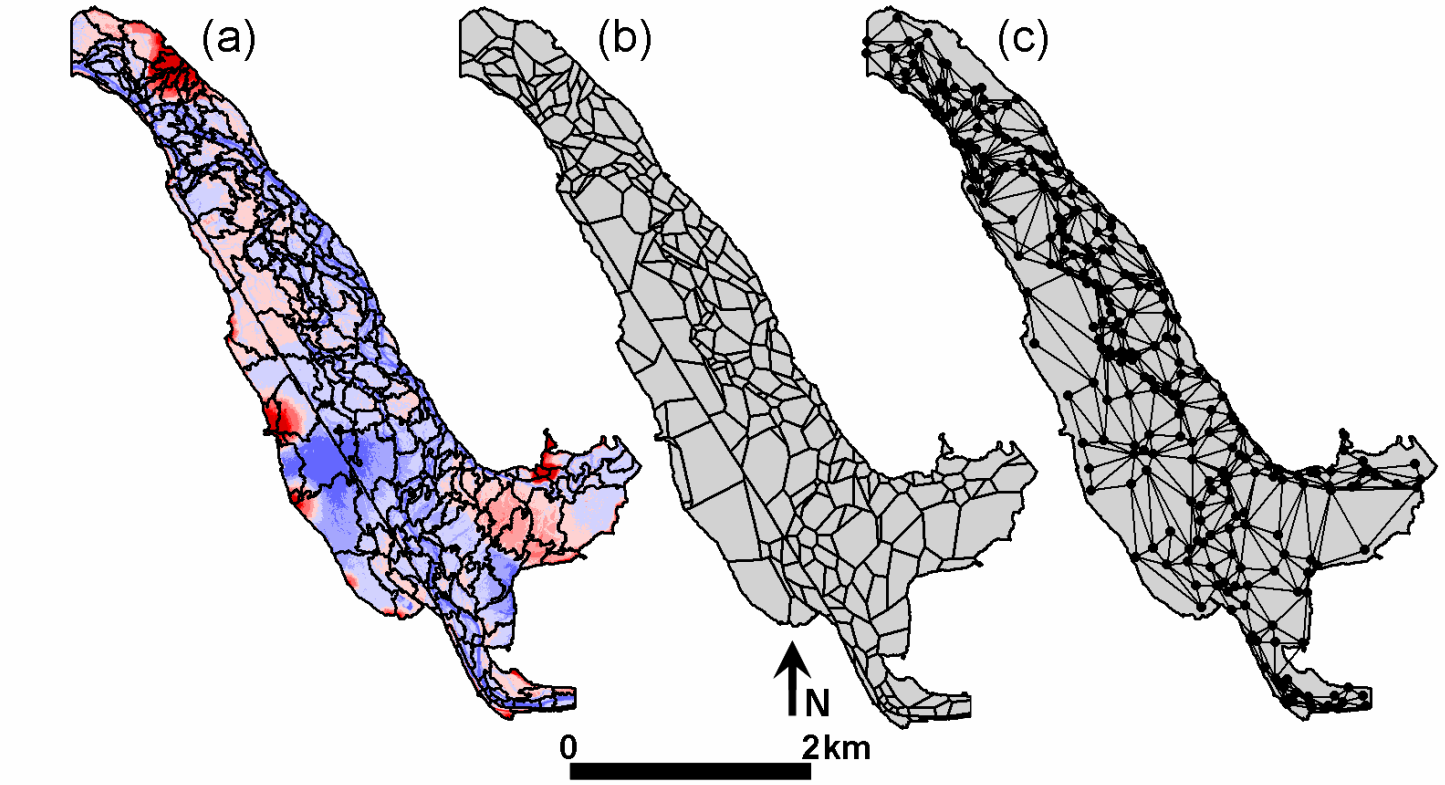

Figure 3.2. Model patches for the Nyack Floodplain a) surface and b) subsurface. c) Example of link-and-node network created from subsurface patches in (b). Color in (a) is relative elevation; blue represents low and red represents high relative elevation.

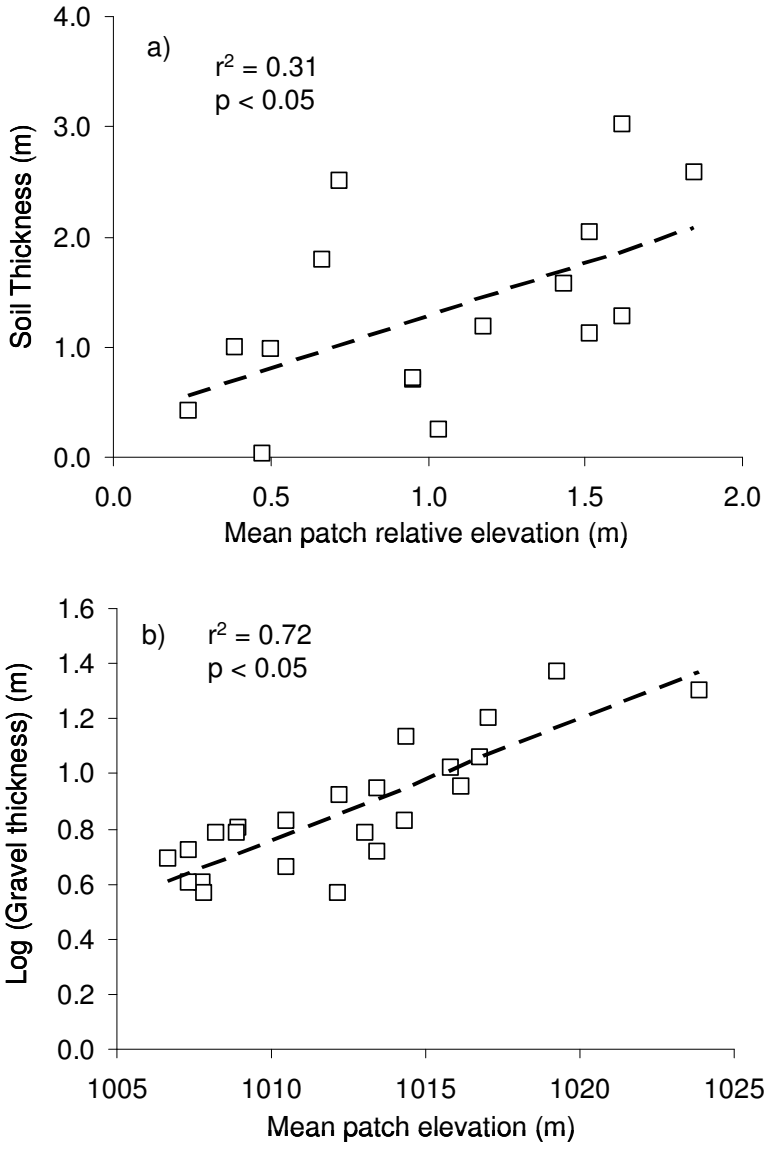

Figure 3.3. Regression relationships used to parameterize subsurface node thickness: a) mean soil thickness versus mean patch relative elevation (Soil Thickness = 0.9525(Mean patch relative elevation) + 0.3332), and b) gravel thickness versus mean patch elevation (Log_{10}(Gravel Thickness) = 0.0442(Mean Patch Elevation) – 43.865).

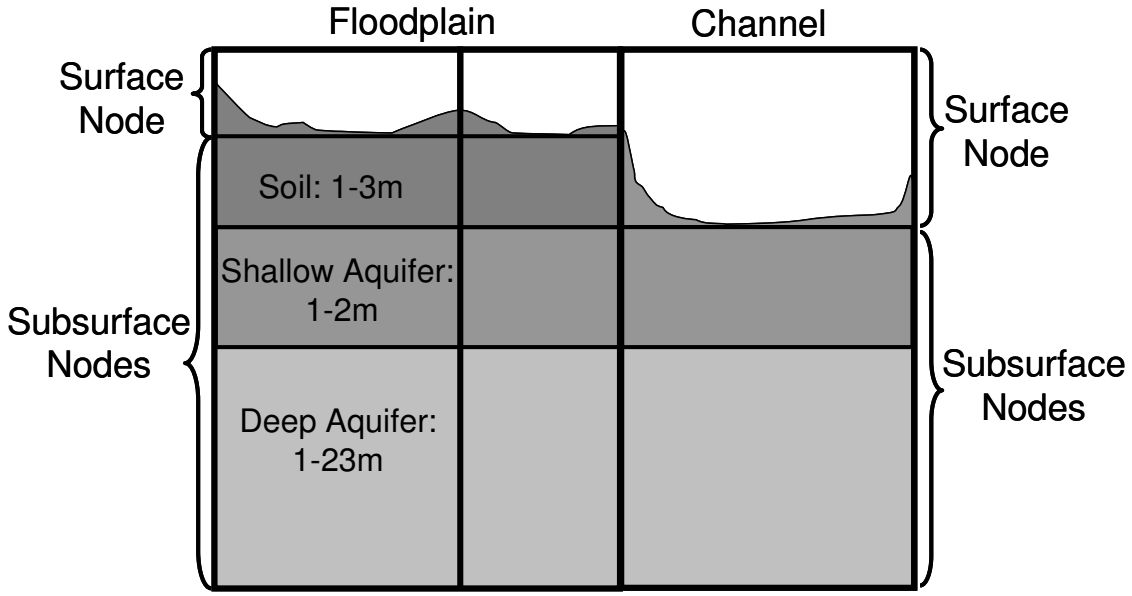

Figure 3.4. Vertical model structure.

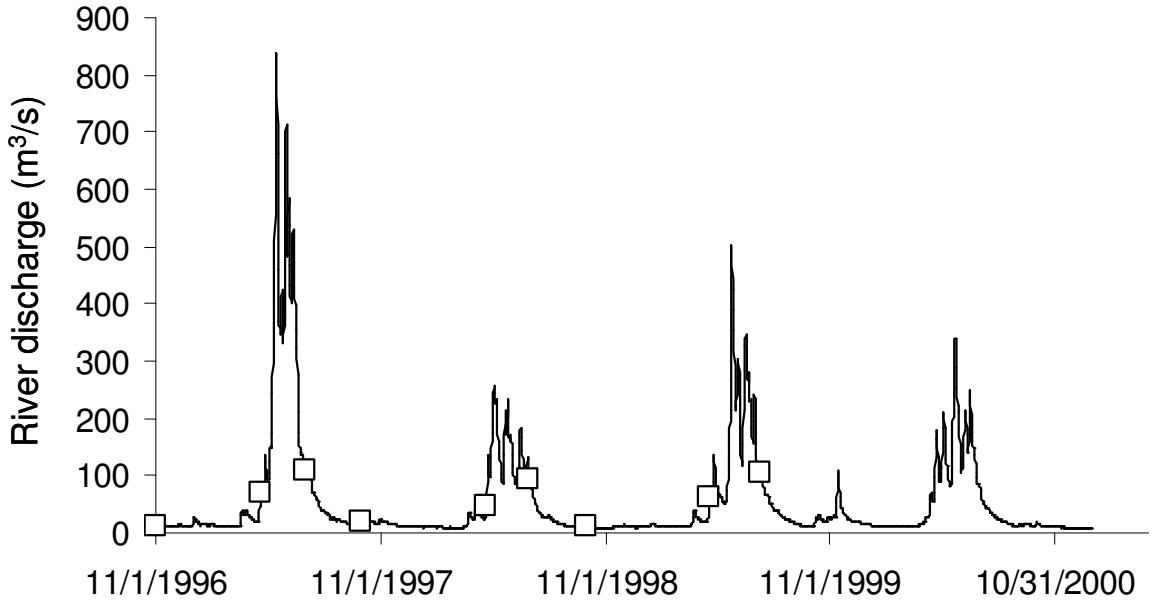

Figure 3.5. Hydrograph of main stem inflow to the Nyack Floodplain during the hydrologic model simulation. Squares indicate dates of simulated conservative tracer particle releases.

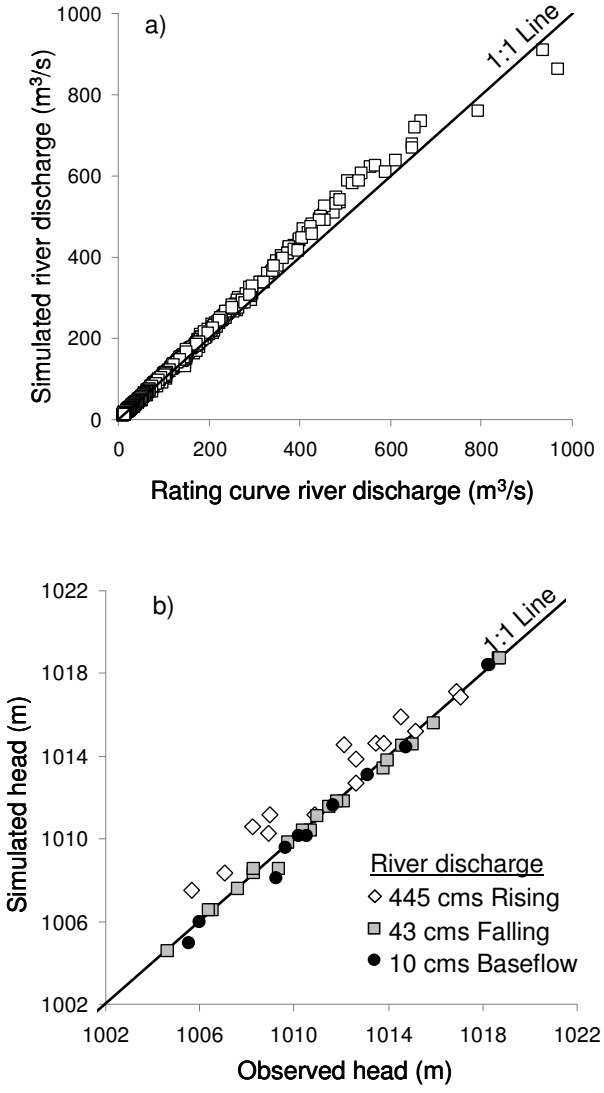

Figure 3.6. a) Rating curve versus simulated river discharge at the Nyack Floodplain outlet (r^2 = 0.99; RMSE = 12.61 m^3/s; slope = 1.04). b) Observed head versus simulated head within the Nyack Floodplain. Observed head data were collected on May 28, 2009, August 17, 2009, and October 15, 2009. Simulated head data are averaged mean daily head values for days when river discharge at the West Glacier gauge was +/- 5% of when observed data were collected. (May, r^2 = 0.97, RMSE = 1.38 m, slope = 0.83; August, r^2 = 0.99, RMSE = 0.26 m, slope = 0.98 ; October, r^2 = 0.99, RMSE = 0.42 m, slope = 1.03)

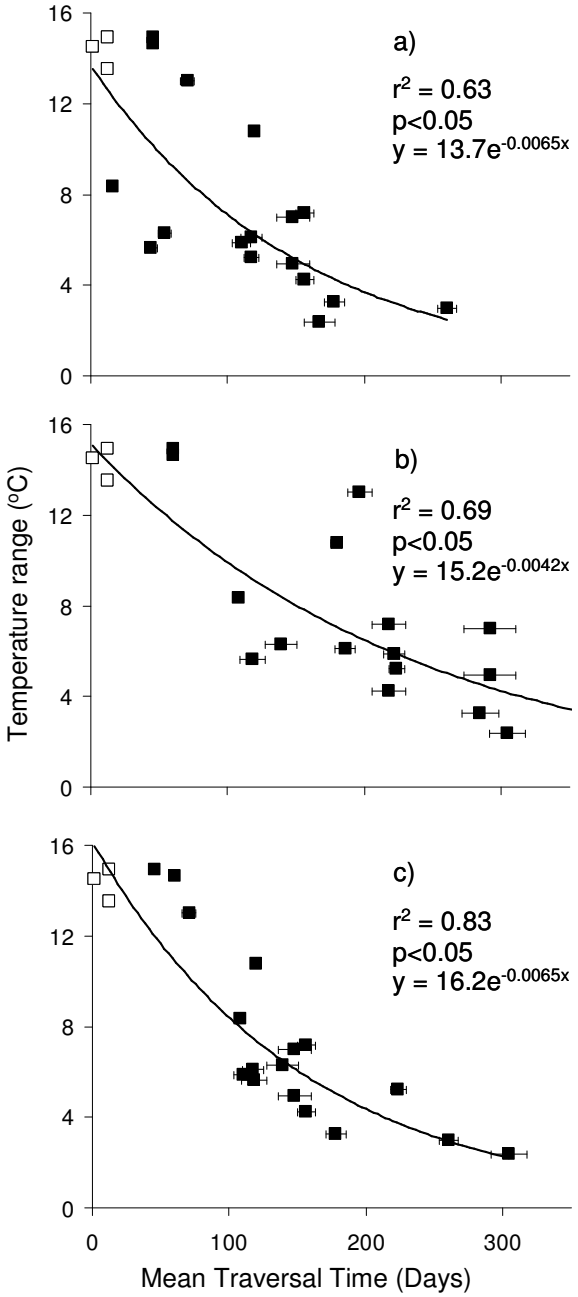

Figure 3.7. Annual temperature range (°C) derived from well temperature logger data versus mean matrix traversal time (days) to the location of the temperature logger. a) Mean matrix traversal time to the shallow aquifer model node, b) deep aquifer model node, and c) shallow or deep aquifer model node corresponding to the temperature logger deployment depth. White squares are surface water locations. Error bars represent ±1SE.

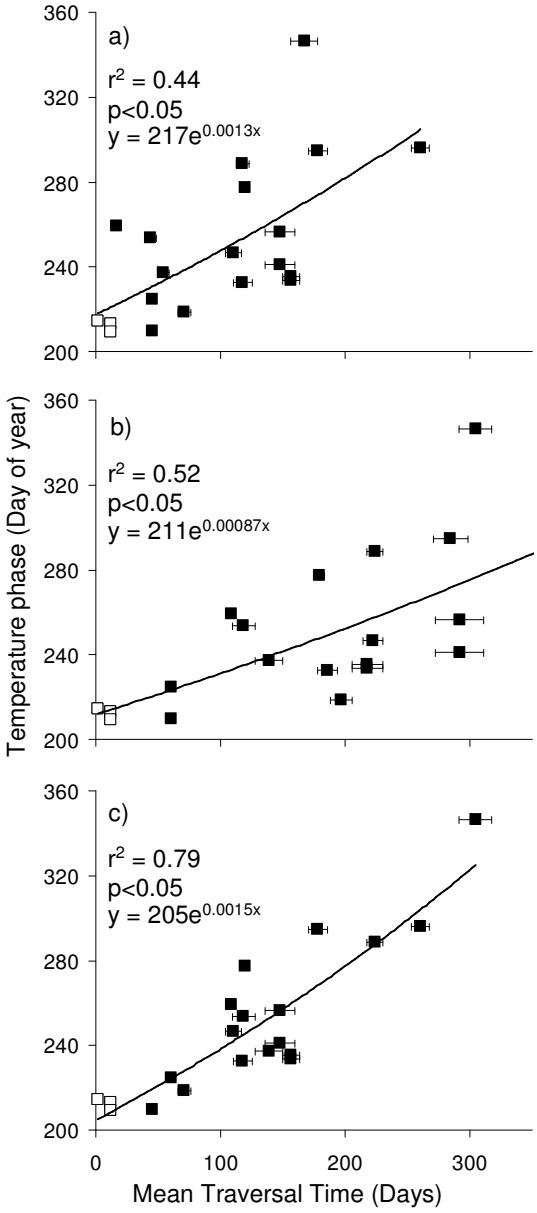

Figure 3.8. Annual temperature phase (i.e., day of the year peak temperature occurs, Jan 1st = 0) derived from well temperature logger data versus mean matrix traversal time (days) to the location of the temperature logger. a) Mean matrix traversal time to the shallow aquifer model node, b) deep aquifer model node, and c) shallow or deep aquifer model node corresponding to the temperature logger deployment depth. White squares are surface water locations. Error bars represent ±1SE.

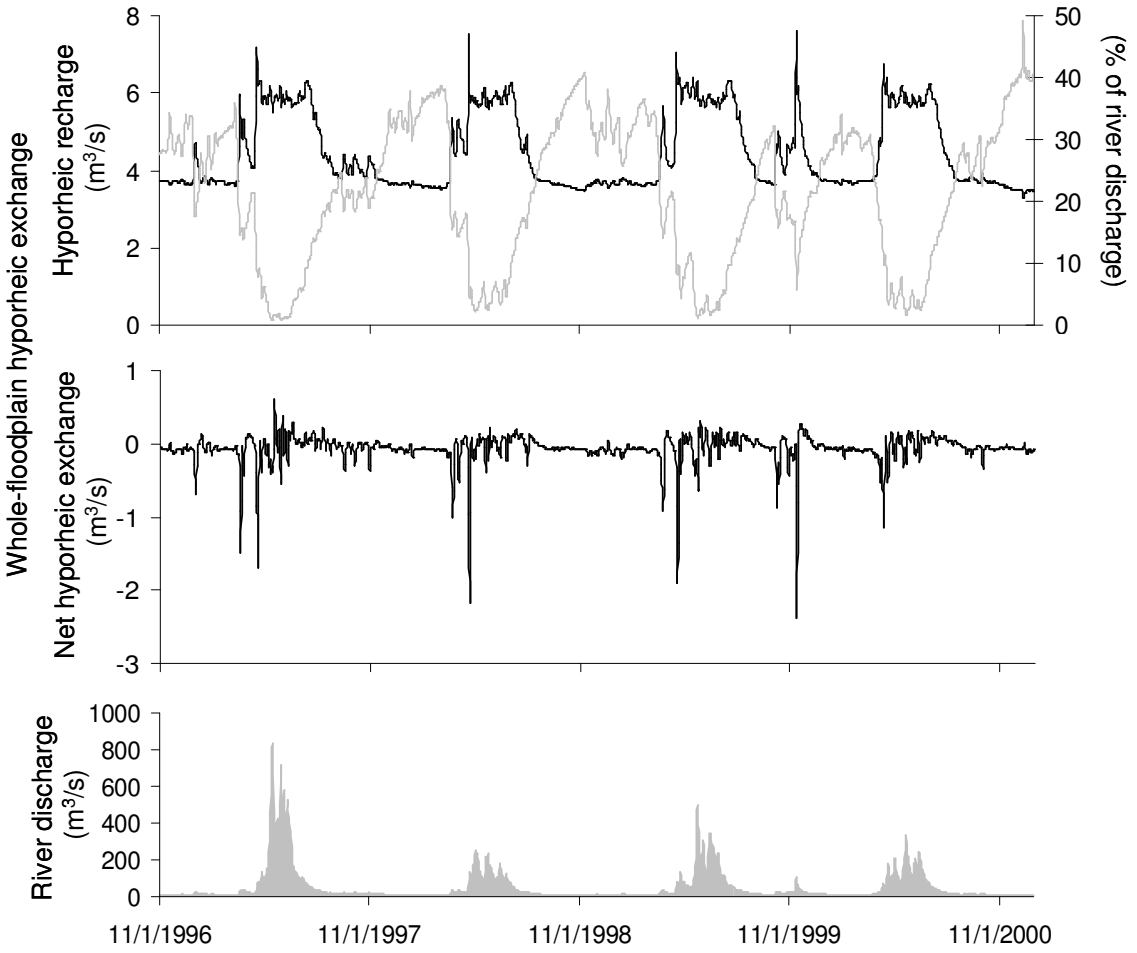

Figure 3.9. Whole-floodplain hyporheic recharge a) as a flux (m^3/s) (black line) and as a percent of river discharge (gray line), and b) net hyporheic exchange (m^3/s). c) Hydrograph for Middle Fork Flathead River at the floodplain inlet.

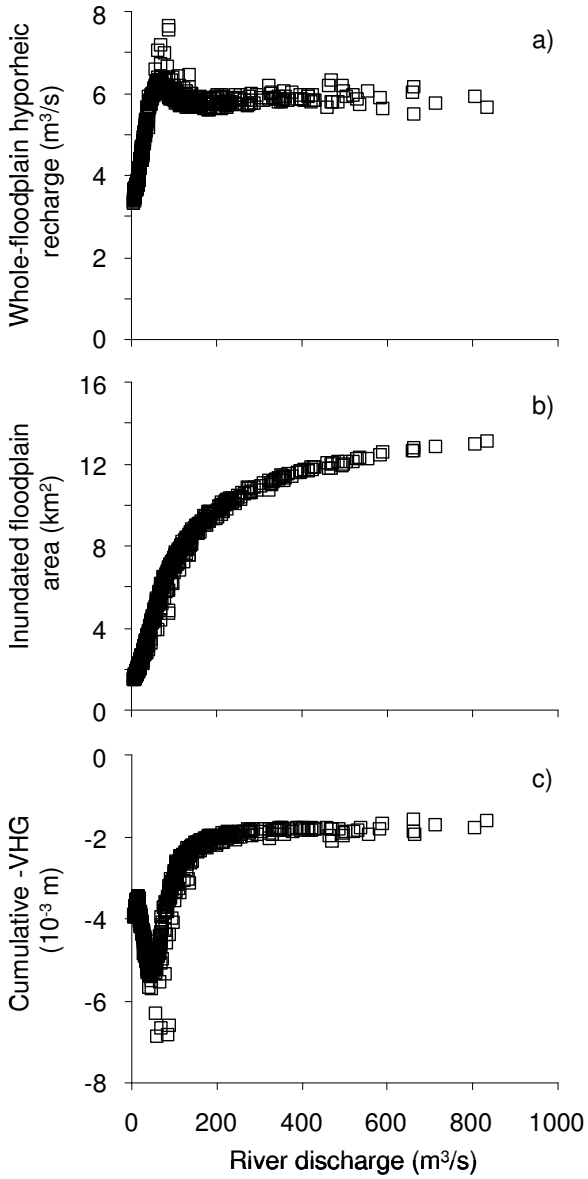

Figure 3.10. a) Whole-floodplain hyporheic recharge, b) inundated floodplain area, and c) cumulative vertical hydraulic gradient (VHG) versus river discharge at the floodplain inlet. Cumulative VHG was calculated as the sum of vertical hydraulic gradients weighted by inundated area across all model patches with net hyporheic recharge (i.e., negative vertical hydraulic gradients).

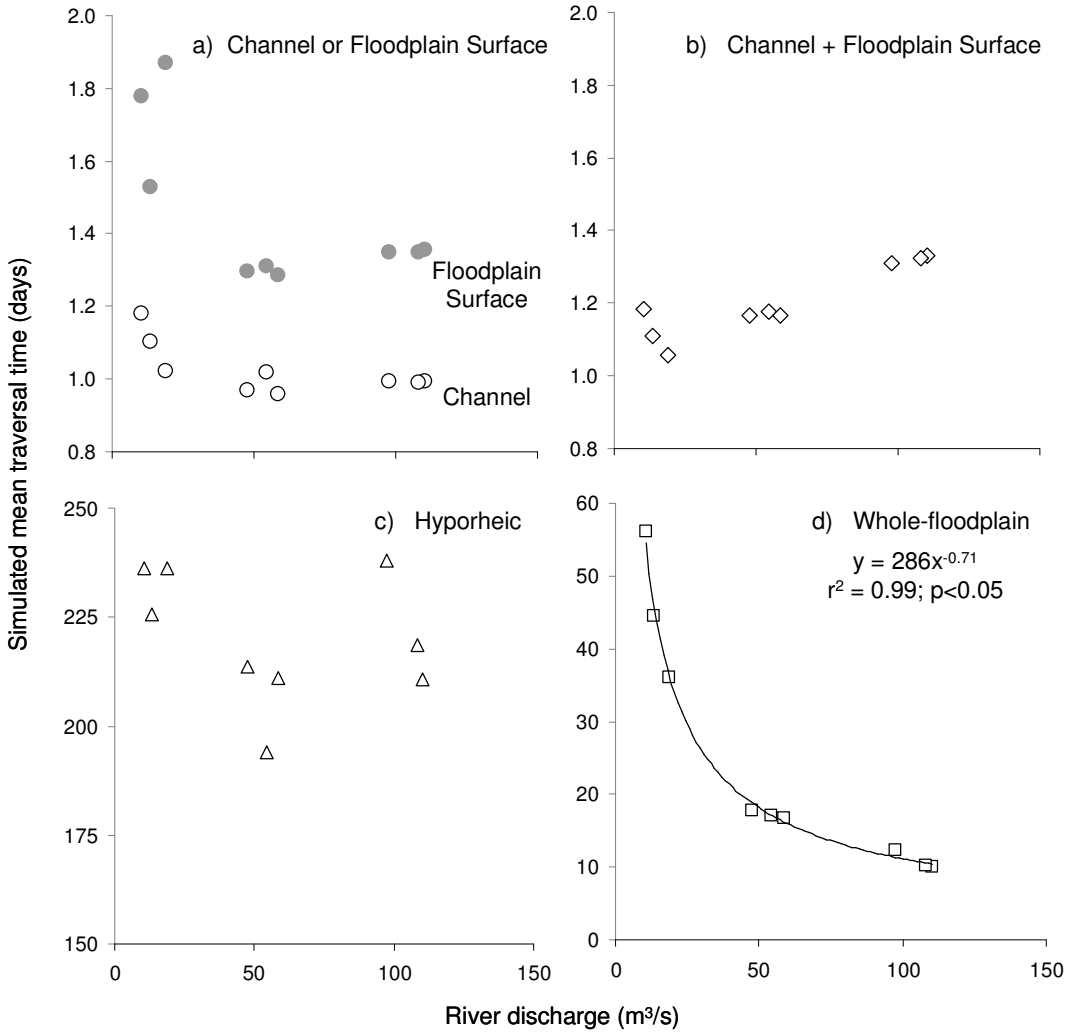

Figure 3.11. Mean matrix traversal time (days) versus river discharge at the time of particle release for a) main river channel (white circles) and floodplain surface (gray circles) particles, b) surface particles (i.e., river channel and floodplain surface particles combined), c) hyporheic particles, and d) all particles released (i.e., the whole-floodplain mean matrix traversal time).

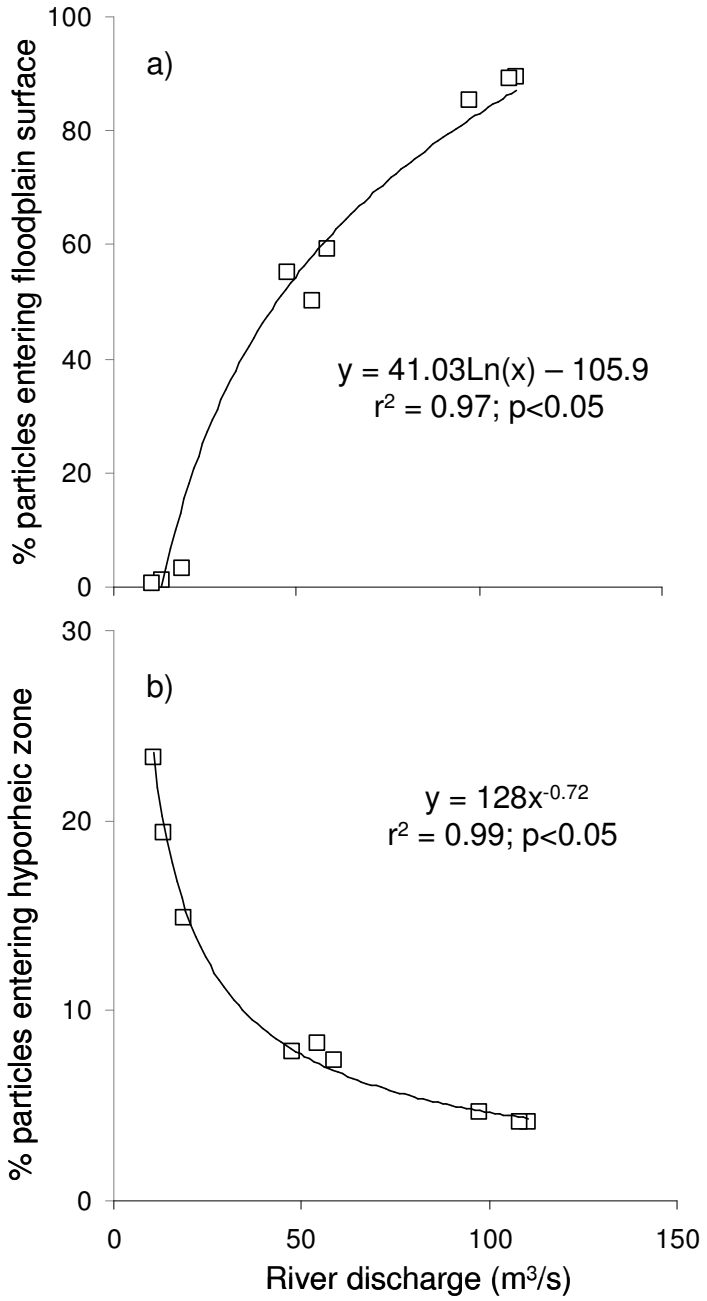

Figure 3.12. Percent of particles that leave the river channel and a) enter the floodplain surface and b) enter the hyporheic zone, versus river discharge at the time of particle release (m^3/s).

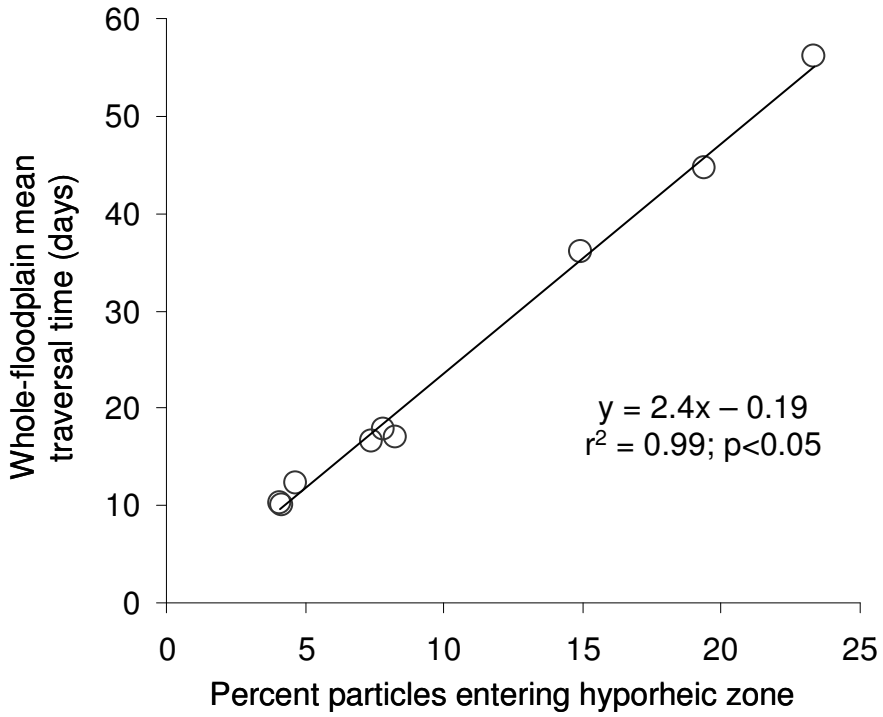

Figure 3.13. Whole-floodplain mean matrix traversal time versus percent of particles that enter the hyporheic zone.

CHAPTER 4

DISSOLVED ORGANIC CARBON DYNAMICS WITHIN THE HYPORHEIC ZONE OF AN ALLUVIAL RIVER-FLOODPLAIN SYSTEM[1]

---

[1] Ashley M Helton, Meredith S Wright, Emily S Bernhardt, Geoffrey C Poole, Rose M Cory, and Jack A Stanford. To be submitted to Limnology and Oceanography.

Abstract

We assessed how residence time in the hyporheic zone altered the quality and quantity of dissolved organic carbon (DOC) in a large alluvial river-floodplain ecosystem. We measured DOC concentration, bioavailable DOC (using laboratory assays), and optical properties of DOC in hyporheic well water sampled throughout the Nyack Floodplain of the Middle Fork Flathead River in Northwest Montana during 10 sampling events in 2008 and 2009. DOC concentrations (mean = 480 μgL^{-1}) and bioavailability (mean = 11%) were typically low. Time-averaged DOC concentration and bioavailable DOC were uncorrelated, but correlations existed for some sampling events, especially during spring and summer. Parallel Factor Analysis of fluorescence Emission-Excitation Matrices revealed two humic-like and two amino acid-like fluorescence groups. DOC concentration and humic-like fluorescence groups decreased with matrix traversal time (MTT), a surrogate measure of hyporheic residence time derived from a hydrologic model of the Nyack Floodplain and alluvial aquifer. However, bioavailable DOC (both as mass and as a percent of DOC concentration) as well as fluorescence metrics indicative of bioavailability (percent of amino acids and fluorescence index) increased with MTT. Although the carbon-poor, oxygen-rich Nyack hyporheic zone is a net sink for DOC, recalcitrant DOC is replaced with more bioavailable DOC along hyporheic flow paths, increasing the lability of DOC transported to downstream ecosystems.

Introduction

Carbon (C) cycling within river ecosystems is an important component of the global C cycle (Cole et al. 2007; Battin et al. 2008). Dissolved organic C (DOC) is typically the dominant form of organic C within river water (Findlay and Sinsabaugh 1999), but DOC is composed of a

complex assortment of molecules with a wide range of bioavailability (Volk et al. 1997; Seitzinger et al. 2005). DOC composition varies widely across space and time depending on the relative contribution of different organic source materials, photochemical and microbial alteration, and sorption onto mineral surfaces.

The fraction of DOC available for microbial degradation (i.e., bioavailable DOC; defined here as the fraction of DOC depleted in laboratory assays) for any specific river and time is highly variable (e.g., 2 – 67%; average 25%; Wiegner et al. 2006), and is generally not correlated to bulk DOC concentrations (del Geiorgia and Davis 2003). Bioavailable DOC of surface water varies temporally and spatially among watershed land use types (Weigner and Seitzinger 2004; Agren et al. 2008), and along the river corridors (Sun et al. 1997).

Within streams and rivers, hyporheic zones (where surface and subsurface waters are exchanged bidirectionally) are important sites for C cycling (Findlay 1995). Hyporheic zones increase water residence times within rivers (e.g., Chapter 2), increasing contact time between bioreactive solutes (e.g., DOC) and microbial biofilms (Bencala 2000). Indeed, hyporheic zone microbial processing can account for the majority of whole ecosystem respiration (Fellows et al. 2001), and play substantial roles in nutrient transformations (Dahm et al. 1998).

Researchers have observed predictable patterns of DOC and associated electron acceptors along hyporheic flow paths (Hedin et al. 1998; Baker et al. 1999), consistent with microbially-mediated degradation of organic materials. Considerable evidence shows that DOC concentration often declines as water flows through the hyporheic zone (Vervier and Naiman 1992; Findlay et al. 1993; Hedin et al. 1998), and in some cases bioavailability may be reduced as well (Sobzack and Findlay 2002; Marmonier et al 1995). Measures of microbial metabolism are consistent with these patterns: they tend to be lower at the end of hyporheic flow paths (Jones

et al 1995; Craft et al. 2002). Physical sorption of DOC to mineral surfaces (McKnight et al. 1992; Fiebig 1997; Findlay and Sobczak 1996) or groundwater dilution (Lapworth et al. 2009; Foulquier et al. 2010) may also contribute to DOC declines along hyporheic flow paths. In other river systems, the hyporheic zone may be an important source for DOC through degradation of particulate organic matter stored in sediments (Schindler and Krabbenhoft 1998), groundwater inputs (Battin et al. 2003), or leaching from the terrestrial ecosystem (Clinton et al. 2007).

Recent studies have used fluorescence Excitation-Emission Matrices (EEMs) combined with Parallel Factor Analysis (PARAFAC) to characterize the chemical composition of DOC (Stedmon and Bro 2008). PARAFAC, a multivariate modeling approach, reduces three-dimensional EEMs into several two-dimensional components that represent different dissolved organic matter functional groups (e.g., amino acids, humic materials, fulvic acids). PARAFAC has been used to characterize DOC fluorescence within a wide range of environments (lakes, Cory and McKnight 2005; marine, Murphy et al. 2008; streams, Fellman et al. 2009; wetlands, Yamashita et al. 2010). PARAFAC components have been used to trace changes in DOC production and consumption along environmental gradients (Murphy et al. 2008; Fellman et al. 2009; Yamashita et al. 2010) and within the laboratory (Stedmon and Markanger 2005; Cory et al. 2007). Thus, PARAFAC provides a useful tool for tracking dynamics of different types of dissolved organic matter, which has the potential to elucidate patterns not evident in bulk DOC concentration measurements alone.

Several studies have directly investigated either DOC bioavailability (Marmonier et al 1995; Baker et al. 2000; Sobczak and Findlay 2002) or fluorescence characteristics (Miller et al. 2006; Mladenov et al. 2008; Lapworth et al. 2009) along subsurface flow paths. Although Fellman et al. (2009) found that amino acid PARAFAC components were positively related to

bioavailable DOC in stream channel water, we are unaware of published research that compares measures of hyporheic DOC bioavailability with fluorescence characteristics. This paper reports results from such comparisons in the hyporheic zone of the Nyack Floodplain on the Middle Fork of the Flathead River, Montana, USA (Figure 4.1).

The hyporheic zone of the Nyack Floodplain is extensive (5 to 25 m deep and up to 1.5 km wide, see Site Description, below), which provides a wide range of hyporheic water residence times (from seconds to months, Diehl 2004; Helton Chapter 2). The Nyack has consistently low DOC concentrations (< 2 mg/L). (DOC concentrations in streams and rivers typically ranges from 0.5 mg/L to 50 mg/L, del Geiorgia and Davis 2003) Previous research within the Nyack hyporheic zone also suggests potentially important gradients in C cycling: *In situ* acetate additions suggest the hyporheic zone is increasingly C-limited (Craft et al. 2002) and bacterial and fungal biovolume decrease (Ellis et al. 1998) with distance from the river channel. Despite apparent C-limitation, an extensive food web with over 70 taxa of interstitial invertebrates exists within the alluvial aquifer of the Nyack Floodplain (Stanford et al. 1994).

Low DOC concentrations and observed gradients in hyporheic C-limitation combined with the wide range of hyporheic water residence times in the Nyack Floodplain suggest multiple approaches to investigate DOC may elucidate patterns of DOC quality within the hyporheic zone that cannot be explained by bulk DOC measurements alone. Here, we report combined measurements of DOC concentration, bioavailable DOC laboratory assays, and PARAFAC modeling of fluorescence EEMs to trace changes in the concentration and chemical quality of DOC among hyporheic waters sampled across seasons and throughout the Nyack Floodplain. We predicted that the relationship between DOC quantity and quality would vary seasonally with seasonal changes in DOC inputs (e.g., leaf fall, snow melt). To determine the influence of the

hyporheic zone on DOC dynamics, we evaluated the effects of hyporheic water residence time on DOC quantity and quality within the Nyack Floodplain. Because hyporheic zones can play substantial roles in whole river ecosystem processes, the influence of the hyporheic water residence time on DOC dynamics is important for understanding the effects of DOC transported to downstream ecosystems.

Methods

Site description

The Nyack Floodplain is a 10 km^2 gravel- and cobble-bedded anastomosed alluvial montane floodplain on the Middle Fork of the Flathead River located in northwest Montana (Figure 4.1). Farming and modest riparian logging have occurred on the floodplain over the last 100 years and a railroad and highway traverse the eastern portion of the floodplain, but the river is unregulated and most of the upstream catchment is in federally protected wilderness, including the hillslopes adjacent to the floodplain. The floodplain is constrained laterally by bedrock valley walls and bounded upstream and downstream by canyon segments with bedrock streambeds. This fifth-order river has a snow-spate driven hydrograph with a mean discharge of 80 m^3/s and mean peak discharge of 600 m^3/s. Complex channel morphology and coarse, well-sorted sediments on the floodplain facilitate high rates of surface-subsurface water flux, creating an extensive hyporheic zone that ranges from ~5 to >25 meters in depth and spans the width of the floodplain (up to 1.5 km). Acoustic Doppler profiler data indicate that the main channel of the river loses ~30% of its base-flow discharge to the underlying alluvial aquifer as it flows across the first 1/3 of the floodplain (Mark Lorang, unpublished data). That water flows downstream within the hyporheic zone and later re-emerges to the floodplain surface in the main

channel or in spring channels scattered across the floodplain, which rejoin the main river channel before entering the downstream canyon (Stanford et al. 1994; Poole et al. 2006). Patterns of surface and subsurface exchange are complex, and vary seasonally as surface water inundates the floodplain (Poole et al. 2006).

Sampling design

We sampled two surface water sites and 12 wells that span a range of lateral and longitudinal positions within the Nyack Floodplain (Figure 4.1) during 10 sampling events from July 2008 to October 2009. Sampling events spanned spring, summer, and fall seasons and a range of river discharges. Surface water sites were located in the main river channel at the inlet and outlet of the floodplain.

Immediately prior to collecting each sample, wells were pumped with a hand-operated diaphragm pump until water ran clear, and then wells were pumped using a 12V electric submersible pump (Whale Submersible 881, Whale Systems Specialists) until dissolved oxygen measurements stabilized. Wells were sampled according to Reid (2007) using a modified straddle packer design to sample at discrete depth intervals. We inserted the submersible pump into a flexible hose that was sealed at the bottom and slotted near the bottom over a 1 m interval to allow the pump to pull water through the hose. Foam packers were inserted around the hose above and below the slotted section, flush with the well casing to limit pumping of water from depths above and below the slotted interval. We raised and lowered the hose with attached packers within the well to sample discrete depths. Each well was sampled at an upper depth (at or near the water table) and a lower depth (at least two meters below the water table).

Physical and chemical analyses

In the field, we measured dissolved oxygen, specific conductance, temperature (YSI 85) and pH (YSI pH100). We collected water for chemical analyses in acid-washed and sample-rinsed polycarbonate or glass bottles. We filtered (0.45 μm nitrocellulose) approximately 200 ml of each sample in the lab within 48 hours of collection for dissolved solute analyses. When samples could not be immediately analyzed, they were frozen and analyzed within three months. We measured nitrate, ammonium, orthophosphate, sulfate, and total dissolved nitrogen (via persulfate digestion) according to standard methods (APHA 1998).

Bioavailable DOC assays

We conducted three-day, dark, oxic laboratory assays using methods similar to Servais et al. (1989) and McDowell et al. (2006), in which we measured initial and final DOC concentrations, and headspace CO_2 production. Within 48 hours of field collection approximately 200 ml of each sample was filtered through a 0.22 μm nylon membrane filter pre-rinsed with ~100 ml of distilled deionized water and ~50 ml of sample. Filtered samples were either frozen or assays were conducted within 48 hours of sample collection. To assess the potential effects of freezing the samples, we analyzed a subset of frozen samples pre- and post-freezing. Freezing did not significantly change measurements of initial or final DOC concentrations ($t = -1.50$, $p = 0.19$, $df = 5$) although CO_2 production decreased significantly with freezing ($t = 3.06$, $p<0.05$, $df = 5$; mean CO_2 decrease with freezing was 858 ppmv).

Assays were conducted in 40 ml glass vials with gas tight septa. For each assay, we added 25 ml of filtered sample and 250 μl of groundwater inoculum, which was prepared by mixing equal volumes of unfiltered well and surface water samples. Fresh samples were

inoculated with groundwater collected on the corresponding sampling event. Frozen samples were inoculated with groundwater from the sampling event closest to the date assays were conducted. The maximum time between inoculum and sample collection was two months. The lack of statistically significant differences in DOC concentrations between assays conducted with fresh versus frozen samples suggests that using inocula made on different dates was not a significant source of variance in the results. Assays were also amended with 50 µl of nutrient solution (0.1% NH_4NO_3 and 0.1% K_2HPO_4) to ensure that N, K and P availability were not limiting. The vials were capped and incubated in the dark at room temperature (~20^oC) for three days.

For each sample, we conducted four assays. One assay was inoculated, amended with nutrients, and immediately acidified with 50 µl phosphoric acid to measure initial DOC concentration. Two assays were inoculated and amended with nutrients. One assay was amended with nutrients, but not inoculated. Although these un-inoculated assays were intended to function as controls, random DAPI cell counts (Porter and Feig 1980) show low levels of microbial contamination (Helton unpublished data), so these data are not reported here We also included two sets of experimental blanks for each sampling event: 1) nutrient-amended distilled water and 2) inoculated, nutrient-amended distilled water. After three days, headspace gas samples were analyzed for CO_2 and each assay was acidified with 50 µl phosphoric acid and analyzed for final DOC concentration. DOC concentrations were analyzed via combustion (APHA 1998) with a Shimadzu Total Organic Carbon analyzer and CO_2 concentrations were analyzed with a SRI Greenhouse Gas Chromatograph.

We calculated two bioavailable DOC metrics: DOC depleted and CO_2 produced. DOC depleted (ΔDOC) was calculated as the initial DOC (µg/L) minus the final DOC (µg/L)

concentrations measured in each set of assays. CO_2 produced (ΔCO_2) was calculated as the final CO_2 measured in the headspace (ppmv) minus the initial CO_2 concentration in the headspace (ppmv). Initial CO_2 was estimated as an average of CO_2 measured within the headspace of the experimental blanks. Blank CO_2 values were not significantly different than values measured from the headspace of initial assays ($t = 1.16$, $p = 0.25$, $df = 28$). ΔDOC and ΔCO_2 reported for each sample are the averaged values from the two inoculated assays. We also calculated $\%\Delta$DOC and $\%\Delta CO_2$ by dividing ΔDOC and ΔCO_2, respectively, by initial DOC concentration and multiplying by 100.

Optical measurements and analyses

We measured UV-visible absorbance at 254 nm for each sample and calculated specific UV absorbance ($SUVA_{254}$) by dividing UV absorbance by DOC concentration (APHA 1998). $SUVA_{254}$ is a measure of aromatic carbon content of the DOC (Weishaar et al 2003). Larger SUVA values are typically associated with more recalcitrant terrestrial C sources whereas smaller SUVA values are associated with more labile aquatic C sources.

We used fluorescence spectroscopy to measure fluorescence Emission-Excitation Matrices (EEMs) in triplicate for bioavailable DOC assays conducted for 2009 sampling events ($n = 793$) (Fluorlog-3; Horiba, Jobin Yvon) (5 nm slit width at a 0.4 second integration time). Fluorescence spectroscopy traces dissolved organic matter dynamics in aquatic systems since the concentration and chemical composition of dissolved organic matter influences the intensity and shape of fluorescence spectra (Stedmon and Bro 2008). EEMs were created by measuring fluorescence intensity across excitation wavelengths 240 to 450 nm (5 nm increment) and across

emission wavelengths 140 to 950 nm (2 nm increment), and were corrected for instrument bias and Raman normalized using the area under the water Raman peak at excitation 350 nm.

From each EEM, we calculated the Fluorescence Index (FI) (McKnight et al. 2001). The FI characterizes the slope of an emission curve as the ratio of the emission intensity at a wavelength of 450 nm to that at 500 nm, obtained at an excitation wavelength of 370 nm. Higher FIs indicate more labile autochthonous microbially-derived organic matter (e.g., 1.56 to 1.9, Fulton et al. 2004; McKnight et al. 2001; Schwede-Thomas et al. 2005) and lower FIs indicated more recalcitrant terrestrially derived organic matter (1.15 to 1.4, McKnight et al. 2001; Schwede-Thomas et al. 2005).

We also used Parallel Factor Analysis (PARAFAC), a multivariate data analysis technique, to reduce the EEMs into unique fluorescence groups representing chemically independent components that describe the total EEM (Stedmon et al. 2003). PARAFAC components are related to the composition of dissolved organic matter (ie humics, amino acids, etc), and provide a more complete representation of each EEM than traditional peak picking methods (ie Fluorescence Index). PARAFAC was conducted according to Stedman and Bro (2008) using the DOMFluor toolbox in MATLAB R2008b (Mathworks). Prior to PARAFAC, EEM wavelength ranges were reduced to excitation 250 to 450 nm and emission 320 to 550 nm, and Raleigh scatter was deleted from EEMs.

Calculation of hyporheic residence time

As a surrogate measure of hydrologic travel time from the river channel, through the hyporheic zone, to each sampling well, we used mean matrix traversal time (MTT), developed by Helton (Chapter 2, this dissertation). To calculate MTT, we implemented a three-dimensional

link and node hydrologic model for water flux and storage within the Nyack Floodplain surface and subsurface (Chapter 2). MTT represents the time required for a water molecule to traverse the three-dimensional lattice network (representing the Nyack Floodplain surface, hyporheic zone, and alluvial aquifer) to a sampling location (e.g., a well) based on this hydrologic simulation.

The model was implemented across years (1996 thru 2000) that encompassed a range flow conditions (e.g., high, median, and low flood spates). We conducted 9 particle releases within the model; three during base flow, three during rising limbs, and three during falling limbs of annual hydrographs (Chapter 2). The MTT was calculated from the particle releases as the mean amount of time (across all nine scenarios) that a particle spent in the modeled representation of the floodplain before it reached each of the sampling wells. See Chapter 2 for a detailed description of modeling methods. We believe that MTT yields an overestimate floodplain residence time at any given location because particles are forced to travel along modeled links between model nodes, even where links are not perpendicular to isopleths of groundwater head. Thus, MTT is a measure of relative, not absolute, hyporheic residence time.

Data Analysis

Simple linear regressions and t-tests were performed using R-Statistical Software (Version 2.2.4, R Foundation for Statistical Computing 2005). PARAFAC components were log-transformed before statistical analyses. Unrealistically high DOC concentrations measured in experimental blanks and assays from 8 October 2008 indicate these samples were contaminated with C and were therefore excluded from the analyses. Because of sample processing time constraints, headspace CO_2 was not analyzed for 16 September 2009 assays.

Results

DOC bioavailability assays

DOC concentrations were low throughout the sampling period (mean: 480, range: 220 – 1250 μg L^{-1}). Mean DOC concentration (i.e., time averaged DOC concentration across all sampling dates at each sampling location) was not correlated to mean ΔDOC or ΔCO_2 (Table 4.1). Mean SUVA decreased with both mean ΔDOC and ΔCO_2 (Table 4.1). Mean ΔDOC and ΔCO_2 were positively correlated, but ΔCO_2 was almost always higher than ΔDOC (Figure 4.2). Higher CO_2 production (ΔCO_2) relative to DOC depletion (ΔDOC) in the assays is likely due to high concentrations of dissolved inorganic carbon (DIC) within the hyporheic zone. Indeed, ΔCO_2 was strongly correlated to DIC concentration ($r^2 = 0.60$; $p<0.001$) whereas ΔDOC was not. Percent ΔDOC ranged from -18% to 59% (mean = 11%), and $\%\Delta CO_2$ ranged from -10% to 146% (mean = 58%). Mean DOC concentration was not correlated to mean %ΔDOC and was negatively correlated to mean $\%\Delta CO_2$ ($r^2 = 0.27$; $p = 0.01$).

Relationships between ΔDOC, ΔCO_2, SUVA and DOC concentration varied between sampling events (Table 4.1). ΔDOC and ΔCO_2 were positively correlated for July sampling events in both years, but were not significantly correlated to each other for the remaining sampling events (again, likely due to the influence of DIC on ΔCO_2). ΔDOC was negatively correlated to SUVA and positively correlated to DOC concentration for July sampling events in both years. ΔDOC was also correlated with SUVA during August 2008, May 2009, and September 2009 sampling events and DOC concentration during August 2009 and October 2009 sampling events. All significant relationships between any pair of variables (time averaged and by sampling event) were in the same direction. Fourteen of the 17 significant correlations occurred during the growing season (May thru August), and all five possible relationships were

significant for both July 2008 and July 2009 sampling events. Additionally, DOC and ΔDOC averaged across locations for each sampling date increased with log-transformed channel discharge (USGS #12358500 Middle Fork Flathead River) (DOC, $r^2 = 0.83$, $p<0.001$; ΔDOC, $r^2 = 0.51$, $p<0.001$) (Figure 4.3).

PARAFAC model

We identified four fluorescent components with the PARAFAC model after removal of outliers EEMs and validated the model using the split-half and random initialization methods (Stedmon and Bro 2008) (Figure 4.4). Comparing the components to previously published PARAFAC models, we found that component 1 (C1) and component 2 (C2) have fluorescence characteristics similar to humic-like material (Table 4.2) and were positively correlated ($r^2 = 0.98$, $p<0.001$). Component 3 (C3) and component 4 (C4) have fluorescence characteristics similar to amino acids (Table 4.2), but were not correlated ($p = 0.65$). C3 was not correlated with any of the other components (C1, p =.0.24; C2, p =0.25), and C4 increased with both C1 ($r^2 = 0.59$, $p < 0.001$) and C2 ($r^2 = 0.56$, $p < 0.001$).

Within assays, approximately half of the component values decreased from initial to final samples (C1: 56%, C2:58%, C3:54%, and C4:42% of assays). The changes in component values from initial to final samples (ie initial F_{max} minus final F_{max}) were not significantly different from zero for any of the four components (C1, $t = 0.62$, $p = 0.54$; C2, $t = 1.02$, $p = 0.31$; C3, $t = 0.14$, $p = 0.89$; C4, $t = -1.39$, $p = 0.17$; $df = 91$). Initial and final values were correlated for C1 ($r^2 = 0.90$), C2 ($r^2 = 0.85$), C3 ($r^2 = 0.21$) and C4 ($r^2 = 0.35$) ($p<0.001$).

Mean DOC concentration was positively correlated with mean component values (C1, $r^2 = 0.85$; C2, $r^2 = 0.87$; C4, $r^2 = 0.44$, $p<0.001$), and negatively correlated to FI ($r^2 = 0.28$, p =

0.006). Mean SUVA was also positively correlated with C1 ($r^2 = 0.57$, $p<0.001$), C2 ($r^2 = 0.52$, $p<0.001$), and C4 ($r^2 = 0.21$, $p=0.02$). However, neither average ΔDOC nor ΔCO_2 were significantly correlated with any of the four components or FI ($p>0.05$).

Mean traversal time

DOC metrics were correlated to mean matrix traversal time (MTT), a surrogate for hydrologic residence time in the hyporheic zone. Mean DOC concentration and SUVA declined with MTT (Figure 4.5), while mean ΔDOC and ΔCO_2 increased with MSTT (Figure 4.6). Mean $\%\Delta$DOC and $\% \Delta CO_2$ also increased with MTT (Figure 4.7).

PARAFAC humic-like components, C1 and C2, decreased with MTT whereas amino-acid like components, C3 and C4, were not related to MTT (Figure 4.8). Fluorescence Index ranged from 1.20 to 1.75 and increased with MTT (Figure 4.9a). Percent amino acids also increased with MTT (Figure 4.9b).

The relationships between MTT and DOC concentration, ΔDOC, ΔCO_2, (Table 4.3) and PARAFAC components (Table 4.4) varied among sampling events. Correlations were negative between MTT and DOC concentration for 3 and SUVA for 5 of 9 sampling events. Correlations were positive between MTT and ΔDOC and $\%\Delta$DOC for 3, ΔCO_2 for 4, and $\%\Delta CO_2$ for 7 sampling events. PARAFAC components C1, C2, and C4 generally decreased MTT. Both FI and percent amino acids increased with MTT for 2 out of 5 sampling events. All significant relationships between any pair of variables (time-averaged and by sampling event) were the same direction.

Other physical and chemical variables were also correlated to MTT. MTT was positively correlated with mean nitrate ($r^2 = 0.15$, $p=0.05$), and negatively correlated with mean sulfate ($r^2 =$

0.21, p = 0.03) and mean dissolved oxygen (r^2 = 0.13, p = 0.05). MTT was also negatively correlated with mean temperature (r^2 = 0.46, p<0.001), and positively correlated to mean specific conductance (r^2 = 0.37, p = 0.002).

Discussion

Spatial DOC dynamics

Our results provide strong evidence that the hyporheic zone had contrasting effects on DOC quantity and DOC quality within the hyporheic zone of the Nyack Floodplain. DOC concentrations decreased with MTT (i.e., a surrogate for hyporheic water residence time) (Figure 4.5, Table 4.3), suggesting that DOC is retained by either or both biological (e.g., hyporheic microbial communities consume available DOC) and geophysical (e.g., physical sorption to hyporheic sediment) processes as water is transported along flow paths. Patterns of DOC depletion along hyporheic flow paths are strongly supported by previous research (Vervier and Naiman 1992; Findlay et al. 1993; Vervier et al. 1993; Marmonier et al. 1995; Hedin et al. 1998; Baker et al. 1999; Sobczak and Findlay 2002). However, we found the opposite pattern with DOC bioavailability: Bioavailable DOC (ΔDOC and ΔCO_2) increased with MTT (in terms of mass, Figure 4.6, and as a percentage of DOC, Figure 4.7). Our results contrast other studies in which high quality DOC at the beginning of flow paths is degraded first, leaving more recalcitrant DOC downstream (e.g., Sobczack and Findlay 2002).

Our PARAFAC components and other optical metrics (i.e., SUVA, FI) shed additional light on our assay results and confirm patterns of increasing DOC lability along hyporheic flow paths. Metrics indicative of more recalcitrant DOC decreased with MTT (SUVA, Figure 4.5; and both humic-like components, Figure 4.8a) suggesting declines in DOC concentration were

likely due to declines in more recalcitrant forms of DOC. While some DOC in the hyporheic zone is degraded by microbial communities, the preferential loss of aromatic DOC (e.g., SUVA) and humic-like DOC (C1 and C2) is indicative of DOC sorption to hyporheic sediments (Marmonier et al. 1995). Conversely, metrics indicative of more labile DOC did not decrease with MTT: amino-acid like components were not correlated with MTT (Figure 4.8b) and percent amino acids and FI both increased with MTT (Figure 4.9). The assay results combined with the PARAFAC results suggest a net depletion of lower-quality humic-like DOC with concurrent production, influx, and/or accumulation of higher-quality amino-acid like and microbially-derived DOC along hyporheic flow paths within the Nyack Floodplain.

Potential mechanisms for increasing bioavailable DOC

There are several potential explanations for the observed increase in bioavailable DOC along hyporheic flow paths.

Leaching from the terrestrial ecosystem provides additional sources of bioavailable DOC. Leaching from terrestrial soils can be a substantial C source to the hyporheic zone (Clinton et al. 2007). However, SUVA (Figure 4.5) and humic-like components (Figure 4.8) decreased with MTT, suggesting that carbon compounds typically associated with terrestrially-derived C likely decreased with increasing hyporheic residence time. Additionally, little root encroachment was observed beneath the water table in soil pits (Alison Appling, Duke University, personal communication).

Because more recalcitrant DOC sorbs to soils, vertically leached DOC to the hyporheic zone may have lower than expected aromatic content (e.g., Qualls and Haines 1992). If the terrestrial ecosystem is responsible for contributing bioavailable DOC, then we would have

expected bioavailable DOC accumulation near the water table. However, we found no relationship between ΔDOC and MTT for time-averaged samples collected near the water table (i.e., upper depth samples, p=0.14), but we did find that ΔDOC significantly increased with MTT for lower depth samples (i.e., at least 2 meters below the water) ($r^2 = 0.80$; $p<0.001$). Thus, our results suggest the terrestrial ecosystem is likely not the primary source responsible for the net increase in bioavailable DOC, but that the increase in bioavailable DOC occurs within the deeper hyporheic zone.

Breakdown of particulate organic matter stored within the hyporheic zone provides an additional source of bioavailable DOC. The hyporheic zone can be an important site for the storage, transport, and breakdown of particulate organic matter (POM) (Metzler and Smock 1990; Pusch 1996; Battin et al. 2003), and the breakdown of stored POM can increase bioavailable DOC within the hyporheic zone (Crocker and Meyer 1987; Schindler and Krabbenhoft 1998). Within the Nyack hyporheic zone large POM pools have been estimated (mean = 1.69 x 105 g C m^{-3}) and may account for a substantial proportion of C fluxes within the hyporheic zone (Reid 2007). Additionally, distinct areas of low dissolved oxygen measured within the Nyack hyporheic zone may be indicative of areas of high microbial activity caused by buried coarse POM (e.g., log jams carried by floods are deposited off-channel and subsequently buried by sedimentation) (Reid 2007). Thus, breakdown of POM may provide a substantial source of bioavailable DOC within the Nyack hyporheic zone.

Internal production of DOC by autochthonous microbial fixation provides an additional source of bioavailable DOC. In situ conditions within the Nyack hyporheic zone, including low DOC (< 2 mg L^{-1}) and high DIC (~30 mg L^{-1}), are conductive to substantial microbial C production via chemoautotrophic pathways, which may represent another important bioavailable

DOC source within the hyporheic zone. For example, high dissolved oxygen, low DOC concentrations, and increases in nitrate with hyporheic residence time indicate potential nitrification. Nitrifiers require oxygen, and have been shown to be inhibited by high C quality (Butturini et al. 2000; Starry et al. 2005), so would likely outcompete heterotrophs in a C-limited system, like the hyporheic zone of the Nyack Floodplain. Using water chemistry measurements, we approximated the potential organic C produced by nitrifiers. Assuming that the range of average nitrate concentrations is an estimate of nitrate produced via nitrification (207 $\mu g\ L^{-1}$) and that the C yield from nitrification is approximately 7% (Glover 1985), a rough estimate of bioavailable DOC production from nitrification is 15 $\mu g\ L^{-1}$, which is about 13% of the observed increase in bioavailable DOC. Thus, nitrification may explain a fraction of bioavailable DOC increase, but not all of it.

Methane (CH_4) is another inorganic C source that may contribute to increasing bioavailable DOC. Methanogenesis reduces DOC to CH_4, which could subsequently be assimilated by microbes, providing bioavailable organic C to downstream ecosystems. Methane-derived C can be an important component of stream food webs (Kohzu et al. 2004; Deines et al. 2007). In fact, measurements of dissolved CH_4 in hyporheic water (Meredith Wright unpublished) and highly depleted ^{13}C within the body mass of hyporheic invertebrates (Reid 2007) both suggest that methanogenesis and methane assimilation may be important C pathways within the hyporheic zone of the Nyack Floodplain.

Bioavailable DOC accumulation: Experimental versus in situ environmental conditions

Since the Nyack hyporheic zone has low DOC concentrations, our finding that bioavailable DOC increases with hyporheic residence time is somewhat surprising given that we

would expect any bioavailable DOC produced to be immediately consumed along a C-limited flow path. The differences between laboratory and *in situ* conditions may provide an explanation: Along the gradient of hyporheic residence times, *in situ* temperatures tend to decrease (during summer sampling events), dissolved oxygen decreases, and microbial biomass likely decreases (Ellis et al. 1998). We conducted laboratory assays at uniform temperatures (much warmer than *in situ* conditions) and dissolved oxygen concentrations (fully saturated; typically higher than *in situ* conditions), and inoculated with equal microbial biomass. Thus, we minimized the environmental gradient observed in the field that may cause *in situ* microbial communities at higher hyporheic residence times to be less capable of using bioavailable DOC, which may allow bioavailable DOC produced at the beginning of flow paths to accumulate within the hyporheic zone to accumulate before upwelling to surface waters.

Temporal DOC dynamics

Although time-averaged bioavailable DOC (ΔDOC) and DOC concentration were not related, we did observe significant positive relationships between bioavailable DOC metrics and DOC concentration during several sampling events (Table 4.1). The mean and range of DOC and ΔDOC were highest during spring and summer sampling events (Figure 4.3), which is typically when observed relationships were significant (Table 4.1). Similarly, other studies have observed higher bioavailable DOC (Weigner and Seitzinger 2004) and steeper gradients in bioavailable DOC along hyporheic flow paths (Marmonier et al. 1995) during spring and summer. We did not observe consistent trends with significance among C metrics and MTT by sampling event, although 56% of the possible relationships were significant (Table 4.3). In the hyporheic zone of the Nyack Floodplain, absolute values of DOC and bioavailable DOC as well

as their relationships to each other and along hyporheic flow paths changed seasonally. Since the quantity and quality of DOC can affect its metabolic role in downstream ecosystems, understanding seasonal changes in DOC quantity and quality are important for understanding larger scale C cycling.

Potential patterns along short Nyack hyporheic flow paths

The current study focused on patterns across well locations that spanned the length of the extensive Nyack hyporheic zone (Figure 4.1). Most studies, conducted on relatively smaller systems, have found the first centimeters to meters of the hyporheic zone can have strong biogeochemical gradients, and the scale at which the study is conducted may determine the conclusions about the effects of the hyporheic zone on the stream ecosystem (Schindler and Krabbenhoft 1998). Indeed, the direction of the trend between our surface water sites (open shapes in Figures 4.5-4.9) and the first well (i.e., well with the shortest MTT; closed shapes in Figures 4.5-4.9) were often the opposite direction of the trend among hyporheic wells sampled along the gradient of MTT. For example, SUVA (Figure 4.5b) and humic-like components (Figure 4.8a) are lower for surface water than for hyporheic samples with lower MTTs. But, ΔDOC (Figure 4.6a) and percent amino acids (Figure 4.9b) are higher for surface water than for hyporheic water with short MTTs. These patterns suggest an accumulation of recalcitrant, possibly terrestrially-derived DOC, and a decrease in bioavailable DOC along the beginning of Nyack hyporheic flow paths. The contradictory patterns between short and long hyporheic flow path dynamics within the Nyack suggest a spatial hierarchy of biogeochemical dynamics, and stress the importance of understanding C cycling at multiple scales, particularly in river systems with extensive and well connected hyporheic zones, like the Nyack Floodplain.

Conclusions

An improved understanding of the controls of DOC quantity and composition within hyporheic habitats will aid in predicting the effects of hyporheic zones on coarser-scale C cycles in river networks. Our metrics provided multiple lines of evidence for a concurrent net decrease in DOC concentration and increase in bioavailable DOC within the extensive hyporheic zone of the Nyack Floodplain. DOC concentrations and metrics indicative of recalcitrant DOC (humic-like DOC fluorescence and SUVA) decreased within the hyporheic zone whereas bioavailable DOC (both as a mass and fraction) and metrics indicative of labile DOC (percent of amino-acids, and fluorescence index) increased within the hyporheic zone. In the Nyack Floodplain, the hyporheic zone may buffer transport of DOC to downstream systems through the sorption of recalcitrant DOC. Conversely, it may be an additional source of bioavailable DOC through microbially-mediated pathways such as chemoautotrophic carbon fixation or POM breakdown. Higher quality DOC supplied from the hyporheic zone to surface water would likely be more rapidly oxidized by downstream communities. These contrasting effects on DOC quantity and quality highlight the potential multiple simultaneous roles the hyporheic zone may play in controlling DOC retention and transport in riverine systems.

Acknowledgments

This research was supported by the Gordon and Betty Moore Foundation for AMH, MSW, ESB, GCP, and JAS, by an EPA Star Fellowship for AMH, and by the Odum School of Ecology for AMH. EPA has not officially endorsed this publication and the views expressed herein may not reflect the views of the EPA. We thank Oriana Grubisic, Rachel Malison, and Tyler Tappenbeck for field assistance, and Kristin Olson and Katie Harrold for laboratory

assistance. Water chemistry and DOC analyses were conducted at the Flathead Lake Biological Station, Polson, MT. This manuscript was improved by comments from John Davis, Cynthia Tant, and Andrew Mehring.

References

Agren, A., I. Buffam, M. Berggren, K. Bishop, M. Jansson, and H. Laudon. 2008. Dissolved organic carbon characteristics in boreal streams in a forest-wetland gradient during the transition between winter and summer. Journal of Geophysical Research-Biogeosciences **113**.

APHA. (1998). Standard method for examination of water and wastewater, Washington DC, American Public Health Association Publication, APHA, AWWA, WEF.

Baker, M. A., C. N. Dahm, and H. M. Valett. 1999. Acetate retention and metabolism in the hyporheic zone of a mountain stream. Limnology and Oceanography **44**:1530-1539.

Baker, M. A., H. M. Valett, and C. N. Dahm. 2000. Organic carbon supply and metabolism in a shallow groundwater ecosystem. Ecology **81**:3133-3148.

Battin, T. J., L. A. Kaplan, S. Findlay, C. S. Hopkinson, E. Marti, A. I. Packman, J. D. Newbold, and F. Sabater. 2008. Biophysical controls on organic carbon fluxes in fluvial networks. Nature Geoscience **1**:95-100.

Battin, T. J., L. A. Kaplan, J. D. Newbold, and S. P. Hendricks. 2003. A mixing model analysis of stream solute dynamics and the contribution of a hyporheic zone to ecosystem function. Freshwater Biology **48**:995-1014.

Bencala, K. E. 2000. Hyporheic zone hydrological processes. Hydrological Processes **14**:2797-2798.

Butturini, A., T. J. Battin, and F. Sabater. 2000. Nitrification in stream sediment biofilms: The role of ammonium concentration and DOC quality. Water Research **34**:629-639.

Clinton, S. M., R. T. Edwards, and R. J. Naiman. 2002. Forest-river interactions: Influence on hyporheic dissolved organic carbon concentrations in a floodplain terrace. Journal of the American Water Resources Association **38**:619-631.

Coble, P. G. 1996. Characterization of marine and terrestrial DOM in seawater using excitation emission matrix spectroscopy. Marine Chemistry **51**:325-346.

Cole, J. J., Y. T. Prairie, N. F. Caraco, W. H. McDowell, L. J. Tranvik, R. G. Striegl, C. M. Duarte, P. Kortelainen, J. A. Downing, J. J. Middelburg, and J. Melack. 2007. Plumbing the global carbon cycle: Integrating inland waters into the terrestrial carbon budget. Ecosystems **10**:171-184.

Cory, R. M., and D. M. McKnight. 2005. Fluorescence spectroscopy reveals ubiquitous presence of oxidized and reduced quinones in dissolved organic matter. Environmental Science & Technology **39**:8142-8149.

Cory, R. M., D. M. McKnight, Y. P. Chin, P. Miller, and C. L. Jaros. 2007. Chemical characteristics of fulvic acids from Arctic surface waters: Microbial contributions and photochemical transformations. Journal of Geophysical Research-Biogeosciences **112**.

Craft, J. A., J. A. Stanford, and M. Pusch. 2002. Microbial respiration within a floodplain aquifer of a large gravel-bed river. Freshwater Biology **47**:251-261.

Crocker, M. T., and J. L. Meyer. 1987. Interstitial Dissolved Organic Carbon in Sediments of a Southern Appalachian Headwater Stream. Journal of the North American Benthological Society **6**:159-167.

Dahm, C. N., N. B. Grimm, P. Marmonier, H. M. Valett, and P. Vervier. 1998. Nutrient dynamics at the interface between surface waters and groundwaters. Freshwater Biology **40**:427-451.

Deines, P., J. Grey, H. H. Richnow, and G. Eller. 2007. Linking larval chironomids to methane: seasonal variation of the microbial methane cycle and chironomid delta C-13. Aquatic Microbial Ecology **46**:273-282.

del Giorgio, P.A., and J. Davis. 2003. Patterns of dissolved organic matter lability and consumption across aquatic ecosystems. In "Aquatic Ecosystems: Interactivity of dissolved organic matter" (S.E.G. Findlay and R.L. Sinsabaugh, eds). Academic Press, San Diego.

Diehl, C. J. 2004. Controls on the magnitude and location of groundwater/surface water exchange in a gravel dominated alluvial floodplain system, northwestern Montana. Unpublished MS Thesis. University of Montana.

Ellis, B. K., J. A. Stanford, and J. V. Ward. 1998. Microbial assemblages and production in alluvial aquifers of the Flathead River, Montana, USA. Journal of the North American Benthological Society **17**:382-402.

Fellman, J. B., E. Hood, D. V. D'Amore, R. T. Edwards, and D. White. 2009a. Seasonal changes in the chemical quality and biodegradability of dissolved organic matter exported from soils to streams in coastal temperate rainforest watersheds. Biogeochemistry **95**:277-293.

Fellows, C. S., H. M. Valett, and C. N. Dahm. 2001. Whole-stream metabolism in two montane streams: Contribution of the hyporheic zone. Limnology and Oceanography **46**:523-531.

Fiebig, D. M. 1997. Microbiological turnover of amino acids immobilized from groundwater discharged through hyporrheic sediments. Limnology and Oceanography **42**:763-768.

Findlay, S. 1995. Importance of Surface-Subsurface Exchange in Stream Ecosystems - the Hyporheic Zone. Limnology and Oceanography **40**:159-164.

Findlay, S., and R. L. Sinsabaugh. 1999. Unravelling the sources and bioavailability of dissolved organic matter in lotic aquatic ecosystems. Marine and Freshwater Research **50**:781-790.

Findlay, S., and W. V. Sobczak. 1996. Variability in removal of dissolved organic carbon in hyporheic sediments. Journal of the North American Benthological Society **15**:35-41.

Findlay, S., D. Strayer, C. Goumbala, and K. Gould. 1993. Metabolism of Streamwater Dissolved Organic-Carbon in the Shallow Hyporheic Zone. Limnology and Oceanography **38**:1493-1499.

Foulquier, A., F. Malard, F. Mermillod-Blondin, T. Datry, L. Simon, B. Montuelle, and J. Gibert. Vertical change in dissolved organic carbon and oxygen at the water table region of an aquifer recharged with stormwater: biological uptake or mixing? Biogeochemistry **99**:31-47.

Fulton, J. R., D. M. McKnight, C. M. Foreman, R. M. Cory, C. Stedmon, and E. Blunt. 2004. Changes in fulvic acid redox state through the oxycline of a permanently ice-covered Antarctic lake. Aquatic Sciences **66**:27-46.

Glover, H. E. 1985. The Relationship between Inorganic Nitrogen Oxidation and Organic-Carbon Production in Batch and Chemostat Cultures of Marine Nitrifying Bacteria. Archives of Microbiology **142**:45-50.

Hedin, L. O., J. C. von Fischer, N. E. Ostrom, B. P. Kennedy, M. G. Brown, and G. P. Robertson. 1998. Thermodynamic constraints on nitrogen transformations and other biogeochemical processes at soil-stream interfaces. Ecology **79**:684-703.

Jones, J. B., S. G. Fisher, and N. B. Grimm. 1995. Vertical Hydrologic Exchange and Ecosystem Metabolism in a Sonoran Desert Stream. Ecology **76**:942-952.

Kohzu, A., C. Kato, T. Iwata, D. Kishi, M. Murakami, S. Nakano, and E. Wada. 2004. Stream food web fueled by methane-derived carbon. Aquatic Microbial Ecology **36**:189-194.

Lapworth, D. J., D. C. Gooddy, D. Allen, and G. H. Old. 2009. Understanding groundwater, surface water, and hyporheic zone biogeochemical processes in a Chalk catchment using fluorescence properties of dissolved and colloidal organic matter. Journal of Geophysical Research-Biogeosciences **114**.

Marmonier, P., D. Fontvieille, J. Gibert, and V. Vanek. 1995. Distribution of Dissolved Organic-Carbon and Bacteria at the Interface between the Rhone River and Its Alluvial Aquifer. Journal of the North American Benthological Society **14**:382-392.

McDowell, W. H., A. Zsolnay, J. A. Aitkenhead-Peterson, E. G. Gregorich, D. L. Jones, D. Jodemann, K. Kalbitz, B. Marschner, and D. Schwesig. 2006. A comparison of methods to determine the biodegradable dissolved organic carbon from different terrestrial sources. Soil Biology & Biochemistry **38**:1933-1942.

McKnight, D. M., K. E. Bencala, G. W. Zellweger, G. R. Aiken, G. L. Feder, and K. A. Thorn. 1992. Sorption of Dissolved Organic-Carbon by Hydrous Aluminum and Iron-Oxides Occurring at the Confluence of Deer Creek with the Snake River, Summit County, Colorado. Environmental Science & Technology **26**:1388-1396.

McKnight, D. M., E. W. Boyer, P. K. Westerhoff, P. T. Doran, T. Kulbe, and D. T. Andersen. 2001. Spectrofluorometric characterization of dissolved organic matter for indication of precursor organic material and aromaticity. Limnology and Oceanography **46**:38-48.

Metzler, G. M., and L. A. Smock. 1990. Storage and Dynamics of Subsurface Detritus in a Sand-Bottomed Stream. Canadian Journal of Fisheries and Aquatic Sciences **47**:588-594.

Miller, M. P., D. M. McKnight, R. M. Cory, M. W. Williams, and R. L. Runkel. 2006. Hyporheic exchange and fulvic acid redox reactions in an alpine stream/wetland ecosystem, Colorado front range. Environmental Science & Technology **40**:5943-5949.

Mladenov, N., P. Huntsman-Mapila, P. Wolski, W. R. L. Masarnba, and D. M. McKnight. 2008. Dissolved organic matter accumulation, reactivity, and redox state in ground water of a recharge wetland. Wetlands **28**:747-759.

Murphy, K. R., C. A. Stedmon, T. D. Waite, and G. M. Ruiz. 2008. Distinguishing between terrestrial and autochthonous organic matter sources in marine environments using fluorescence spectroscopy. Marine Chemistry **108**:40-58.

Poole, G. C. 2002. Fluvial landscape ecology: addressing uniqueness within the river discontinuum. Freshwater Biology **47**:641-660.

Poole, G. C., J. A. Stanford, S. W. Running, and C. A. Frissell. 2006. Multiscale geomorphic drivers of groundwater flow paths: subsurface hydrologic dynamics and hyporheic habitat diversity. Journal of the North American Benthological Society **25**:288-303.

Poole, G. C., J. A. Stanford, S. W. Running, C. A. Frissell, W. W. Woessner, and B. K. Ellis. 2004. A patch hierarchy approach to modeling surface and subsurface hydrology in complex flood-plain environments. Earth Surface Processes and Landforms **29**:1259-1274.

Porter, K. G., and Y. S. Feig. 1980. The Use of Dapi for Identifying and Counting Aquatic Microflora. Limnology and Oceanography **25**:943-948.

Pusch, M. 1996. The metabolism of organic matter in the hyporheic zone of a mountain stream, and its spatial distribution. Hydrobiologia **323**:107-118.

Qualls, R. G., and B. L. Haines. 1992. Biodegradability of Dissolved Organic-Matter in Forest Throughfall, Soil Solution, and Stream Water. Soil Science Society of America Journal **56**:578-586.

Reid, B.L. 2007. Energy flow in a floodplain aquifer ecosystem. Unpublished PhD Thesis. University of Montana.

Schindler, J. E., and D. P. Krabbenhoft. 1998. The hyporheic zone as a source of dissolved organic carbon and carbon gases to a temperate forested stream. Biogeochemistry **43**:157-174.

Schwede-Thomas, S. B., Y. P. Chin, K. J. Dria, P. Hatcher, E. Kaiser, and B. Sulzberger. 2005. Characterizing the properties of dissolved organic matter isolated by XAD and C-18 solid phase extraction and ultrafiltration. Aquatic Sciences **67**:61-71.

Seitzinger, S. P., H. Hartnett, R. Lauck, M. Mazurek, T. Minegishi, G. Spyres, and R. Styles. 2005. Molecular-level chemical characterization and bioavailability of dissolved organic matter in stream water using electrospray-ionization mass spectrometry. Limnology and Oceanography **50**:1-12.

Servais, P., A. Anzil, and C. Ventresque. 1989. Simple Method for Determination of Biodegradable Dissolved Organic-Carbon in Water. Applied and Environmental Microbiology **55**:2732-2734.

Sobczak, W. V., and S. Findlay. 2002. Variation in bioavailability of dissolved organic carbon among stream hyporheic flow paths. Ecology **83**:3194-3209.

Sobczak, W. V., S. Findlay, and S. Dye. 2003. Relationships between DOC bioavailability and nitrate removal in an upland stream: An experimental approach. Biogeochemistry **62**:309-327.

Stanford, J. A., J. V. Ward, and B. K. Ellis. 1994. Ecology of the alluvial aquifers of the Flathead River, Montana. Pages 367-390 in J. Gibert, D. L. Danielopol, and J. A. Stanford, eds. Groundwater Ecology. Academic Press, San Diego, California.

Starry, O. S., H. M. Valett, and M. E. Schreiber. 2005. Nitrification rates in a headwater stream: influences of seasonal variation in C and N supply. Journal of the North American Benthological Society **24**:753-768.

Stedmon, C. A., and R. Bro. 2008. Characterizing dissolved organic matter fluorescence with parallel factor analysis: a tutorial. Limnology and Oceanography-Methods **6**:572-579.

Stedmon, C. A., and S. Markager. 2005. Tracing the production and degradation of autochthonous fractions of dissolved organic matter by fluorescence analysis. Limnology and Oceanography **50**:1415-1426.

Stedmon, C. A., S. Markager, and R. Bro. 2003. Tracing dissolved organic matter in aquatic environments using a new approach to fluorescence spectroscopy. Marine Chemistry **82**:239-254.

Sun, L., E. M. Perdue, J. L. Meyer, and J. Weis. 1997. Use of elemental composition to predict bioavailability of dissolved organic matter in a Georgia river. Limnology and Oceanography **42**:714-721.

Vervier, P., M. Dobson, and G. Pinay. 1993. Role of Interaction Zones between Surface and Ground Waters in Doc Transport and Processing - Considerations for River Restoration. Freshwater Biology **29**:275-284.

Vervier, P., and R. J. Naiman. 1992. Spatial and Temporal Fluctuations of Dissolved Organic-Carbon in Subsurface Flow of the Stillaguamish River (Washington, USA). Archiv Fur Hydrobiologie **123**:401-412.

Volk, C. J., C. B. Volk, and L. A. Kaplan. 1997. Chemical composition of biodegradable dissolved organic matter in streamwater. Limnology and Oceanography **42**:39-44.

Weishaar, J. L., G. R. Aiken, B. A. Bergamaschi, M. S. Fram, R. Fujii, and K. Mopper. 2003. Evaluation of specific ultraviolet absorbance as an indicator of the chemical composition and reactivity of dissolved organic carbon. Environmental Science & Technology **37**:4702-4708.

Wiegner, T. N., and S. P. Seitzinger. 2004. Seasonal bioavailability of dissolved organic carbon and nitrogen from pristine and polluted freshwater wetlands. Limnology and Oceanography **49**:1703-1712.

Wiegner, T. N., S. P. Seitzinger, P. M. Glibert, and D. A. Bronk. 2006. Bioavailability of dissolved organic nitrogen and carbon from nine rivers in the eastern United States. Aquatic Microbial Ecology **43**:277-287.

Yamashita, Y., L. J. Scinto, N. Maie, and R. Jaffe. 2010. Dissolved Organic Matter Characteristics Across a Subtropical Wetland's Landscape: Application of Optical Properties in the Assessment of Environmental Dynamics. Ecosystems **13**:1006-1019.

Table 4.1. Simple linear regression results for ΔDOC and versus DOC concentration, SUVA, and ΔCO_2 by sampling event and averaged across sampling events (time-average). All r^2 and p-values (in parentheses) shown. ND = no data. Direction indicates a positive (+) or negative (-) slope. All slopes derived from correlation between any specific pair of variables were in the same direction.

Sampling Date	[DOC]	SUVA	ΔCO_2
15 Jul 2008	**0.51 (<0.001)**	**0.33 (0.006)**	**0.34 (0.005)**
8 Aug 2008	0.00006 (0.97)	**0.24 (0.05)**	0.0002 (0.95)
10 Sep 2008	0.18 (0.09)	0.02 (0.63)	0.032 (0.48)
20 Apr 2009	0.009 (0.66)	0.006 (0.72)	0.016 (0.56)
28 May 2009	0.16 (0.18)	**0.26 (0.05)**	0.012 (0.72)
15 Jul 2009	**0.90 (<0.001)**	**0.20 (0.04)**	**0.69 (<0.001)**
17 Aug 2009	**0.47 (0.001)**	0.009 (0.70)	0.12 (0.15)
16 Sep 2009	0.06 (0.26)	**0.18 (0.04)**	ND
15 Oct 2009	**0.40 (0.002)**	0.014 (0.61)	0.003 (0.83)
Time-averaged	0.002 (0.85)	**0.47 (<0.001)**	**0.30 (0.007)**
Direction	+	-	+

Table 4.2. Characteristics of the four PARAFAC components identified in this study compared with those previously identified.

Comp-onent	Ex. Max.	Em. Max.	Description	References
1	<250 (350)	476	Terrestrial, humic-like	P3(<260,380/498) - Murphy et al. 2008; C2 (<250, 385/504) – Stedmon and Markager 2005; C (350/420-480) - Coble 1996;
2	<250 (320)	399	Autochthonous and Terrestrial, humic-like	P1 (<260,310/414) - Murphy et al. 2008; C3 (<250, 305/412) & C4 (<250, 360/440) -Stedmon and Markager 2005; A (260 / 380-460) and M (312 / 380-420) - Coble 1996;
3	275	322	Autochthonous, amino acid-like (Tyrosine-like)	AK9 (270/306) – Fellman et al. 2009; P5 (270/310), P6 (275/318) - Murphy et al. 2008; C13 (280/<350) – Cory and McKnight 2005; C8 (275/304) - Stedmon and Markager 2005 B (275/310) - Coble 1996
4	<250 (290)	342	Autochthonous, amino acid-like (Tryptophan-like)	AK10 (280/336) – Fellman et al. 2009; P7 (280/342) - Murphy et al. 2008; C8 (270/<350) – Cory and McKnight 2005; C7 (280/344) – Stedmon and Markager 2005 T (275/340) - Coble 1996;

Table 4.3. Simple linear regression results for mean simulated traversal time versus assay metrics by sampling event and averaged across sampling events (Time-averaged). All r^2 and p-values (in parentheses) shown. ND = no data. Direction indicates a positive (+) or negative (-) slope. All slopes derived from correlation between any specific pair of variables were in the same direction.

Sampling Date	[DOC]	ΔDOC	ΔCO_2
15 Jul 2008	0.03 (0.46)	0.13 (0.11)	**0.25 (0.02)**
11 Aug 2008	0.06 (0.38)	0.02 (0.60)	**0.29 (0.04)**
10 Sep 2008	0.08 (0.28)	0.06 (0.34)	**0.49 (0.002)**
20 Apr 2009	**0.44 (<0.001)**	0.08 (0.20)	0.11 (0.13)
28 May 2009	0.02 (0.64)	0.003 (0.86)	0.02 (0.68)
15 Jul 2009	0.06 (0.26)	**0.20 (0.03)**	**0.34 (0.004)**
17 Aug 2009	**0.49 (<0.001)**	**0.25 (0.03)**	0.0004 (0.93)
16 Sep 2009	0.06 (0.24)	**0.21 (0.02)**	ND
15 Oct 2009	**0.18 (0.05)**	0.006 (0.74)	0.10 (0.15)
Time-averaged	**0.12 (0.05)**	**0.54 (<0.001)**	**0.52 (<0.001)**
Direction	-	+	+

[a] Statistical analysis performed on $\log_{10}$ transformed data

Table 4.4. Simple linear regression results for mean simulated traversal time versus optical metrics by sampling event. All r^2 and p-values (in parentheses) shown. ND = no data. Direction indicates a positive (+) or negative (-) slope. All slopes derived from correlation between any specific pair of variables were in the same direction.

Sampling Date	SUVA	C1[a]	C2[a]	C3[a]	C4[a]	FI[a]	% amino acids[a]
15 Jul 2008	**0.46 (<0.001)**	ND	ND	ND	ND	ND	ND
11 Aug 2008	0.0006 (0.93)	ND	ND	ND	ND	ND	ND
10 Sep 2008	0.009 (0.72)	ND	ND	ND	ND	ND	ND
20 Apr 2009	**0.24 (0.02)**	**0.57 (<0.001)**	**0.49 (<0.001)**	0.04 (0.35)	**0.29 (0.008)**	0.004 (0.78)	**0.42 (0.001)**
28 May 2009	0.08 (0.35)	ND	ND	ND	ND	ND	ND
15 Jul 2009	**0.22 (0.03)**	**0.50 (<0.001)**	**0.40 (0.001)**	0.0003 (0.93)	0.004 (0.79)	0.006 (0.72)	**0.41 (0.001)**
17 Aug 2009	0.14 (0.12)	**0.46 (0.03)**	**0.46 (0.03)**	0.08 (0.42)	0.11 (0.34)	0.18 (0.23)	0.002 (0.90)
16 Sep 2009	**0.28 (0.01)**	**0.34 (0.005)**	**0.30 (0.01)**	0.13 (0.10)	**0.38 (0.002)**	**0.19 (0.04)**	0.006 (0.73)
15 Oct 2009	**0.31 (0.008)**	**0.49 (<0.001)**	0.10 (0.17)	0.05 (0.32)	**0.23 (0.03)**	**0.39 (0.002)**	0.003 (0.81)
Time-averaged	**0.64 (<0.001)**	**0.66 (<0.001)**	**0.60 (<0.001)**	0.006 (0.72)	0.10 (0.16)	**0.22 (003)**	**0.56 (<0.001)**
Direction	-	-	-	-	-	+	+

[a] Statistical analysis performed on $\log_{10}$ transformed data

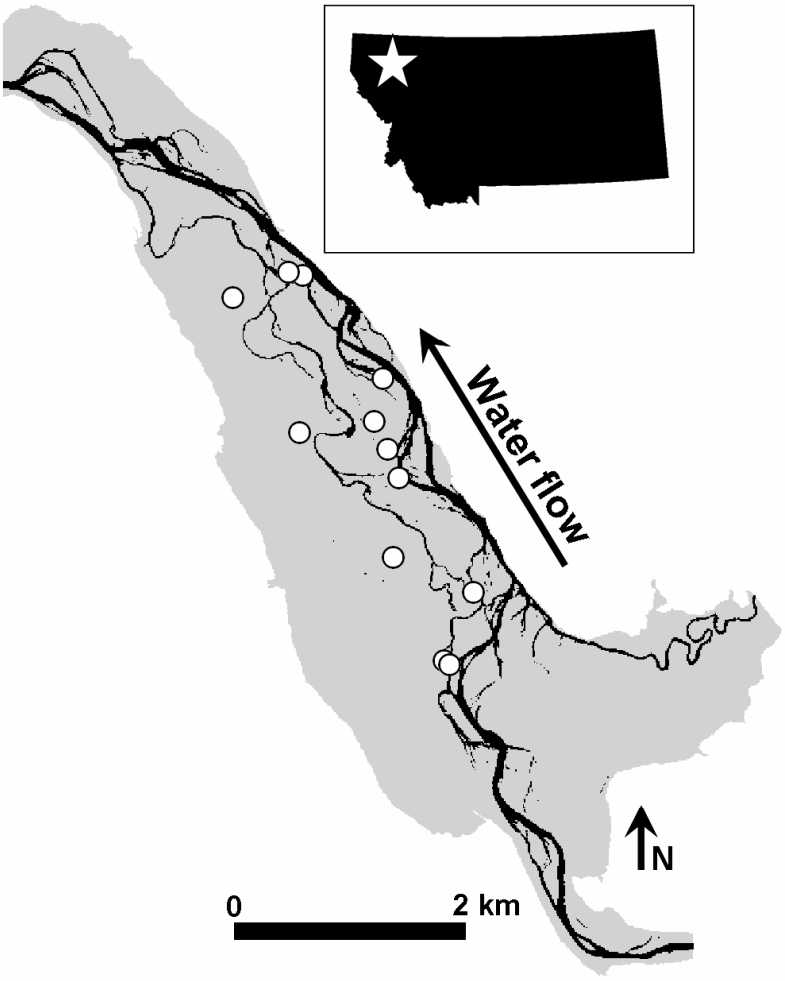

Figure 4.1. Plan view of Nyack Floodplain extent (grey), on the Middle Fork Flathead River located in Northwest Montana (shown in inset). White circles indicate well locations. Black zone is modeled surface water extent at base flow.

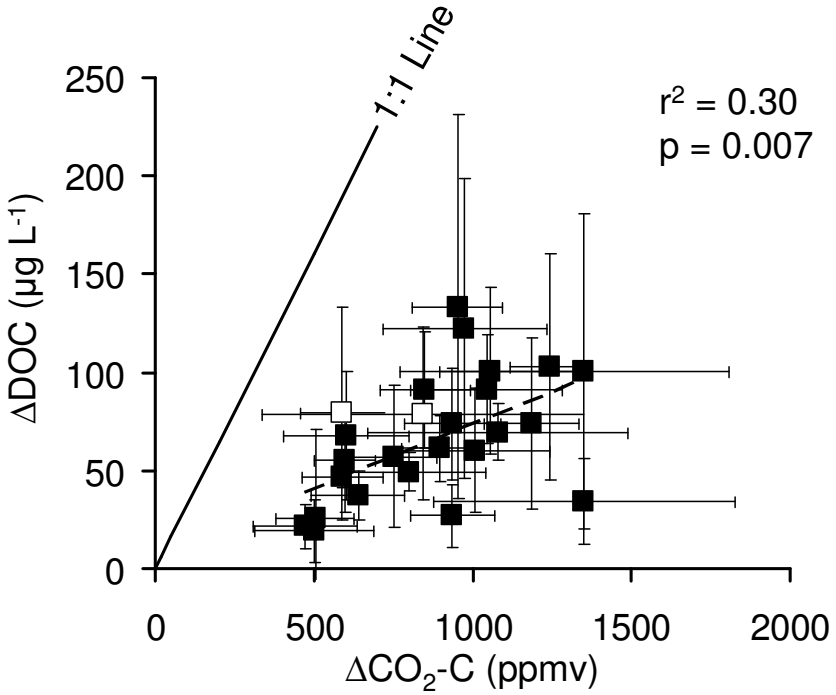

Figure 4.2. DOC depleted versus CO_2 produced within lab assays. Values are average by location across sampling period +/- 1 SE. Black squares are hyporheic and white squares are river water samples.

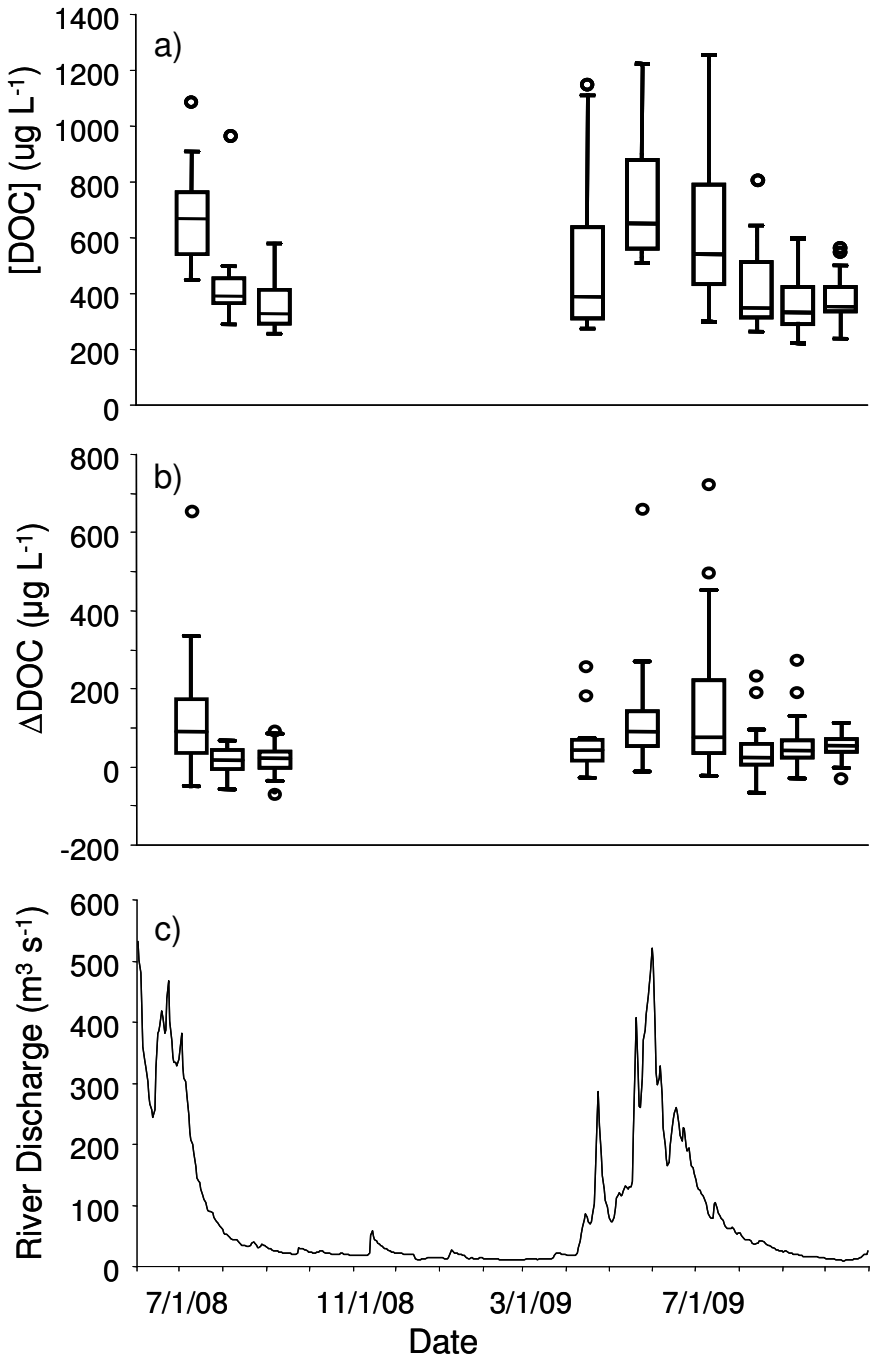

Figure 4.3. Box plots of a) DOC concentration and b) DOC depleted in lab assays by sampling event. c) Hydrograph of the Middle Fork Flathead River at USGS Gage ##12358500.

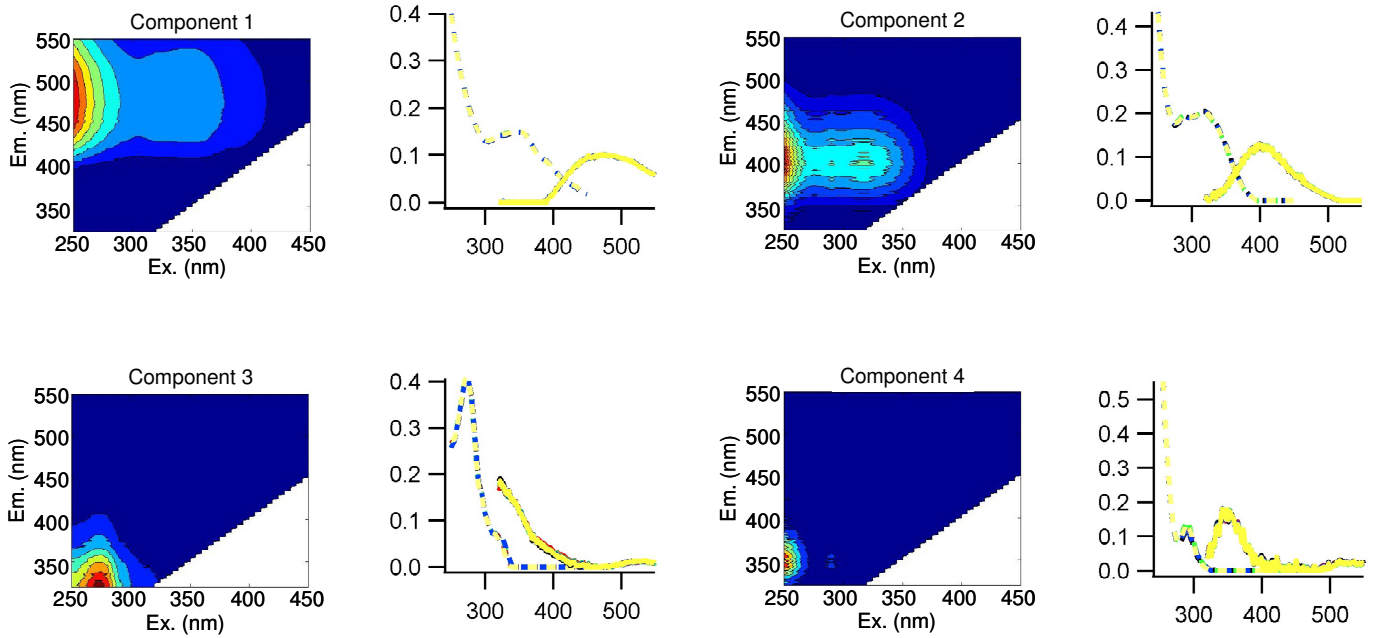

Figure 4.4. Fluorescence signatures of the four PARAFAC components identified in the Nyack dataset. Contour plots of components C1-C4 are ordered by decreasing percent explained. Corresponding line plots to the right of each contour plot compare the split-half validation results, in which each component's excitation (left, dashed) and emission (right, solid) spectra are estimated from four independent splits of the dataset, to the results from the complete dataset. See Table 4.2 for component descriptions.

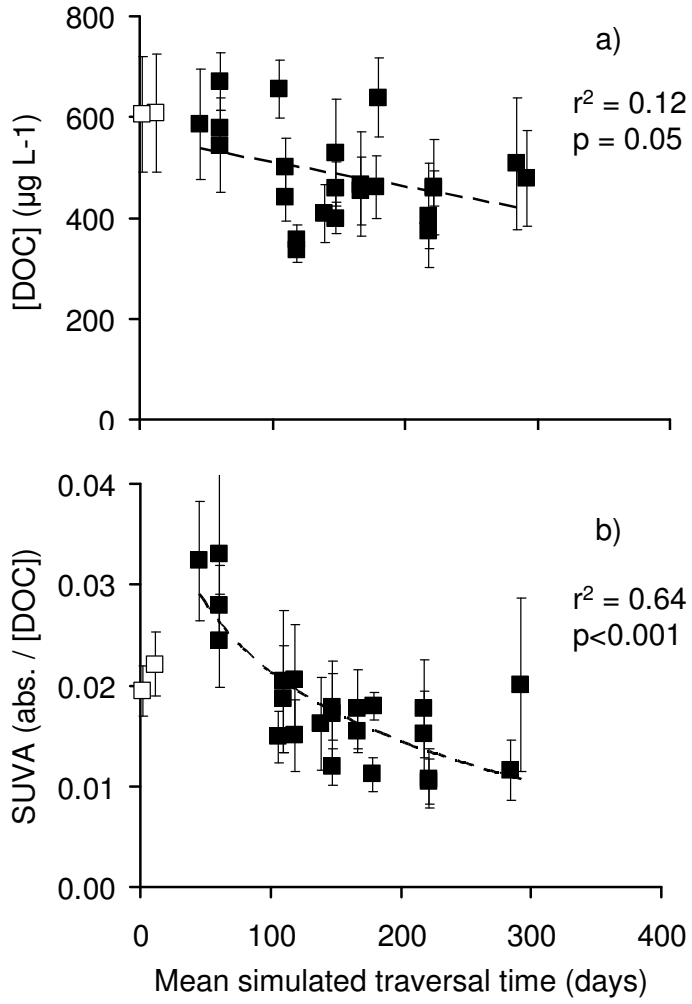

Figure 4.5. a) DOC concentration, and b) SUVA versus mean simulated traversal time. Values are average by location across sampling period +/- 1 SE. Black squares are hyporheic and white squares are river water samples. River water samples are not included in the regression analysis.

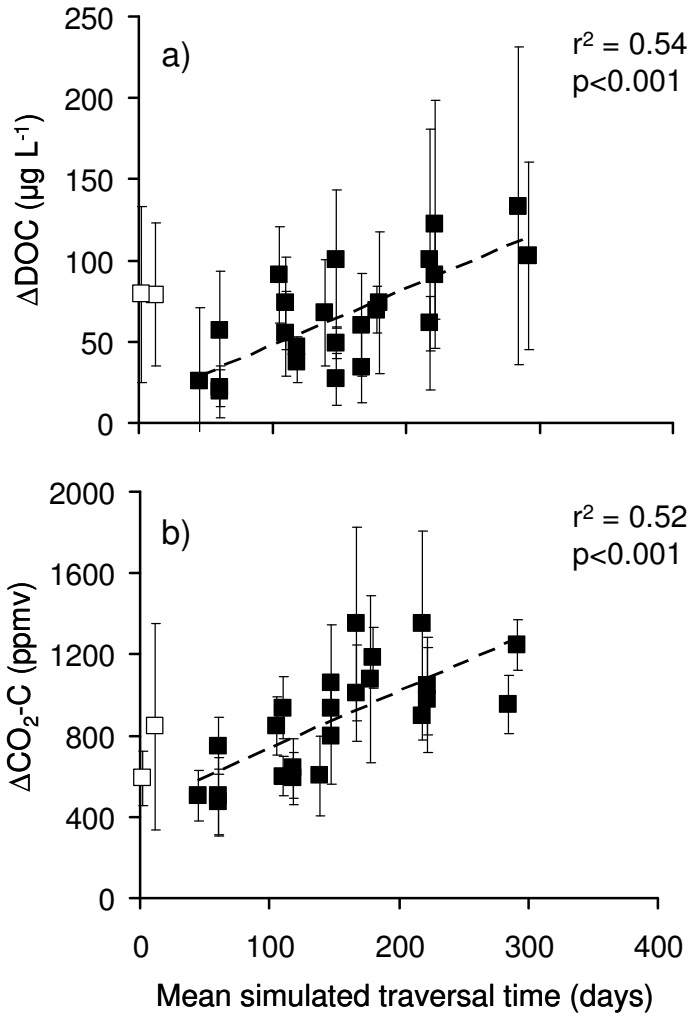

Figure 4.6. a) DOC depleted and d) CO_2 produced within lab assays versus mean simulated traversal time. Values are average by location across sampling period +/- 1 SE. Black squares are hyporheic and white squares are river water samples. River water samples are not included in the regression analysis.

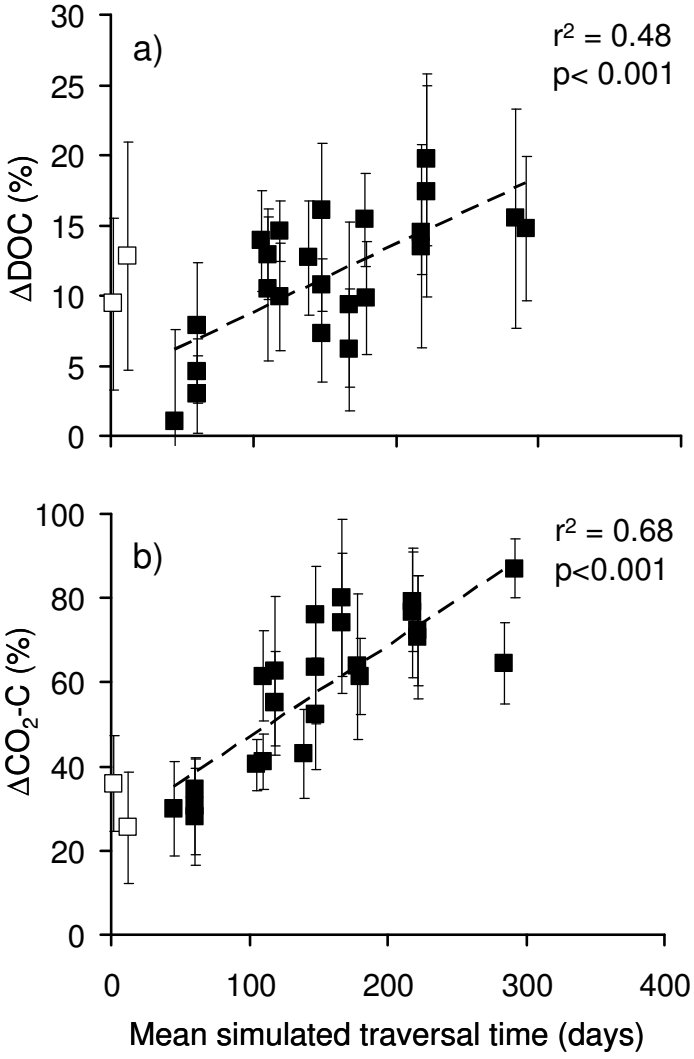

Figure 4.7. a) Percent DOC depleted and b) percent CO_2 produced within lab assays versus mean simulated traversal time. Values are average by location across sampling period +/- 1 SE. Black squares are hyporheic and white squares are river water samples. River water samples are not included in the regression analysis.

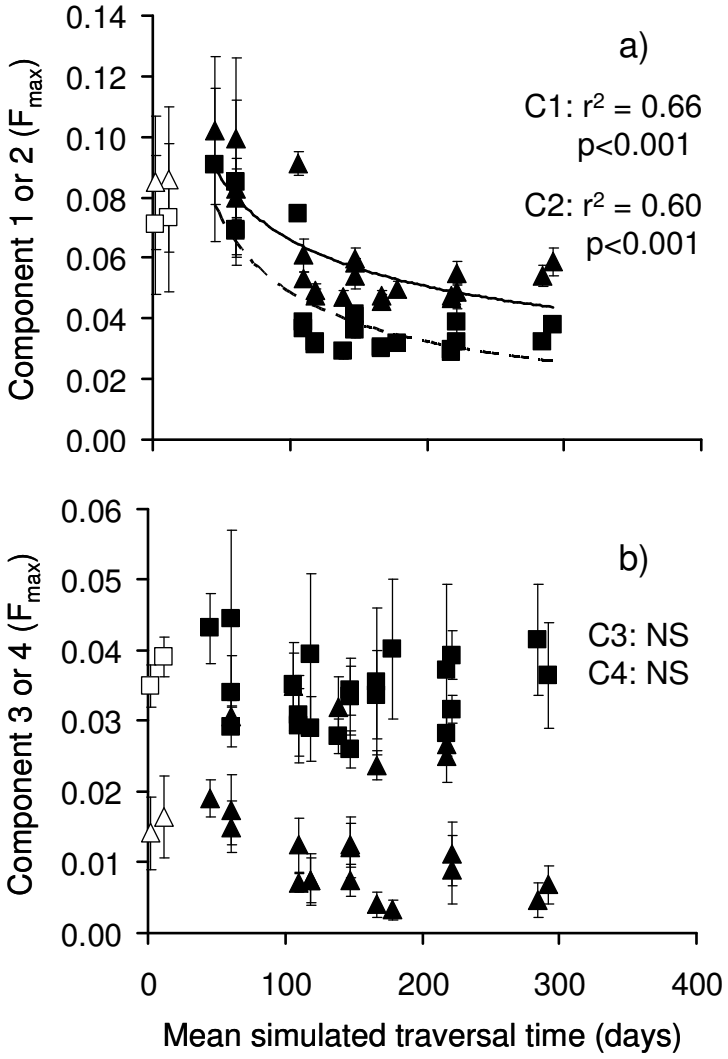

Figure 4.8. PARAFAC component loadings, a) C1 (squares) and C2 (triangles), and b) C3 (squares), and C4 (triangles), versus mean simulated traversal time. Values are average by location +/- 1 SE across sampling period. Black squares are hyporheic and white squares are river water samples. River water samples are not included in the regression analysis.

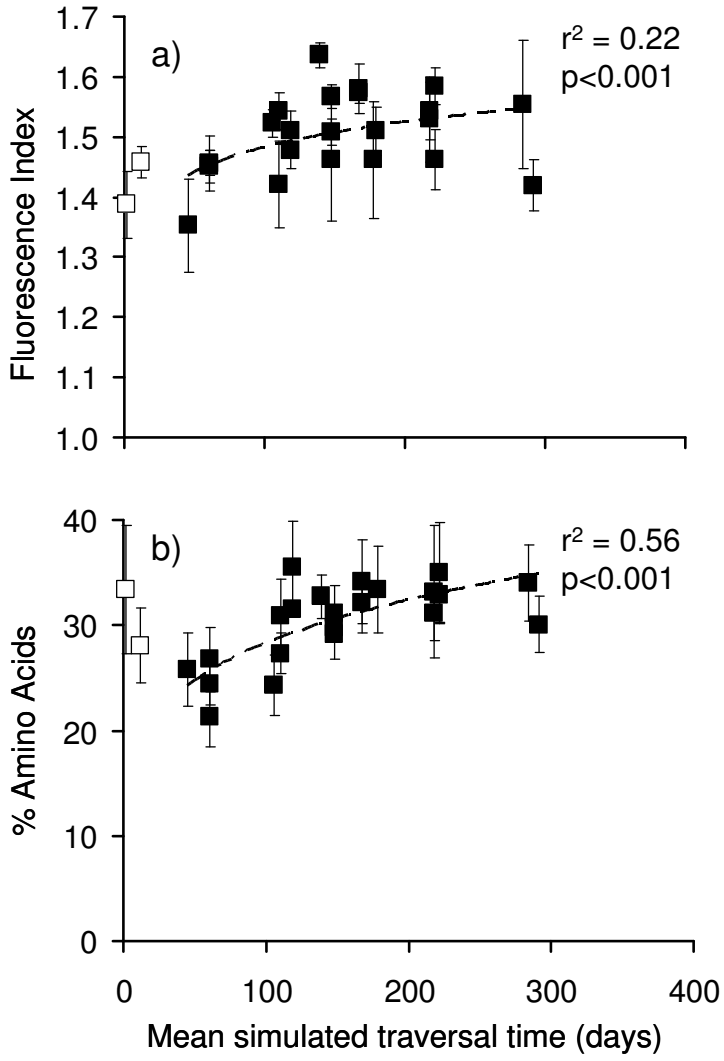

Figure 4.9. a) Fluorescence Index and b) Percent amino acids versus mean simulated traversal time. Values are average by location across sampling period +/- 1 SE. Black squares are hyporheic and white squares are river water samples. River water samples are not included in the regression analysis.

CHAPTER 5

SCALING FLOW PATHS TO FLOODPLAINS: SIMULATING DISSOLVED OXYGEN AND NITRATE DYNAMICS WITHIN AN ALLUVIAL RIVER-FLOODPLAIN SYSTEM[1]

---

[1]Ashley M. Helton and Geoffrey C. Poole. To be submitted to an undecided journal.

Abstract

River ecosystem dynamics are controlled and constrained by a river's physical template, but representations of geomorphology, hydrology, and temperature are often highly simplified and abstracted in biogeochemical models of river ecosystems. If paired with a realistic model of floodplain hydrogeomorphology and water temperature, we posited that relatively simple biogeochemical models could explain complex patterns of oxygen and nitrate dynamics observed throughout the 16km^2 hyporheic zone of the Nyack Floodplain, Middle Fork Flathead River, Montana, USA. To test this hypothesis, we developed an interdependent set of simple, flow-path scale empirical models to simulate biotic oxygen utilization and nitrate uptake and production in hyporheic sediments. We then embedded these integrated models within an existing hydrogeomorphic model of the Nyack Floodplain. The resulting hydro-biogeochemical model incorporates several aspects fundamental to biogeochemical cycling typically missing from coarse-scale river biogeochemical models, including: 1) a detailed, three-dimensional representation of the river's physical template (floodplain inundation dynamics, ground-surface water exchange, hyporheic hydrology, and temperature dynamics), 2) the biogeochemistry of multiple interactive elements, and 3) cycling of nitrogen (microbially-mediated nitrate uptake and production). We simulated floodplain hydro-biogeochemistry under dynamic hydrologic conditions for one year, and compared model results to a large dataset of observed dissolved oxygen and nitrate values measured throughout the Nyack hyporheic zone. The model explained 67% of the variance in 820 dissolved oxygen measurements and 27% of the variance in 447 nitrate measurements that spanned the floodplain longitudinally, laterally, vertically, and across river discharge conditions and seasons. Our results underscore the importance of geomorphology, hydrology, and temperature in driving river ecosystem dynamics, and

demonstrate how a more realistic representation of hydrogeomorpholgy, combined with simple biogeochemical models, can explain complex patterns of solute availability observed across hyporheic water over time.

Introduction

Recent research indicates rivers likely play important roles in global biogeochemical cycles, particularly in their ability to retain and transform nutrients (Cole et al. 2007; Mulholland et al. 2008). An understanding of riverine biogeochemical cycling is essential to the study and management of changing biogeochemical cycles as landscapes are increasingly subjected to perturbations, such as global climate change and urbanization. However, our understanding of spatiotemporal patterns of ecosystem processes, such as denitrification and respiration, across fluvial landscapes is limited by current modeling approaches (Helton et al. In Press).

Traditional watershed-scale riverine biogeochemical models have focused on predicting nutrient export to receiving water bodies (e.g., Smith et al. 1997). More recently the same models have been applied to scale denitrification rates throughout river networks (Alexander et al. 2000; Mulholland et al. 2008). Although these models typically have high predictive accuracy for coarse scale nutrient export from large watersheds (Alexander et al. 2002), large uncertainties are associated with their estimates of denitrification (Boyer et al. 2006) because they lack fundamental representations of biogeochemical cycles and hydrology that drive spatiotemporal patterns of biogeochemical dynamics. These models simulate the nitrogen cycle as a one-way flux of nitrogen from the river channel independent of other elemental cycles, and represent the river as simply a channel, ignoring connections between the channel, hyporheic zone, and floodplain/riparian surface (Helton et al. In Press). Because biogeochemical processes

in rivers cannot be empirically measured at large spatial scales, simulation models are important tools for understanding riverine biogeochemical cycling. Therefore, large uncertainties in modeling make understanding the role of rivers in landscape-scale biogeochemical cycling particularly difficult.

Predictable patterns of electron donors and acceptors tend to occur along flow paths at the scale of centimeters to meters (Hedin et al. 1998; Baker et al. 2000; Vidon and Hill 2004). For example, dissolved oxygen and organic carbon tend to decrease, consistent with microbial degradation of organic matter (Hedin et al. 1998). Nitrate may decrease or increase, depending on the availability of carbon and oxygen, which drive the prevalence of microbial pathways that remove (e.g., denitrification) or produce (e.g., nitrification) nitrate (Vidon and Hill 2004; Fernald et al. 2006). As individual hydrologic flow paths diverge and converge within a river system, different combinations of solutes are brought together, creating a three-dimensional landscape that encompasses a wide range of biogeochemical possibilities (McClain et al. 2003; Fisher et al. 2004). Developing methods to scale observed one-dimensional flow path patterns to hydrologically complex and dynamic three-dimensional river-floodplain systems is fundamental for understanding spatiotemporal patterns of biogeochemical cycling. To our knowledge, no ecosystem model for fluvial systems exists that links a three-dimensional representation of fluvial landscape hydrology (patterns of channel water flux, surface water inundation, ground-surface water exchange, hyporheic hydrology, and water temperature) to a multi-element biogeochemical model.

Here, we developed an interdependent set of simple, flow-path scale empirical models to simulate biotic oxygen utilization and nitrate uptake and production in hyporheic sediments. We then embedded these models within an existing hydrogeomorphic model of the 16km^2 Nyack

Floodplain on the Middle Fork Flathead River, Montana, USA. The resulting hydro-biogeochemical model incorporates several aspects fundamental to biogeochemical cycling typically missing from coarse-scale river biogeochemical models, including: 1) a detailed, three-dimensional representation of the river's physical template (floodplain inundation dynamics, ground-surface water exchange, hyporheic hydrology, and temperature dynamics), 2) the biogeochemistry of multiple interactive elements, and 3) cycling of nitrogen (microbially-mediated nitrate uptake and production).

We simulated the paired hydro-biogeochemical model under dynamic hydrologic conditions for one year, and compared model results to a large dataset of observed dissolved oxygen and nitrate values that spanned the floodplain longitudinally, laterally, vertically, and across river discharge conditions and seasons. We posited that relatively simple flow-path scale biogeochemical models could explain complex spatial and temporal patterns in hyporheic oxygen and nitrate dynamics across the Nyack Floodplain when coupled with a detailed representation of the hydrogeomorphic template.

Methods

Site description

The Nyack Floodplain is a 16 km^2 gravel- and cobble-bedded anabranched alluvial montane floodplain on the Middle Fork of the Flathead River located in northwest Montana (Figure 5.1). The hydrology and geomorphology of the Nyack hyporheic zone are well characterized (Poole et al. 2002; Poole et al. 2004; Helton Chapter 2). The floodplain is constrained laterally by bedrock valley walls and bounded upstream and downstream by canyon segments with bedrock streambeds. The fifth-order river has a snow-spate driven hydrograph

with a mean discharge of 80 m^3/s and mean peak discharge of 600 m^3/s. Complex channel morphology and coarse, well-sorted sediments on the floodplain facilitate high rates of surface-subsurface water flux, creating an extensive hyporheic zone that ranges from ~5 to >25 meters in depth and spans the width of the floodplain (up to 1.5 km). Acoustic Doppler profiler data indicate that the main channel of the river loses ~30% of its base-flow discharge to the underlying alluvial aquifer as it flows across the first 1/3 of the floodplain (Mark Lorang, unpublished data). Water recharged to the alluvial aquifer flows downstream within the hyporheic zone and later re-emerges to the floodplain surface in the main channel or in spring channels scattered across the floodplain, which rejoin the main river channel before entering the downstream canyon (Poole et al. 2004).

Model description

We developed an integrated model of dissolved oxygen (DO) and nitrate (NO_3^-) cycling within the Nyack Floodplain (Figure 5.2), parameterized the model based on observed patterns of DO and NO_3^- with hyporheic residence time, and linked the biogeochemistry model to an existing Nyack Floodplain hydrologic model (Helton Chapter 3). The hydrology model is a three-dimensional finite volume, or link and node, model in which the floodplain is divided into discrete nodes and one-dimensional flows are calculated for links between adjacent nodes (Figure 5.3). The model subdivides the floodplain into four layers: the surface, soil, shallow alluvial aquifer, and deep alluvial aquifer, and represents horizontal surface water flow, horizontal and vertical subsurface flow, and vertical flow between surface and subsurface waters. The model also estimates daily average temperature for each model node, based on relationships between mean floodplain traversal time (a surrogate for floodplain residence time derived from

particle tracking model analyses) and extensive empirical temperature data records from the Nyack Floodplain (Helton Chapter 3).

The biogeochemistry model simulates mass advection of DO and NO_3^- between model nodes by multiplying simulated solute concentration by the rate of water flux between model nodes (derived from the hydrology model). For subsurface model nodes (i.e., the hyporheic zone) the model also simulates DO and NO_3^- uptake and NO_3^- production. We simulated hyporheic DO uptake (u_{DO}) with a temperature-dependent Michaelis-Menten uptake function:

$$u_{DO} = u_{maxDO} * [DO] / (K_{sDO} + [DO]) \quad (1)$$

where [DO] is the DO concentration (mg / L), u_{maxDO} is the maximum uptake rate of DO (mg / L / s), and K_{sDO} is the half-saturation coefficient of DO (mg / L). Because u_{maxDO} was positively correlated with water temperature (see *Model Parameterization*, below), the model assumes u_{maxDO} increases linearly with water temperature (T, ^oC):

$$u_{maxDO} = mT \quad (2)$$

We modeled hyporheic NO_3^- uptake and production within the Nyack hyporheic zone as a function of both NO_3^- concentration and DO dynamics. We simulated NO_3^- uptake (u_{NO3}) with a Michaelis-Menten uptake function:

$$u_{NO3} = u_{maxNO3} * [NO3] / (K_{sNO3} + [NO3]) \quad (3)$$

where [NO3] is the NO_3^- concentration (µg / L), u_{maxNO3} is the maximum uptake rate (µg / L / s), and K_{sNO3} is the half-saturation coefficient (µg / L). Because NO_3^- is more readily used as an electron acceptor when DO concentrations are low, we assumed u_{maxNO3} was negatively related to DO concentration, so that lower DO concentrations would yield higher u_{maxNO3} values.

$$u_{maxNO3} = ae^{-b[DO]} \quad (4)$$

Empirical observations revealed that NO_3^- concentrations increased with hyporheic residence time during some months (see *Model Parameterization*, below), suggesting that at times NO_3^- production is apt to exceed NO_3^- uptake. Likely, a fraction of DO consumption produces NO_3^- through nitrification. Thus, we assumed that NO_3^- production was positively related to u_{maxDO}, so that higher rates of DO uptake would be associated with higher rates of NO_3^- production.

$$prod_{NO3} = c\ u_{maxDO}^2$$

Data description

We parameterized and evaluated the DO and NO_3^- models with data from 6 surface water sampling sites and 58 monitoring wells dispersed across the floodplain (Figure 5.1). Data included measured DO from 2003 and 2004, and measured DO and NO_3^- from 2008 and 2009. Samples were collected during 28 sampling events for DO and 22 sampling events for NO_3^-. Between 7 and 21 wells and 2 and 5 main stem surface water sites were sampled during each sampling event. Wells were typically sampled at two discrete depths: near the water table and at least 2 meters below the water table. A box-plot revealed that one well was a statistical outlier for NO_3^- concentration (Figure 5.10). All but three of the outliers for measured NO_3^- concentrations over time were recorded in a single well, so data from that well were not used to parameterize or evaluate model performance.

The final monitoring dataset included a total of 820 DO and 447 NO_3^- measurements that spanned the Nyack Floodplain longitudinally, laterally, vertically, and across river discharges and seasons. The monitoring dataset was divided into two, with 5% of the DO data and 15% of the NO_3^- data used to derive model parameters ("parameterization dataset"), and the remainder

reserved for evaluation of model performance. The parameterization dataset for the DO model included one surface water and four hyporheic well sites collected along a relatively short flow path (Figure 5.1) sampled on six dates (Figure 5.4). Because detailed measurements of NO_3^- were not collected along short flow paths over time, and because NO_3^- dynamics occurred over larger scales, the parameterization dataset for the NO_3^- model included all surface and hyporheic well data collected during three separate sampling events with varying patterns in NO_3^- concentration versus hydrologic residence time (Figure 5.6).

Model parameterization

We fit DO uptake parameters, u_{max} and K_s, to observed DO concentrations within the Nyack floodplain hyporheic zone (Figure 5.1) for six sampling dates (Figure 5.4) by minimizing RMSE between predicted and observed DO concentrations in the parameterization dataset. We ordered measured DO values along the flow path based on estimates of mean traversal time (a surrogate for floodplain residence time) from our hydrologic model (Helton Chapter 3). Parameter estimates for K_s were relatively constant across sampling dates, so we used the average K_s value (4.5 mg / L) for floodplain-scale simulations, and u_{maxDO} was positively correlated with water temperature (Figure 5.5). The model uses this observed relationship between u_{maxDO} and temperature to simulate u_{maxDO} within each model node over time.

We fit NO_3^- uptake (K_s, u_{maxNO3}) and NO_3^- production parameters to the model with hyporheic well data from three dates with varying spatial patterns in NO_3^- concentrations (Figure 5.6) by minimizing RMSE between predicted and observed NO_3^- concentrations in the parameterization dataset. Like the DO model, for parameterization, we ordered hyporheic

samples by mean traversal time derived from the hydrologic model. Modeled relationships for DO and NO_3^- uptake and NO_3^- production are shown in Figure 7.

Model inputs

The model requires temporal patterns of DO and NO_3^- concentrations in surface water as model inputs. We modeled surface water DO and NO_3^- concentrations based on statistical relationships for the Middle Fork Flathead River at the Nyack Floodplain. We assumed that DO concentrations remained at atmospheric equilibrium based on the observed relationship between saturated DO concentration and river water temperature for the Middle Fork Flathead River at Nyack Floodplain (Figure 5.8). We modeled NO_3^- concentration in the surface water based on NO_3^- concentration-discharge relationships from river water samples. We observed different relationships between concentration and discharge for the rising and falling limbs of the hydrograph (Figure 5.9): NO_3^- concentrations on the rising limb were higher than those on the falling limb for similar river discharges. We incorporated both of these relationships into the model such that days that fell before the peak of the flood spate were considered to be on the rising limb and days that fell after the peak of the flood spate were considered to be on the falling limb.

Model simulation and evaluation

We simulated hourly DO and NO_3^- dynamics for one year, which corresponded to the median flow year from the previously run hydrologic simulations (Helton Chapter 3), 11/1/1998 to 10/31/1999. We ran the model for one simulation year prior to 11/1/1998 to assure that initial conditions did not affect model output.

We evaluated the DO and NO_3^- models by comparing model output to observed data from 2003 and 2004 (for DO only), and 2008 and 2009 (see *Data description*, above). Since we did not have observed data for the simulation year, we compared simulated values to observed values collected in the same month of the year and with a similar river discharge (Table 5.1). River discharges for observed dates were within 5% of river discharge for simulated dates. We categorized each simulated versus observed comparison (i.e., "comparison type") by season and river discharge condition (Table 5.1). Seasons included winter, summer, spring, and fall. Discharge conditions included base flow, peak flow, the rising limb of the flood spate before peak flow ("rising"), and the falling limb of the flood spate after peak flow ("falling").

Results

By integrating a simple biogeochemical model with a detailed temperature and hydrology model, we were able to scale flow path DO and NO_3^- dynamics to the floodplain. The model explained 67% of the variance in 820 DO measurements that spanned the floodplain longitudinally, laterally and vertically, and different river discharge conditions and seasons (Figure 5.11) by linking a temperature-dependent Michaelis-Menten uptake model to the existing hydrology and temperature model. The DO model also simulated concentrations well among seasons and flow conditions, with r^2 values ranging from 0.58 for "spring peak" to 0.73 for "winter base" flow conditions (Figure 5.12).

The NO_3^- model explained 27% of the variance in 412 NO_3^- measurements that spanned the floodplain longitudinally, laterally, and vertically, and different river discharge conditions and seasons (Figure 5.13). The model tended to over-predict NO_3^- at low concentrations and under-predict NO_3^- at high concentrations. The ability of the model to accurately estimate NO_3^-

changed across seasons and flow conditions (Figure 5.14). Simulated and observed values were most strongly correlated during "spring rising" and "spring peak" flow conditions, were weakly correlated during "winter base" and "summer falling" flow conditions, and were not correlated during either "summer base" or "fall base" flow conditions.

Discussion

The relationship between simulated and observed DO was strong among seasons and river discharge conditions (Figure 5.12), indicating the model incorporated the appropriate drivers of oxygen dynamics (advection, uptake, and temperature) within the Nyack floodplain. The predictive ability of the NO_3^- model was not as strong as the DO model (Figure 5.13), and, in general, the NO_3^- model over-predicted NO_3^- at low concentrations and under-predicted NO_3^- at high concentrations. The NO_3^- model had a wide range of predictive abilities among seasons and river discharge conditions (Figure 5.14). Simulated and observed NO_3^- data were most strongly correlated during the spring for higher river discharges, but were not significantly correlated during summer and fall base flow conditions. Thus, we were able to incorporate fundamental fluxes (advection, uptake, and production) and drivers (temperature and oxygen) during some seasons and river discharge conditions, but not others.

Model uncertainties

Several factors contributed to model uncertainty, and thus our ability to reliably scale biogeochemical dynamics within the Nyack Floodplain. First, simulated hyporheic DO and NO_3^- concentrations were highly sensitive to patterns of surface water model input concentrations. The empirical relationship between saturated surface water DO and temperature was strong

(Figure 5.8), and therefore the model simulated surface water DO concentration inputs well. However, surface water NO_3^- concentrations were more difficult to predict. The surface water NO_3^- model inputs were based on a smaller dataset, and surface water NO_3^- concentrations had a weak relationship with discharge, which varied relative to rising or falling river flow conditions (Figure 5.9). Large uncertainties associated with surface water NO_3^- model inputs created large uncertainties in simulated hyporheic concentrations, which contributed to poor model performance. Improving the representation of surface water NO_3^- dynamics in the model would improve our ability to simulate NO_3^- advection from surface to hyporheic waters, and thus more accurately evaluate the hyporheic NO_3^- uptake and production model.

Second, the model likely omits important additional NO_3^- removal and/or production mechanisms. The nitrogen cycle in river systems is complex (e.g., Helton et al. In Press), and consists of multiple forms of nitrogen than undergo numerous transformations. Nitrogen transformations may also be tightly coupled to other elemental cycles (e.g., iron-driven denitrification or sulfate-driven NO_3^- reduction. Burgin and Hamilton 2007), and the prevalence of nitrogen transformation rates (e.g., nitrification versus denitrification) may be controlled by carbon availability and quality (Butturini et al. 2000; Starry et al. 2005). Indeed, correlations between carbon bioavailability (Helton Chapter 4) and sulfate (Helton unpublished data) with hydrologic residence time have been observed in the Nyack hyporheic zone. Furthermore, NO^{3-} is highly mobile in soils and neither our model nor our empirical measurements account for potential NO_3^- leached from the floodplain surface.

Finally, our methodology to fit DO and NO_3^- model parameters likely affected model performance. Model parameters should be fit to Lagrangian representations of biogeochemical transformations along flow paths (measurements taken of a single parcel of water as it moves

along a flow path). Our monitoring dataset, however, yielded Eulerian representations of flow path biogeochemistry (repeated measurements taken at specific locations over time). Thus, our parameter estimation presumed that the Eulerian and Lagrangian representations were similar for DO and NO_3^- within the Nyack hyporheic zone. This assumption is appropriate when initial flow path conditions (e.g., surface water DO and NO_3^- concentrations at the time of downwelling) are constant across the hydrologic residence times of sampled flow paths. Thus, this assumption was appropriate for the DO parameterization dataset (where variation of surface water DO was relatively low over the hydrologic residence time in the parameterization flow paths), but the NO_3^- parameterization dataset violated the assumption (NO_3^- concentrations were highly variable over the hydrologic residence time of the parameterization flow paths). The larger discrepancies between Eulerian and Lagrangian flow path representations in the NO_3^- dataset yielded poor parameter estimates for NO_3^- uptake and production, contributing to the poorer performance of the model for NO_3^- than for DO. Developing methods to parameterize the model based on transforming the Eulerian to a Lagrangian representation of parameterization flow paths will improve model parameters, and likely improve model performance.

Model implications

Our simulation model includes drivers of biogeochemical cycles essential for understanding biogeochemistry across scales. Most notably, our model utilizes a detailed representation of floodplain hydrogeomorphology to simulate hydrology and temperature dynamics within the river channel, hyporheic zone, and floodplain surface. Hydrologically-driven transport of solutes is fundamental for understanding and predicting when and where "hot moments and spots" of biogeochemical cycling occur that may drive whole-system rates

(McClain et al. 2003). Our modeling framework for river-floodplain systems provides an analog to ecohydrologic models for terrestrial systems (reviewed by Boyer et al. 2006; Kulkarni et al. 2008). Ecohydrologic models simulate hydrologically explicit hillslope nitrogen dynamics, even predicting observed patterns and timing of water and nutrient delivery to streams (Band et al. 2001).

Although our biogeochemical model is relatively simple, it includes two important conceptualizations of biogeochemical cycles typically excluded from coarse-scale river biogeochemical models (Helton et al. In Press). First, we represent nitrogen dynamics as a cycle of gross uptake and release rather than a one-way flux of net uptake from the river channel. Thus, our model can predict a net uptake or production of NO_3^-, depending on the environmental context (i.e., NO_3^- concentration, DO concentration and uptake as a measure of respiration, and temperature). Second, we link two elemental cycles within our model – in this case NO_3^- dynamics are related to DO dynamics. Dissolved oxygen drives the prevalence of the aerobic pathway that produces NO_3^-, nitrification, versus the anaerobic pathway that removes NO_3^-, denitrification. Incorporating removal and production as well as linkages to DO dynamics allowed our model to simulate contrasting NO_3^- dynamics within the same system (Figure 5.6), where nitrogen may increase, decrease, or both along a given flow path. Our approach that reproduces multiple patterns of NO_3^- dynamics within the same system is a first step toward scaling diverse biogeochemical flow path dynamics to larger scales.

Scaling river biogeochemical cycles across geomorphic conditions

Hydrologic dynamics within the Nyack study site are complex. Floodplain inundation patterns coupled with an extensive hyporheic zone and alluvial aquifer drive complex spatial and

temporal patterns of surface-groundwater exchange. River segments with channels that are less connected to their surrounding floodplain and alluvial aquifers, for example bedrock river channels or rivers that have been artificially channelized, may require a less detailed representation of non-channel hydrogeomorphology. For example, Helton et al. (In Press) found that by representing river channel hydrogeomorphology alone, denitrification rates could be scaled from small headwater stream reaches to whole stream networks. However, because large gravel-bedded rivers systems, like the Nyack Floodplain, are prevalent in many regions around the world, the influence of non-channel storage could have a substantial influence on biogeochemical cycling across large scales. Thus, understanding where a river segment lies on the continuum of geomorphic complexity will improve our ability to upscale ecologically relevant dynamics across fluvial landscapes.

Conclusions

Our simulation model was able to explain substantial amounts of variance in DO and NO_3^- across seasons and river discharge conditions for the Nyack Floodplain. Our results illustrate how one-dimensional flow path biogeochemical dynamics can be realistically scaled to a larger three-dimensional river-floodplain system by integrating a simple biogeochemical model to a detailed floodplain hydrology model. This approach provides the first step for scaling spatially and temporally dynamic biogeochemical patterns from flow paths to floodplains, which improves our ability to predict locations and times within fluvial landscapes most influential for biogeochemical cycles. Our work underscores the importance of the hydrogeomorphic template that drives hydrologic flux and storage of biogeochemical constituents for both scaling and understanding biogeochemical cycles across large spatial and temporal scales.

Acknowledgements

This research was supported by the National Research Initiative of the USDA Cooperative State Research, Education and Extension Service (2005-35102-16288), by the Gordon and Betty Moore Foundation, and by an EPA Star Fellowship for AMH. EPA has not officially endorsed this publication and the views expressed herein may not reflect the views of the EPA.

References

Alexander, R. B., R. A. Smith, and G. E. Schwarz. 2000. Effect of stream channel size on the delivery of nitrogen to the Gulf of Mexico. Nature **403**:758-761.

Alexander, R. B., P. J. Johnes, E. W. Boyer, and R. A. Smith. 2002. A comparison of models for estimating the riverine export of nitrogen from large watersheds. Biogeochemistry **57**:295-339.

Baker, M. A., H. M. Valett, and C. N. Dahm. 2000. Organic carbon supply and metabolism in a shallow groundwater ecosystem. Ecology **81**:3133-3148.

Band L.E., C.L. Tague, P. Groffman, K. Belt. 2001. Forest ecosystem processes at the watershed scale: hydrological and ecological controls of nitrogen export. *Hydrol Process* **15**: 2013–28.

Boyer, E. W., R. B. Alexander, W. J. Parton, C. S. Li, K. Butterbach-Bahl, S. D. Donner, R. W. Skaggs, and S. J. Del Gross. 2006. Modeling denitrification in terrestrial and aquatic ecosystems at regional scales. Ecological Applications **16**:2123-2142.

Burgin, A. J., and S. K. Hamilton. 2007. Have we overemphasized the role of denitrification in aquatic ecosystems? A review of nitrate removal pathways. Frontiers in Ecology and the Environment **5**:89-96.

Butturini, A., T. J. Battin, and F. Sabater. 2000. Nitrification in stream sediment biofilms: The role of ammonium concentration and DOC quality. Water Research **34**:629-639.

Cole, J. J., Y. T. Prairie, N. F. Caraco, W. H. McDowell, L. J. Tranvik, R. G. Striegl, C. M. Duarte, P. Kortelainen, J. A. Downing, J. J. Middelburg, and J. Melack. 2007. Plumbing the global carbon cycle: Integrating inland waters into the terrestrial carbon budget. Ecosystems **10**:171-184.

Fernald, A. G., D. H. Landers, and P. J. Wigington. 2006. Water quality changes in hyporheic flow paths between a large gravel bed river and off-channel alcoves in Oregon, USA. River Research and Applications **22**:1111-1124.

Fisher, S. G., R. A. Sponseller, and J. B. Heffernan. 2004. Horizons in stream biogeochemistry: Flowpaths to progress. Ecology **85**:2369-2379.

Hedin, L. O., J. C. von Fischer, N. E. Ostrom, B. P. Kennedy, M. G. Brown, and G. P. Robertson. 1998. Thermodynamic constraints on nitrogen transformations and other biogeochemical processes at soil-stream interfaces. Ecology **79**:684-703.

Helton, A. M., G. C. Poole, J. L. Meyer, W. M. Wollheim, B. J. Peterson, P. J. Mulholland, E. S. Bernhardt, J. A. Stanford, C. Arango, L. R. Ashkenas, L. W. Cooper, W. K. Dodds, S. V. Gregory, R. O. Hall Jr, S. K. Hamilton, S. L. Johnson, W. H. McDowell, J. D. Potter, J. L. Tank, S. M. Thomas, H. M. Valett, J. R. Webster, and L. Zeglin. Thinking outside the channel: modeling nitrogen cycling in networked river ecosystems. Frontiers in Ecology and the Environment.

Kulkarni, M. V., P. M. Groffman, and J. B. Yavitt. 2008. Solving the global nitrogen problem: it's a gas! Frontiers in Ecology and the Environment **6**:199-206.

McClain, M. E., E. W. Boyer, C. L. Dent, S. E. Gergel, N. B. Grimm, P. M. Groffman, S. C. Hart, J. W. Harvey, C. A. Johnston, E. Mayorga, W. H. McDowell, and G. Pinay. 2003. Biogeochemical hot spots and hot moments at the interface of terrestrial and aquatic ecosystems. Ecosystems **6**:301-312.

Mulholland, P. J., A. M. Helton, G. C. Poole, R. O. Hall, S. K. Hamilton, B. J. Peterson, J. L. Tank, L. R. Ashkenas, L. W. Cooper, C. N. Dahm, W. K. Dodds, S. E. G. Findlay, S. V. Gregory, N. B. Grimm, S. L. Johnson, W. H. McDowell, J. L. Meyer, H. M. Valett, J. R. Webster, C. P. Arango, J. J. Beaulieu, M. J. Bernot, A. J. Burgin, C. L. Crenshaw, L. T. Johnson, B. R. Niederlehner, J. M. O'Brien, J. D. Potter, R. W. Sheibley, D. J. Sobota, and S. M. Thomas. 2008. Stream denitrification across biomes and its response to anthropogenic nitrate loading. Nature **452**:202-U246.

Poole, G. C. 2002. Fluvial landscape ecology: addressing uniqueness within the river discontinuum. Freshwater Biology **47**:641-660.

Poole, G. C., J. A. Stanford, S. W. Running, C. A. Frissell, W. W. Woessner, and B. K. Ellis. 2004. A patch hierarchy approach to modeling surface and subsurface hydrology in complex flood-plain environments. Earth Surface Processes and Landforms **29**:1259-1274.

Smith, R. A., G. E. Schwarz, and R. B. Alexander. 1997. Regional interpretation of water-quality monitoring data. Water Resources Research **33**:2781-2798.

Starry, O. S., H. M. Valett, and M. E. Schreiber. 2005. Nitrification rates in a headwater stream: influences of seasonal variation in C and N supply. Journal of the North American Benthological Society **24**:753-768.

Vidon, P., and A. R. Hill. 2004. Denitrification and Patterns of Electron Donors and Acceptors in Eight Riparian Zones with Contrasting Hydrogeology. Biogeochemistry **71**:259-283.

Table 5.1. Simulated and observed comparison dates for model evaluation

Sample Date	Simulation Date	Comparison Type
11/7/2003 to 11/10/2003	11/21/1998 to 11/22/1998	Fall base flow
2/18/2004 to 2/23/2004	2/15/1999 to 2/24/1999	Winter base flow
4/5/2004 to 4/12/2004	4/20/1999 to 4/25/1999	Spring rising
5/25/2004 to 5/30/2004	5/19/1999 to 5/22/1999	Spring peak
7/25/2004 to 8/4/2004	8/13/1999 to 8/20/1999	Summer falling
10/26/2004 to 10/30/2004	9/25/1999 to 9/30/1999	Fall base flow
5/1/2008 to 5/2/2008	5/12/1999 to 5/15/1999	Spring rising
6/13/2008 to 6/14/2008	6/14/1999 to 6/15/1999	Spring peak
6/26/2008 to 6/27/2008	6/21/1999 to 6/23/1999	Spring peak
7/2/2008 to 7/8/2008	7/2/1999 to 7/5/1999	Summer falling
7/15/2008 to 7/16/2008	7/17/1999 to 7/19/1999	Summer falling
7/30/2008	8/10/1999 to 8/11/1999	Summer falling
8/11/2008 to 8/12/2008	8/23/1999 to 8/29/1999	Summer base flow
8/28/2008	8/28/1999 to 9/1/1999	Summer base flow
9/10/2008 to 9/11/2008	9/10/1999 to 9/14/1999	Fall base flow
9/25/2008 to 10/23/2008	9/25/1999 to 9/30/1999	Fall base flow
12/3/2008 to 12/4/2008	12/2/1998 to 12/4/1998	Winter base flow
1/14/2009 to 1/15/2009	1/11/1999 to 1/14/1999	Winter base flow
3/4/2009 to 3/14/2009	3/8/1999 to 3/10/1999	Winter base flow
3/26/2009 to 3/28/2009	3/20/1999 to 3/21/1999	Winter base flow
4/20/2009 to 4/21/2009	4/20/1999 to 4/25/1999	Spring rising
5/28/2009 to 6/1/2009	5/25/1999 to 5/29/1999	Spring peak
6/18/2009	6/14/1999	Summer falling
7/1/2009	7/16/1999	Summer falling
7/15/2009 to 7/16/2009	7/25/1999 to 7/26/1999	Summer falling
8/17/2009 to 8/20/2009	8/23/1999 to 9/1/1999	Summer base flow
9/16/2009 to 9/17/2009	9/23/1999 to 9/25/1999	Fall base flow
10/15/2009 to 10/16/2009	10/24/1998 to 10/30/1998	Fall base flow

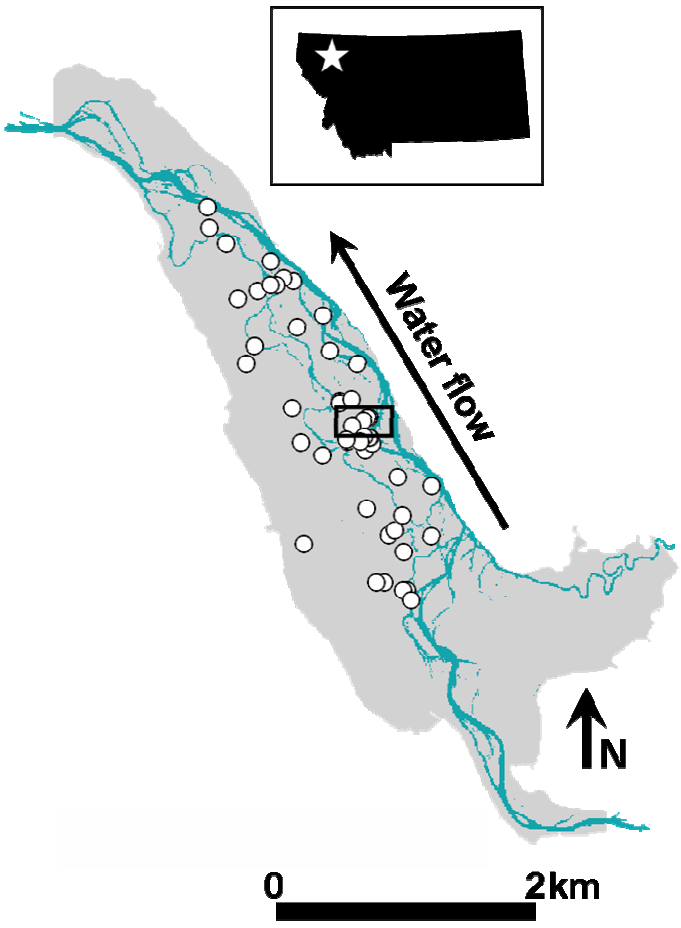

Figure 5.1. Plan view of Nyack floodplain extent (grey), on the Middle Fork Flathead River located in Northwest Montana (shown in inset). Circles indicate well locations where dissolved oxygen and/or nitrate were measured. Black square indicates location of flow path used to parameterize the dissolved oxygen model (Figure 5.4).

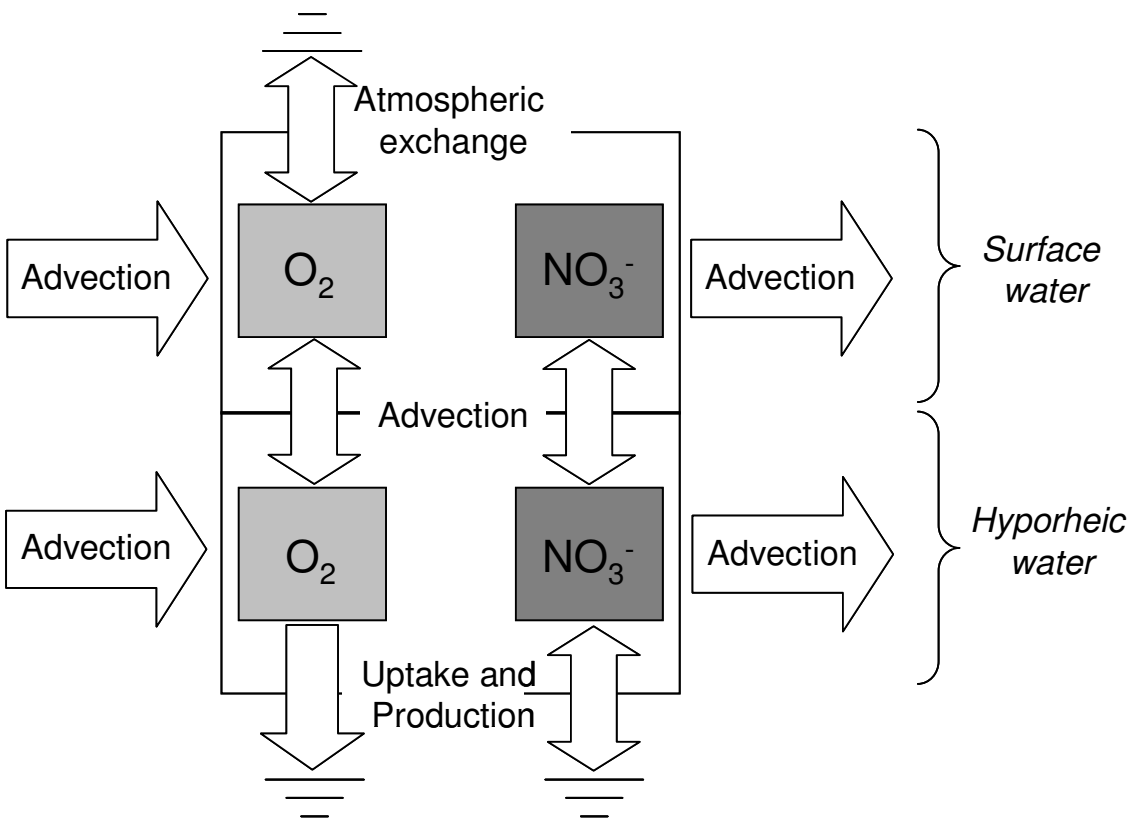

Figure 5.2. Box and arrow diagram of the dissolved oxygen and nitrate model. The model simulates dissolved oxygen (O_2) and nitrate (NO_3^-) advection and atmospheric exchange in surface water. In addition to advection, the model simulates dissolved oxygen and nitrate uptake and nitrate production in hyporheic water. The oxygen and nitrate models are linked to the hydrology model via advection, and the oxygen and nitrate models are linked to each other via uptake and production (see text for detailed equations).

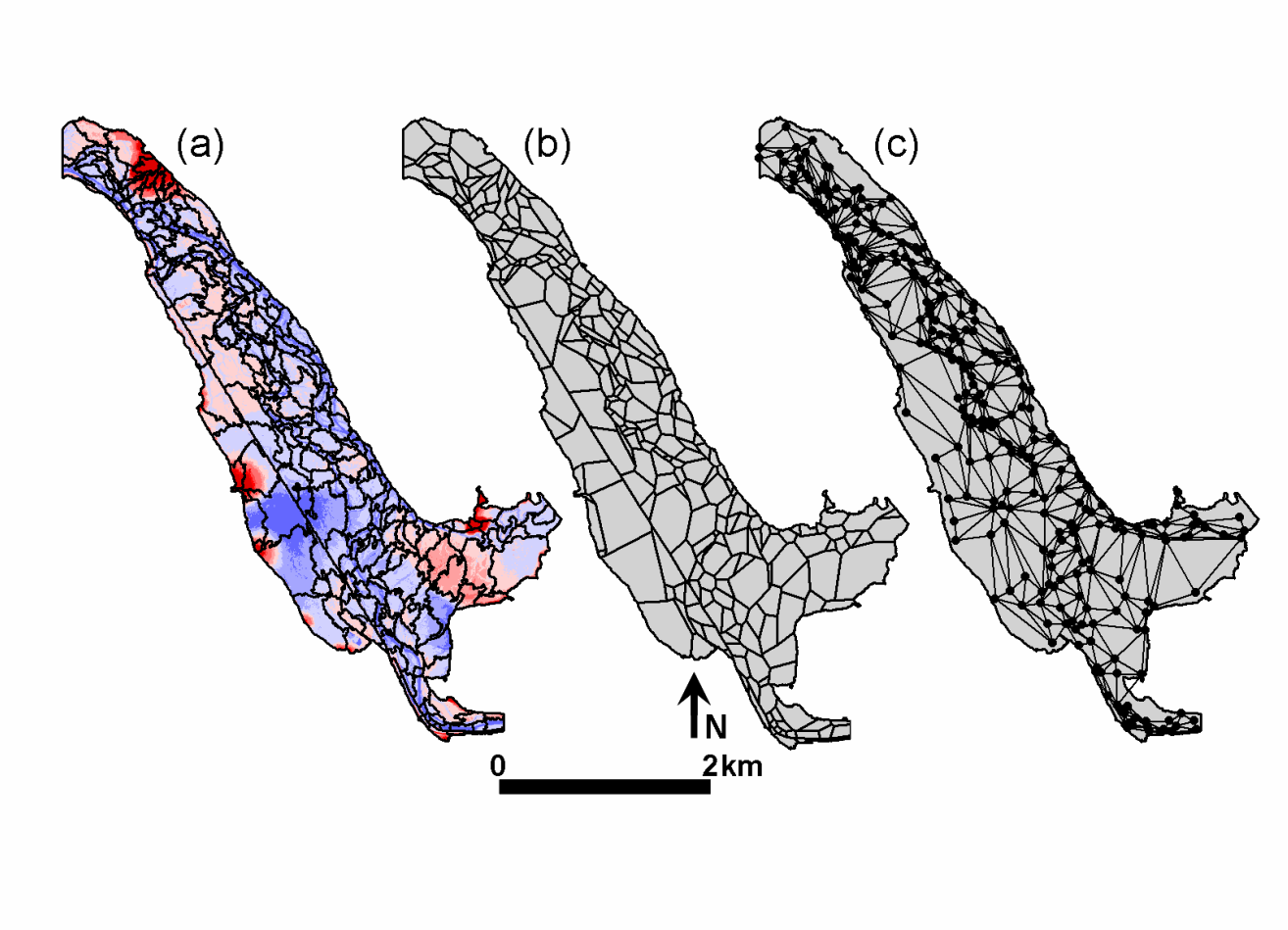

Figure 5.3. Model patches for the Nyack floodplain a) surface and b) subsurface. c) Example of link-and-node network created from subsurface patches in (b). Color in (a) is relative elevation; blue represents low and red high relative elevation.

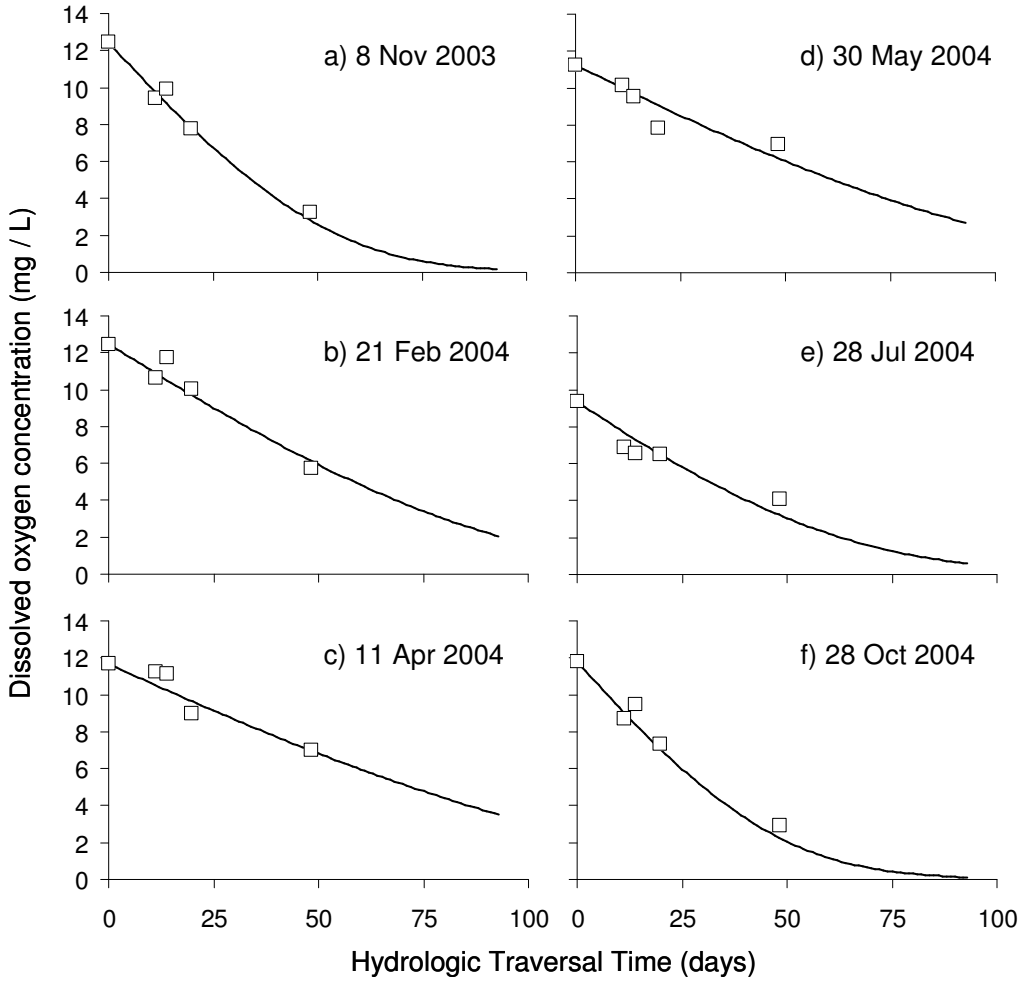

Figure 5.4. Observed (white squares) and parameterized model fit (black lines) dissolved oxygen concentrations versus mean traversal time for a) 8 Nov 2003 b) 21 Feb 2004 c) 11 Apr 2004 d) 30 May 2004 e) 28 Jul 2004, and f) 28 Oct 2004.

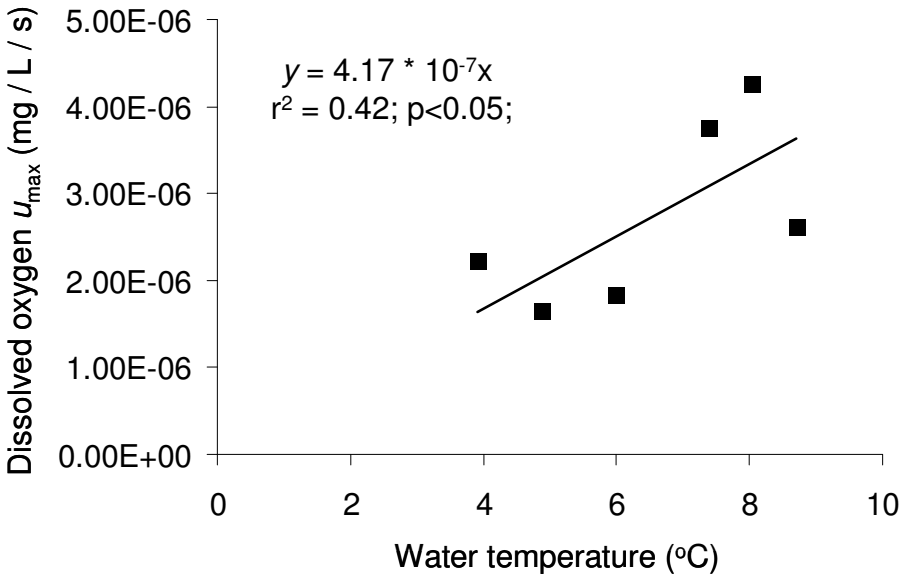

Figure 5.5. Maximum uptake rate for dissolved oxygen versus observed temperature for the six sampling dates shown in Figure 5.4.

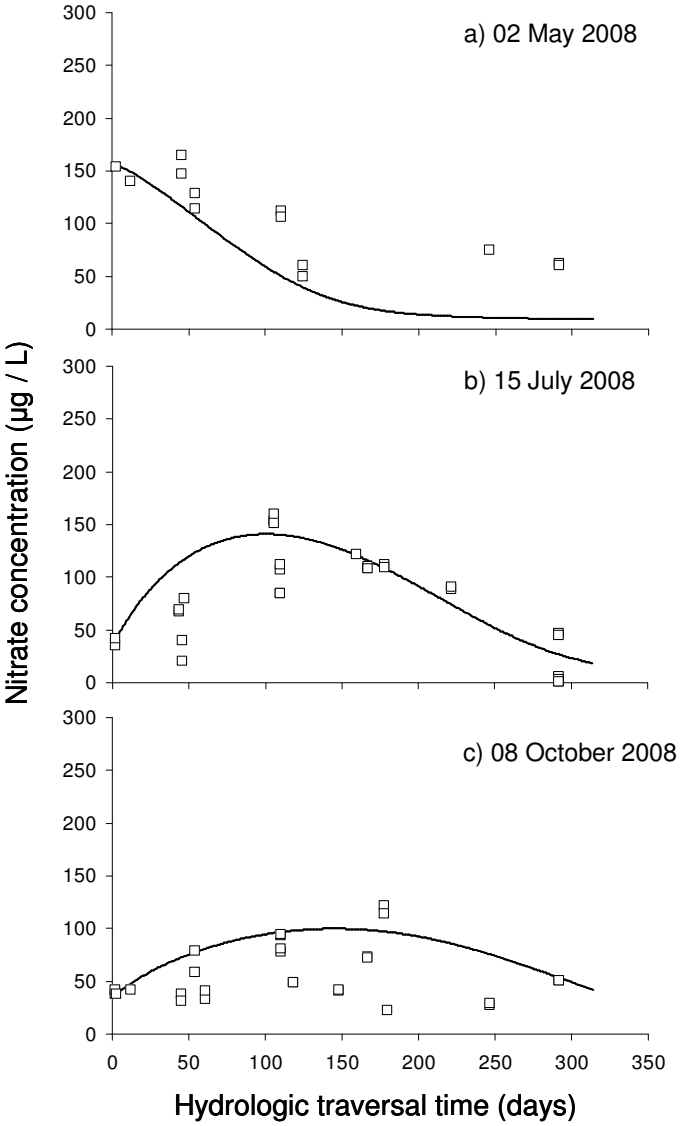

Figure 5.6. Observed (white squares) and parameterized model fit (black lines) nitrate concentrations versus mean traversal time for a) 2 May 2008, b) 15 June 2008, and c) 8 October 2008. Parameter estimates: K_s = 42 µg / L, $u_{maxNO3} = (2.52 * 10^{-6})e^{-0.2[DO]}$, and $NO_3^-{}_{prod} = (8.9 * 10^7)u_{maxDO}^2$.

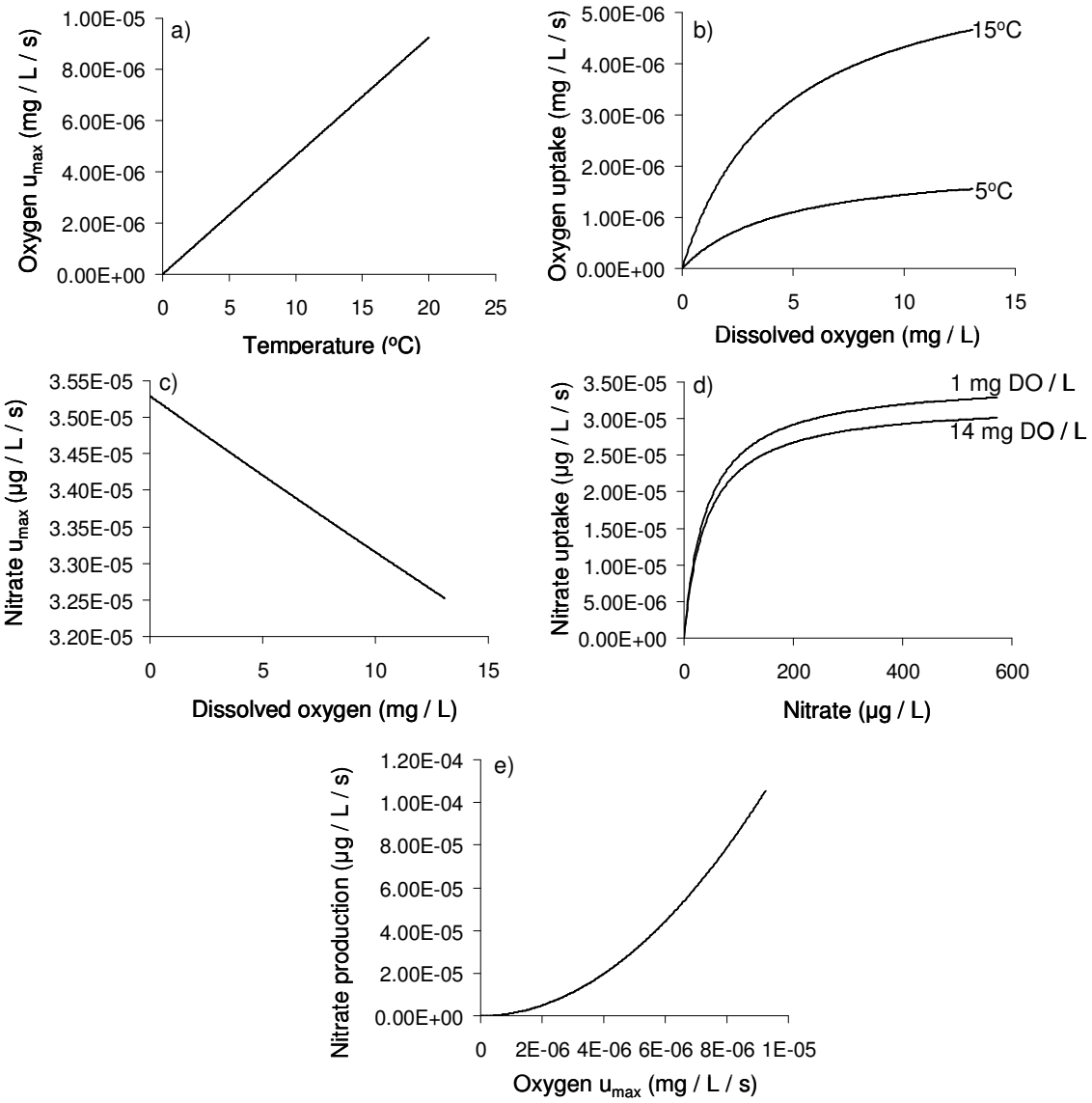

Figure 5.7. Modeled relationships between a) Oxygen maximum uptake rate (u_{maxDO}) and temperature, b) Oxygen uptake and concentration, c) Nitrate maximum uptake rate (u_{maxNO3}) and dissolved oxygen concentration, d) nitrate uptake and concentration, and e) nitrogen production and oxygen maximum uptake rate.

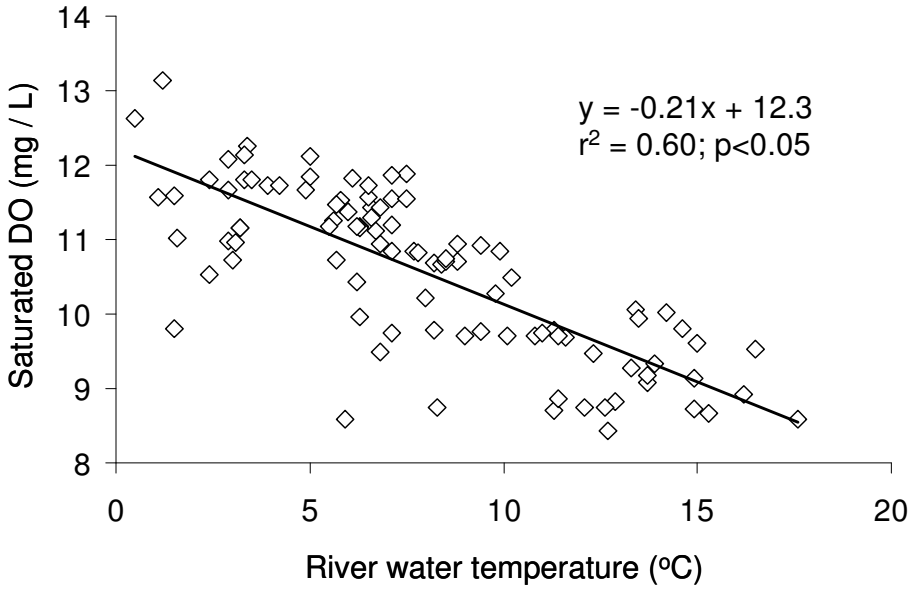

Figure 5.8. Saturated dissolved oxygen (mg / L) versus river water temperature for the Middle Fork Flathead River.

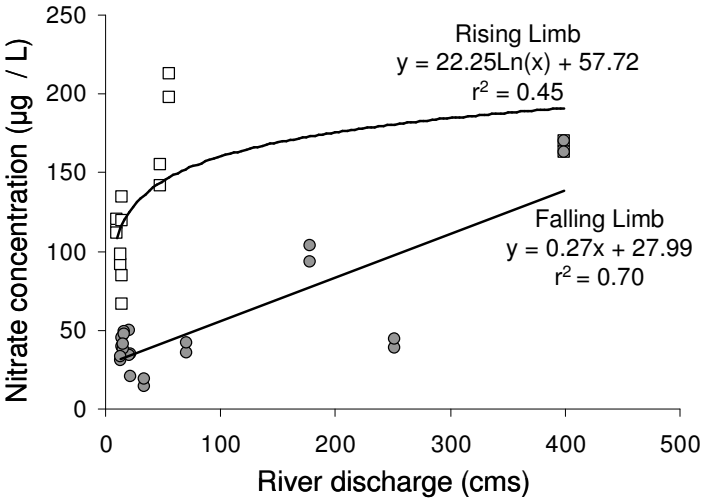

Figure 5.9. Observed surface water nitrate concentration (µg/L) versus river discharge collected during rising and falling river flow conditions during 2008 and 2009.

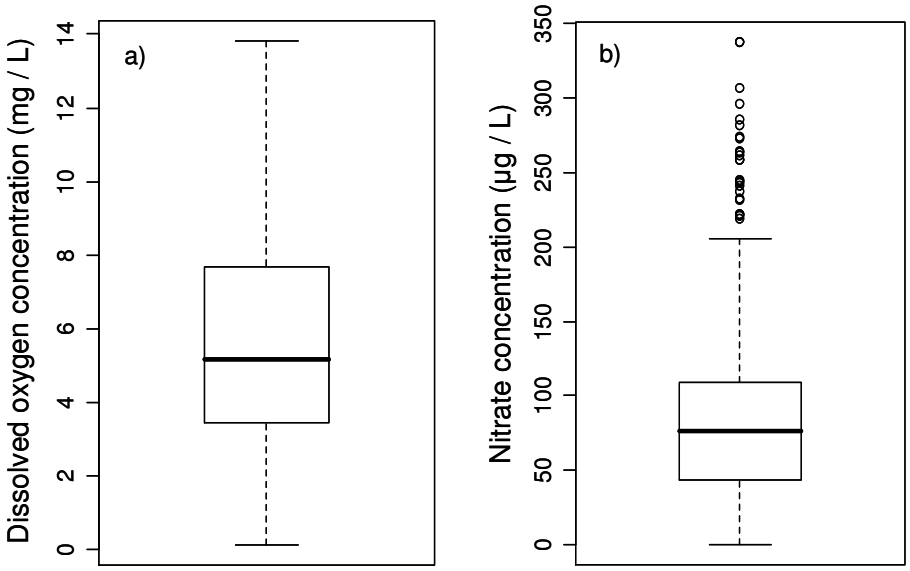

Figure 5.10. Box plot of observed a) dissolved oxygen (n = 820) and b) nitrate concentrations (n = 475) measured within the Nyack floodplain across seasons and river discharge conditions (Table 5.1).

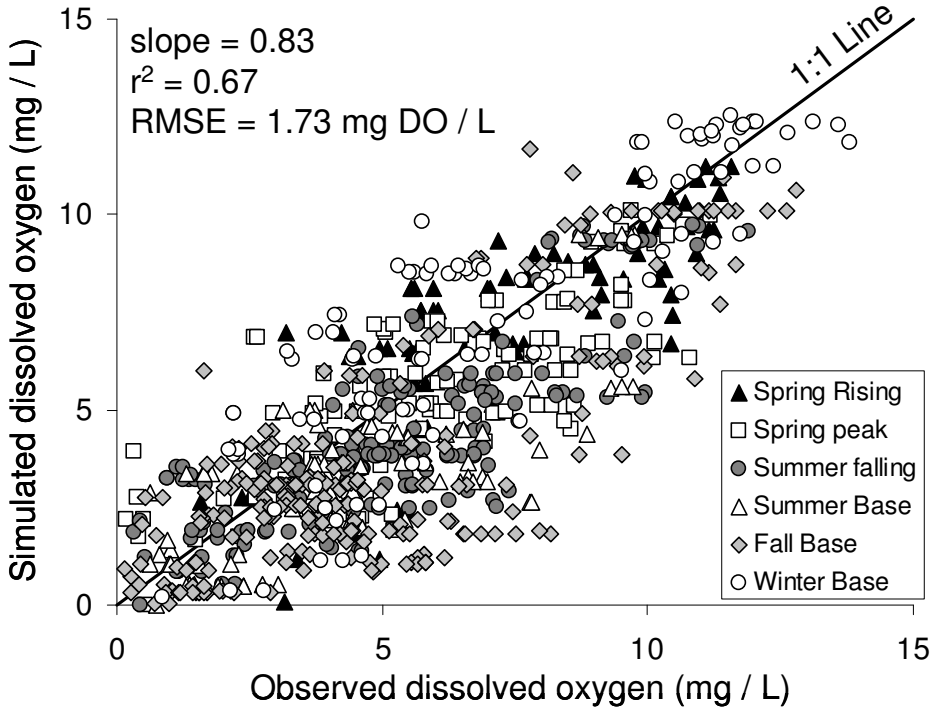

Figure 5.11. Simulated versus observed dissolved oxygen concentration. The legend represents comparison types (Table 5.1).

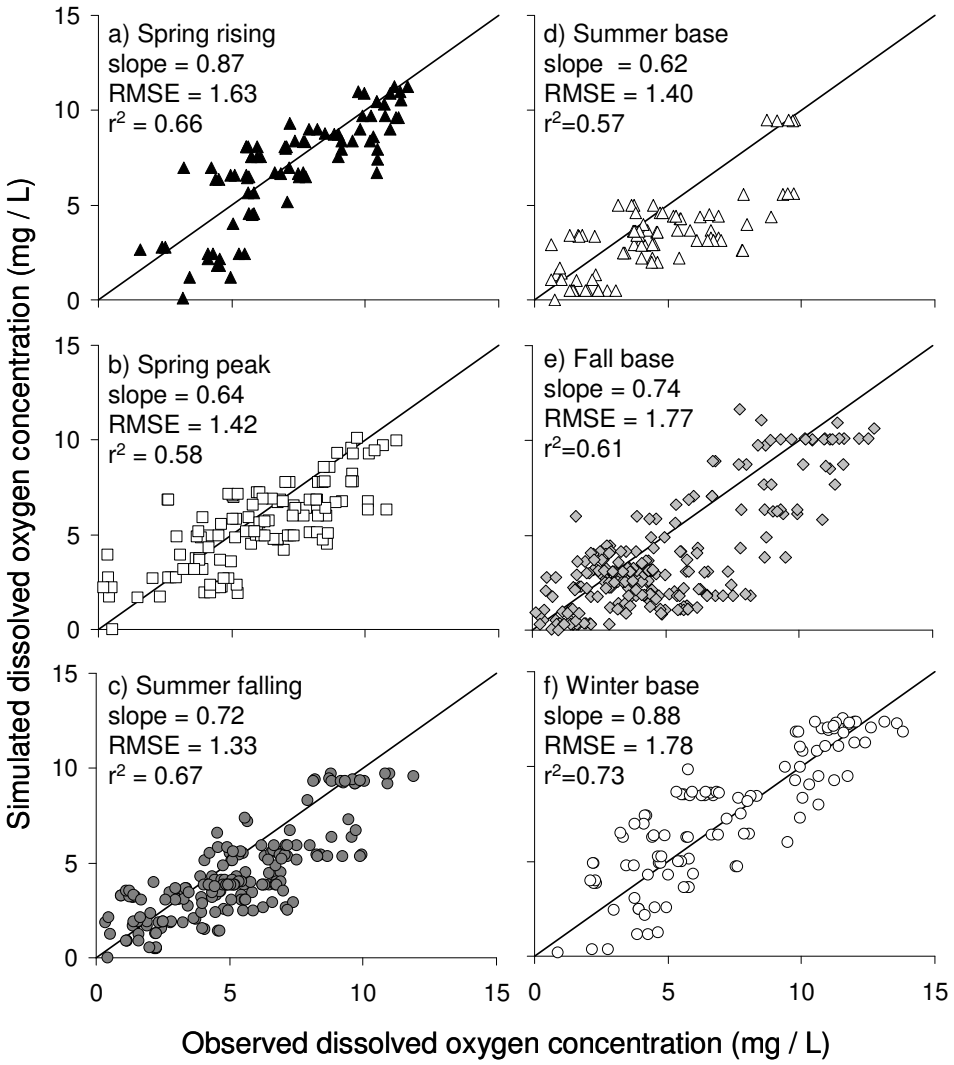

Figure 5.12. Simulated versus observed dissolved oxygen concentration across comparison types: a) spring rising, b) spring peak, c) summer falling, d) summer base, e) fall base, and f) winter base. Solid line is a 1:1 line. All relationships were significant at p = 0.05. RMSE is reported in mg / L of dissolved oxygen.

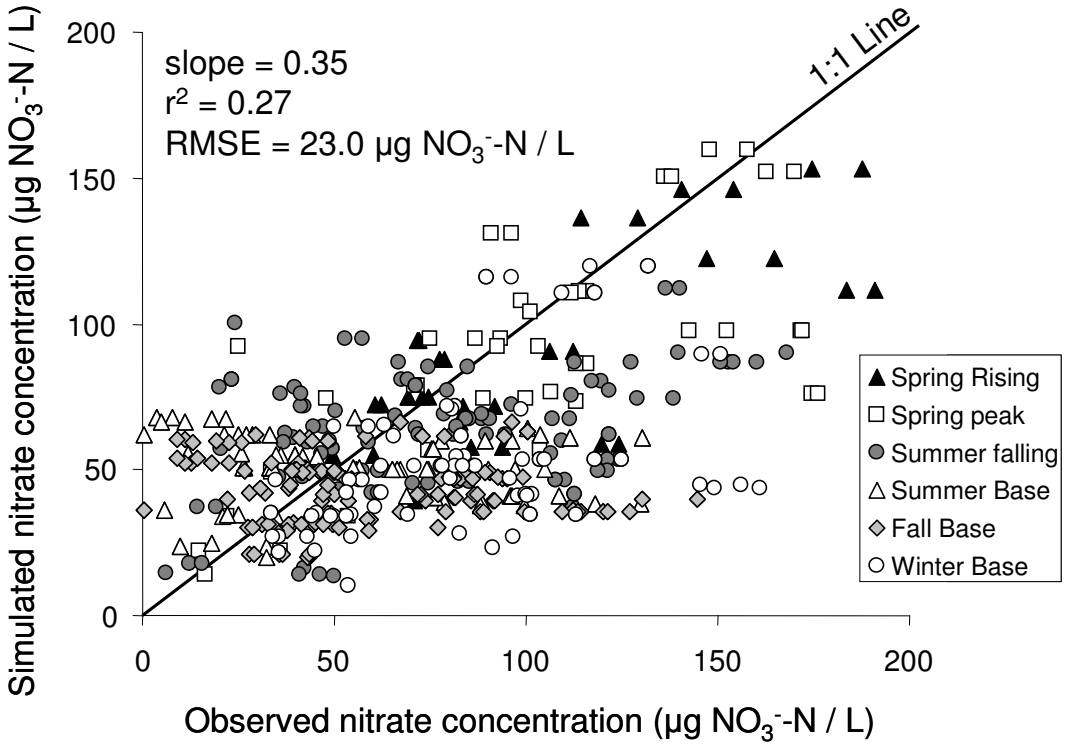

Figure 5.13. Simulated versus observed nitrate concentration. The legend represents comparison types (Table 5.1).

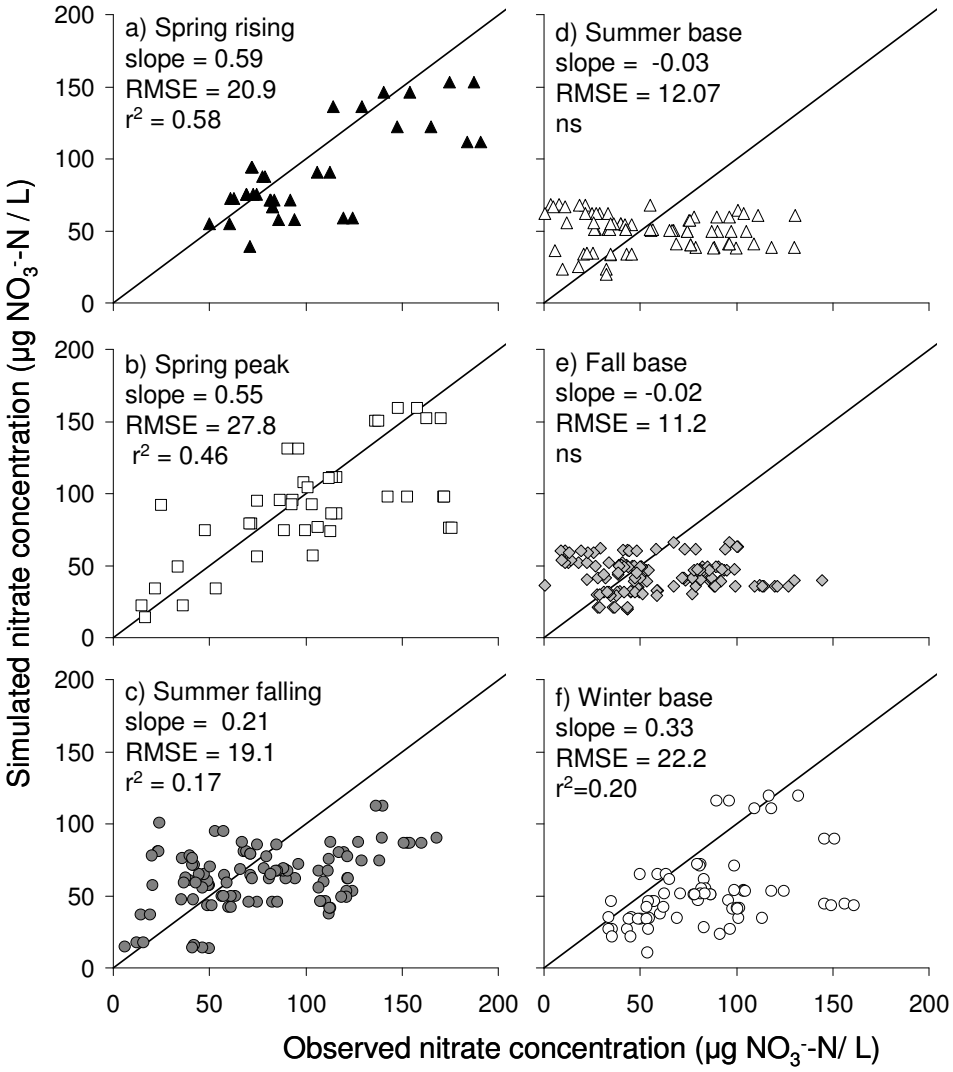

Figure 5.14. Simulated versus observed nitrate concentration across comparison types: a) spring rising, b) spring peak, c) summer falling, d) summer base, e) fall base, and f) winter base. Solid line is a 1:1 line. ns = not significant at p = 0.05. RMSE is reported in µg NO_3^--N/ L.

CHAPTER 6

CONCLUSIONS

Riverine processes play important roles in larger-scale biogeochemical cycles. In this dissertation, several approaches were used to improve our understanding of scaling riverine biogeochemical processes. In Chapter 2, I evaluated common modeling approaches and assumptions about river and catchment hydrogeomorphology and biogeochemistry, by scaling headwater stream denitrification measurements to eight small river networks. Using the model results, I identified additional dynamics and catchment characteristics important for understanding biogeochemical cycling, illustrated strategies for improving river biogeochemistry simulation, and prioritized steps for future model development.

Chapter 2 outlined three specific paths to improve river-network biogeochemistry models, which can be accomplished incrementally and independently of one another. First, I proposed using ecohydrologic models to improve estimated spatiotemporal patterns of water and nutrient delivery to river networks. Human alterations will complicate these patterns, and methods to scale their effects – for example, effects of storm-sewer and tile drainage systems on nutrient and water routing to whole river networks – will be essential, particularly as human impacts become increasingly prevalent. Second, I proposed incorporating multiple elemental cycles and ecological stoichiometry into river-network models. My initial proposed approach integrates first principles of thermodynamics (i.e., free energy yield from metabolic pathways) with governing equations for surface and groundwater fluxes, and should therefore be widely applicable. Maturation of such an approach will require increased collaboration between

empirical, simulation, remote sensing, geographical, and computer sciences to create, model, and understand datasets describing biogeochemical fluxes across an array of environmental conditions and scales. Finally, I proposed integrating biogeochemical models and floodplain-scale hydrology models, which will provide important insights into the biogeochemical dynamics of multiple interacting flow paths within fluvial landscapes. The challenge will be to develop methods to scale these integrated biogeochemistry–hydrology models to whole river networks.

A primary finding from the modeling experiment was the importance of incorporating hydrologic linkages between the river channel, floodplain surface, and hyporheic zone as a basis for scaling biogeochemical cycles. Thus, in Chapter 3 I parameterized a detailed three-dimensional hydrologic model for the 16km^2 Nyack Floodplain on the Middle Fork Flathead River, Montana, and evaluated the influence of different ecosystem components on hydrologic residence time (i.e., matrix traversal time; MTT). Whole-floodplain rates of hyporheic recharge showed a general positive relationship with river discharge, but peaks in hyporheic recharge and net exchange were associated with minor floods and/or the rising limbs of larger flood events. Particle tracking simulations revealed when river discharge was below bankfull, MTT of surface water was inversely correlated to river discharge. However, during overbank flows, MTT increased with discharge due to storage of surface water on the floodplain. Conversely, when both surface and hyporheic water were considered, whole-floodplain MTT was more than an order of magnitude greater than the residence time of surface water alone, and decreased exponentially with river discharge, due to a smaller percentage of channel water entering the hyporheic zone at high discharges.

Our analyses illustrate the importance of considering channel, floodplain, and hyporheic hydrologic residence times in determining the overall residence time of water within a river

segment. When ecosystem components are well connected, adequate representation of hydrologic linkages among channels and floodplain surface and subsurface waters is likely fundamental for understanding hydrologic patterns that drive ecological dynamics. As researchers continue to extrapolate fine scale hydrologic and biogeochemical measurements, a more holistic representation of river system hydrology will be fundamental in describing patterns across large spatial and temporal scales.

In Chapter 4, I used simulated MTT throughout the Nyack hyporheic zone to evaluate measured patterns of hyporheic carbon quality and quantity. Relationships between carbon metrics and MTT (i.e., simulated hydrologic residence time at each carbon sampling location) provided multiple lines of evidence for a concurrent net decrease in dissolved organic carbon (DOC) concentration and increase in bioavailable DOC within the hyporheic zone of the Nyack Floodplain. DOC concentrations and metrics indicative of recalcitrant DOC (humic-like DOC fluorescence and SUVA) decreased with MTT whereas bioavailable DOC (both as a mass and fraction) and metrics indicative of labile DOC (percent of amino-acids, and fluorescence index) increased with MTT. In the Nyack Floodplain, the hyporheic zone may buffer transport of DOC to downstream systems through the sorption of recalcitrant DOC. Conversely, it may be an additional source of bioavailable DOC through microbially-mediated pathways such as chemoautotrophic carbon fixation or POM breakdown. Thus, although the carbon-poor, oxygen-rich Nyack hyporheic zone is a net sink for DOC, recalcitrant DOC is replaced with more bioavailable DOC along hyporheic flow paths, increasing the lability of DOC transported to downstream ecosystems. These contrasting effects on DOC quantity and quality highlight the potential multiple simultaneous roles the hyporheic zone may play in controlling DOC retention and transport in riverine systems.

Finally, in Chapter 5, we integrated a simple linked oxygen and nitrate model with our existing hydrology model to scale observed flow path dynamics to the Nyack Floodplain. We found that simple biogeochemical models can explain large amounts of variability in field data when incorporated with a detailed representation of the floodplain hydrology. Our model explained 67% and 27% of the variance in dissolved oxygen and nitrate measurements, respectively, that spanned the floodplain longitudinally, laterally, and vertically, and river discharge conditions and seasons. Our results illustrate how one-dimensional flow path biogeochemical dynamics can be realistically scaled to a larger three-dimensional river-floodplain system by integrating simple a biogeochemical model to a detailed floodplain hydrology model. This approach provides a initial step for scaling spatially and temporally dynamic biogeochemical patterns from flow paths to floodplains, enhancing the possibility of predicting locations and times within fluvial landscapes most influential for biogeochemical cycles. Our work underscores the importance of the hydrogeomorphic template that drives hydrologic flux and storage of biogeochemical constituents for both scaling and understanding biogeochemical cycles across large spatial and temporal scales.

Developing models that can accurately represent hydrogeomorphic and biogeochemical dynamics across fluvial landscapes ranging from floodplains to river networks will require the melding of concepts and approaches from both terrestrial and aquatic biogeochemical modeling, as well as hydrologic modeling and remote-sensing sciences. Application of these models will yield insights into the river-network biogeochemistry necessary for understanding carbon and nutrient cycling across a variety of fluvial landscapes and among diverse biomes. As anthropogenic activities, such as land-use conversion and fossil-fuel production, push ecosystems toward unprecedented states, a holistic and mechanistic approach to biogeochemical

modeling of rivers will provide a valuable tool for forecasting the responses of biogeochemical cycles across river networks worldwide.

Appendix A. A model for scaling denitrification to river networks

We developed a model of NO_3^- loading, transport, and denitrification in stream and river networks (described in detail by Mulholland *et al.* 2008) to scale-up empirical measures of stream-reach denitrification. The model is based on a steady-state, mass-balance approach and hydrogeomorphic scaling principles commonly used to represent river geomorphology and hydrology, including (1) steady-state hydrologic flux; (2) accumulation of water in streams and rivers from their drainage areas as they flow downstream; (3) uniform water yield for each sampled subcatchment (Figure 2.2); and (4) channel width increasing downstream in proportion to discharge. In accordance with typical river-network model assumptions, denitrification is the primary nitrogen removal pathway (Wollheim *et al.* 2006).

The model calculates denitrification within stream segments and routes water (Q; $m^3\ d^{-1}$) and NO_3^- ($NO3$; $g\ d^{-1}$) between segments linked together into networks (Figure 2.1). Upstream inputs to a stream segment (i) of water (Q_{ui}) and NO_3^- ($NO3_{ui}$) are equal to the sum of exports from upstream segments.

$$Q_{ui} = \Sigma(Q_{i-1}) \quad \text{(Eq 1)}$$

$$NO3_{ui} = \Sigma(NO3_{i-1}) \quad \text{(Eq 2)}$$

Lateral inputs from the terrestrial landscape are equal to the product of the area draining directly to stream segment i (A, m^2) and the area specific loading rate (Y) of water ($m^3\ m^{-2}\ d^{-1}$) and NO_3^- ($kg\ m^{-2}\ d^{-1}$).

$$Q_{Li} = A_i Y_{Qi} \quad \text{(Eq 3)}$$

$$NO3_{Li} = A_i Y_{NO3i} \quad \text{(Eq 4)}$$

We calculated downstream exports using a steady-state mass-balance approach where downstream fluxes of water (Q_{ei}) and NO_3^- ($NO3_{ei}$) equal the sum of inputs minus outputs.

$$Q_{ei} = Q_{ui} + Q_{Li} \quad \text{(Eq 5)}$$

$$NO3_{ei} = NO3_{ui} + NO3_{Li} - NO3_{Ri} \quad \text{(Eq 6)}$$

$NO3_{Ri}$ is the NO_3^- removed from stream segment *i* via denitrification, and is the product of the fraction of NO_3^- denitrified (R) and the sum of NO_3^- inputs to the segment.

$$NO3_{Ri} = R_i(NO3_{ui} + NO3_{Li}) \quad \text{(Eq 7)}$$

The fraction of NO_3^- denitrified from each stream segment is determined by:

$$R = 1 - e^{-\upsilon_{fden}/H_L} \quad \text{(Eq 8)}$$

where hydraulic load (H_L, m s^{-1}) is the ratio of discharge to streambed surface area (length times width of each stream segment; Wollheim *et al.* 2006). Stream length was determined from USGS stream hydrography data (1:24 000). Stream width (w) was calculated using modeled discharge (Q) for each stream segment (Leopold and Maddock 1953):

$$w = aQ^b \quad \text{(Eq 9)}$$

Parameters a and b were estimated empirically for low-flow conditions within each catchment (Appendix B). Because water yields and width parameters were derived from low-flow measurements, the model scenarios apply to low-flow conditions within each catchment.

Conceptually, uptake velocity for denitrification (υ_{fden}) is the downward velocity of NO_3^- molecules through the water column necessary to meet observed streambed denitrification demand for NO_3^-. Mulholland *et al.* (2008) demonstrated that υ_{fden} decreases with increasing in-stream NO_3^- concentration (*[NO3]*), following a power function. Thus, the model determines υ_{fden} for each stream segment according to:

$\upsilon_{fden} = c\ [NO3]^{\ d}$ (Eq 10)

We derived parameters c and d empirically for each catchment using observed values of υ_{fden} and *[NO3]* from 5–9 experimental stream reaches located within or adjacent to each modeled network (Appendix B).

References

Leopold LB and Maddock T. 1953. The hydraulic geometry of streams and some physiographic implications. US Geological Survey Professional Paper 252. United States Government Printing Office, Washington DC.

Mulholland PJ, Helton AM, Poole GC, *et al.* 2008. Stream denitrification across biomes and its response to anthropogenic nitrate loading. *Nature* **452**: 202–46.

Wollheim WM, Vorosmarty CJ, Peterson BJ, *et al.* 2006. Relationship between river size and nutrient removal. *Geophys Res Lett* **33**: doi:10.1029/2006GL025845.

Appendix B. Site-specific parameter values for river-network modeling

Site abbreviation	*Channel width* *a, b (r^2)*	*Uptake velocity (υ_{fden})* *c, d (r^2)*
NC	7.3, 0.45 (0.90)	8.2E-1, –1.2 (0.72)
KS	7.2, 0.35 (0.74)	2.3E-4, –0.48 (0.61)
OR	7.2, 0.35 (0.74)	7.6E-1, –1.2 (0.18)
WY	7.0, 0.33 (0.50)	8.5E-1, –0.10 (0.88)
MA	7.4, 0.27 (0.37)	4.0E-4, –0.47 (0.60)
MI	10.4, 0.45 (0.93)	1.1E-1, –0.93 (0.53)
PR	6.6, 0.35 (0.27)	3.4E-6, –0.063 (0.01)
NM	nd	4.2E-5, –0.36 (0.23)

Notes: The width coefficient (a) and exponent (b) were used to determine channel width for each stream segment (using Eq 9 in Appendix A). The denitrification coefficient (c) and exponent (d) were used to determine denitrifcation uptake velocity (υ_{fden}) for each stream segment (using Eq 10 in Appendix A). nd = no data.

Appendix C. Literature review used to determine the realistic range of modeled NO_3^- loading estimates.

Location	Number of catchments	Catchment area (km^2)	% Agriculture	% Urban	Loading estimate (kg N km^{-2} d^{-1})	Method used to estimate loading	Reference
Loch Vale Watershed, Colorado Front Range	1	6.6	0	0	0.69	Modeled direct total N loading to aquatic ecosystems	Baron and Campbell (1997)
Upper Mississippi	3	492 000 (422 000 – 1 320 000)	nd	nd	1.93 (0.28 – 2.52)	Measured NO_3^- river export	Carey *et al.* (2001)
Embarrass River, Illinois	1	482	91	4.5	6.54	Measured NO_3^- river export	David *et al.* (1997)
Gwynns Falls, Maryland	3	0.32 (0.08 – 0.81)	0 (0 – 100)	0 (0 – 47)	1.78 (0.14 – 4.49)	Measured total N river export	Groffman *et al.* (2004)
Lake Michigan Basin	18	2398 (153 – 15 825)	42 (5 – 82)	2 (0.2 – 20)	0.86 (0.47 – 3.63)	Measured total N river export	Han *et al.* (2009)
Southeast US	14	2125 (63 – 56 894)	16 (2 – 42)	0.5 (0.05 – 5)	1.30 (0.71 – 2.50)	Measured total N river export	Harned *et al.* (2004)
LTER sites across North America	13	0.38 (0.06 – 10)	nd	nd	0.19 (0.03 – 1.18)	Measured dissolved inorganic N river export	Kane *et al.* (2008)
Oldman River, Alberta, Canada	1	28 200	nd	nd	0.76	Measured total N river export	Rock and Mayer (2006)
US West Coast	18	8995 (1531 – 279 438)	6 (0.4 – 24)	1 (0 – 20)	0.32 (0.19 – 4.57)	Measured total N river export	Schaefer *et al.* (2009)
Sierra Nevada and Rocky Mountains	28	1.6 (0.2 – 19.1)	nd	nd	0.20 (0.008 – 0.85)	Measured dissolved inorganic N river export	Sickman *et al.* (2002)
Central Valley, California	23	2736 (461 – 61 721)	6 (0 – 74)	2 (0 – 6)	0.31 (0.06 – 2.59)	Measured total N river export	Sobota *et al.* (2009)
Northeast US	16	11 945 (475 – 70 189)	10 (1 – 61)	3 (0 – 22)	5.51 (2.74 – 6.96)	Modeled estimates of NO_3^- leaching to ground and surface waters	Van Breeman *et al.* (2002)
Ipswich River basin, Massachusetts	1	404	7	35	1.85	Estimated direct total N loading to river network by 1st-order streams	Williams *et al.* (2004)
Summary	140	1791 (0.06 – 1 320 000)	10 (0 – 100)	1.2 (0 – 47)	0.49 (0.008 – 6.96)		

Notes: Catchments in the literature review span a wide range of geographic regions, catchment areas, and land-use conditions. When references included more than one year of loading data for a particular catchment, the average value was used. Data are reported as median (range). The highest reported nitrogen loading rate was 6.96 kg N km^{-2} d^{-1}. nd = no data.

References

Baron JS and Campbell DH. 1997. Nitrogen fluxes in a high elevation Colorado Rocky Mountain basin. *Hydrol Process* **11**: 783–99.

Carey AE, Lyons WB, Bonzongo JC, and Jehrter JC. 2001. Nitrogen budget in the Upper Mississippi River watershed. *Environ Eng Geosci* **7**: 251–65.

David MB, Gentry LE, Kovacic DA, and Smith KM 1997. Nitrogen balance in and export from an agricultural watershed. *J Environ Qual* **26**: 1038–48.

Groffman PM, Law NL, Belt KT, *et al.* 2004. Nitrogen fluxes and retention in urban watershed ecosystems. *Ecosystems* **7**: 393–403.

Han H, Allan JC, and Scavia D. 2009. Influence of climate and human activities on the relationship between watershed nitrogen input and river export. *Environ Sci Technol* **43**: 1916–22.

Harned DA, Atkins JB, and Harvill JS. 2004. Nutrient mass balance and trends, mobile river basin, Alabama, Georgia and Mississippi. *J Am Water Resour As* **40**: 765–93.

Kane ES, Betts EF, Burgin AJ, *et al.* 2008. Precipitation control over inorganic nitrogen import–export budgets across watersheds: a synthesis of long-term ecological research. *Ecohydrol* **1**: 105–17.

Rock L and Mayer B. 2006. Nitrogen budget for the Oldman River Basin, southern Alberta, Canada. *Nutr Cycl Agroecosyst* **75**: 147–62.

Schaefer SC, Hollibaugh JT, and Alber M. 2009. Watershed nitrogen input and riverine export on the west coast of the US. *Biogeochemistry* **93**: 219–33.

Sickman JO, Melack JM, and Stoddard JL. 2002. Regional analysis of inorganic nitrogen yield and retention in high-elevation ecosystems of the Sierra Nevada and Rocky Mountains. *Biogeochemistry* **57**: 341–74.

Sobota DJ, Harrison JA, and Dahlgren RA. 2009. Influences of climate, hydrology, and land use on input and export of nitrogen in California watersheds. *Biogeochemistry* **94**: 43–62.

Van Breemen N, Boyer EW, and Goodale CL. 2002. Where did all the nitrogen go? Fate of nitrogen inputs to large watersheds in the northeastern USA. *Biogeochemistry* **57**: 267–93.

Williams M, Hopkinson C, Rastetter E, and Vallino J. 2004. N budgets and aquatic uptake in the Ipswich River basin, northeastern Massachusetts. *Water Resour Res* **20**: doi: 10.1029/2004WR003172.

Appendix D. Modeled NO_3^- loading estimates from the Ipswich River, Massachusetts versus upstream percent wetland stream length (ie ratio of stream length passing through wetlands to total stream length). Wetland extent determined from 2001 National Land Cover Dataset (http://seamless.usgs.gov). Loading estimates derived from network modeling were negatively correlated with percent wetland stream length for both years of estimated loading rates (2003 $r^2 = 0.21$, $P < 0.002$, solid line and diamonds and 2004 $r^2 = 0.31$, $P < 0.002$, dashed line and open squares), suggesting that the model underpredicts denitrification in channels flowing through wetlands.